The Interactions of Stance Width and Feedback Control Gain: A Modeling Study of Bipedal Postural Control

A Dissertation
Presented to
The Academic Faculty

by

Jevin Eugene Scrivens

In Partial Fulfillment
of the Requirements for the Degree
Doctor of Philosophy in the Interdisciplinary Bioengineering Program
School of Mechanical Engineering

Georgia Institute of Technology
August 2007

The Interactions of Stance Width and Feedback Control Gain: A Modeling Study of Bipedal Postural Control

Approved by:

Dr. Stephen P. DeWeerth, Co-Advisor
Department of Biomedical Engineering
Georgia Institute of Technology

Dr. Young-Hui Chang
School of Applied Physiology
Georgia Institute of Technology

Dr. Lena H. Ting, Co-Advisor
Department of Biomedical Engineering
Emory University and Georgia Institute of Technology

Dr. T. Richard Nichols
School of Physiology
Emory University

Dr. Wayne J. Book
School of Mechanical Engineering
Georgia Institute of Technology

Date Approved: June 28, 2007

ACKNOWLEDGMENTS

I would like to thank a number of people who have supported me throughout my doctorial work. Thanks to my advisors Steve DeWeerth and Lena Ting, for encouraging me and helping me to form my research ideas. To my committee, Dr. Wayne Book, Dr. Young-Hui Chang, and Dr. Richard Nichols, whose direction and input was indispensable. I have also had the pleasure of working with many wonderful people in the Neuro Lab who have provided me with camaraderie, assistance, and advice: Kartik Sundar, Carrie Williams, Jim Ross, Shane Migliore, Richard Blum, Kate Williams, Gelsy Torres-Oviedo, Torrence Welch, Lucas McKay, Nate Bunderson, Amanda Pryor, Murat Sekerli, and Ivan Rikov. Thanks to Kunal Gosrani and Hugh Kinsel, for your many hours of labor, running thousands of robot trials. I would particularly like to thank Edgar Brown, Stefan Clemens, and Stacie Chevatal for being technical sounding boards and providing the critical support that I needed as I prepared this document. Special thanks to Malaika Kamunanwire, Aimee Lui-Thomas, Holly Neal, and Cherie Pimento, for helping to keep me sane with encouragement, motivation, laughs, and empathy. Thanks to my family, Mom, Dad, Jay, Janelle, Ted, Ann, and Kerry, whose support has been absolutely critical to my success.

Most importantly, I would like to thank my wife, Diane, and my sons, Jevin and Justin, for being ……EVERYTHNG to me.

TABLE OF CONTENTS

Page

LIST OF TABLES

Page

LIST OF FIGURES

Page

LIST OF SYMBOLS AND ABBREVIATIONS

BoS	Base of Support
CNS	Central Nervous System
CoM	Center of Mass
COP	Center of Pressure
G	Active Delayed Feedback Gain (Lumped Parameter)
G_{i}	Intrinsic Feedback Gain (Lumped Parameter)
G_{ip}	Intrinsic Position Feedback Gain
G_{iv}	Intrinsic Velocity Feedback Gain
G_{p}	Active Delayed Position Feedback Gain
G_{v}	Active Delayed Velocity Feedback Gain
ζ	Damping Ratio

SUMMARY

By understanding and mimicking characteristics of postural control used by animals, scientist and engineers may develop standing autonomous robots that work safely within home environments, and treatment strategies that help people overcome postural impairments. To increase our understanding of postural control we developed physical and computational models of standing posture to explain the interrelation of stance width and feedback gain in controlling the stability and dynamics of the postural response. These models facilitated precise analysis of mechanical dynamics and their effects on compliant feedback control, and provided a physical implementation to verify predictions developed from simulation. We show that a scaling of active feedback gain is required to maintain postural stability. These results are consistent with previous studies that have shown that a correlation exists between increased stance width and decreased postural responses. However, these studies have not quantified the relation between stance and the active control of standing posture. This scaling of gains that we show is dependent on the changing kinematic relations of the mechanical structure as it undergoes stance width adjustments. Specifically, we show that increasing stance width increases the leverage of the mechanical system. Feedback gains must be reduced by the reciprocal of the increase in mechanical leverage in order to maintain a consistent postural response; otherwise, the system may become unstable with increasing oscillations. We also showed that increasing magnitudes of intrinsic stiffness increases postural stability by facilitating stable responses over larger ranges of active feedback gain and increasing the stability of responses by decreasing settling time, oscillations, and displacement magnitude. The conclusions of this study were that the variation of mechanical leverage is responsible for changing the dynamics of the response during stance width variation, and that scaling of feedback gains with the changing mechanical leverage of stance width variations is required to maintain consistent response dynamics across stance widths.

CHAPTER 1

INTRODUCTION

Compliant postural strategies employed by animal neuromuscular systems may provide robust solutions and inspiration for robotic and prosthetic design. In traditional robotic systems for manufacturing applications, control algorithms are designed to enable precise control over joint trajectories, overriding the natural dynamics of the mechanical system. However, in all devices including those that both interact with and emulate humans, these algorithms produce very stiff systems that can create potentially dangerous levels of contact force. Thus, applying traditional control algorithms to an unstable, upright, bipedal configuration such as in the humanoid robot Asimo™ (Honda Corp.) results in joint stiffness and energetic expenditures that far exceed those found in humans and animals (Collins et al. 2005). In contrast, animals display fluid movements with compliant behaviors that generate relatively low reaction forces when contacted or perturbed. The fluidity of these movements results from the relatively low actuator forces combined with the passive dynamics of the mechanical system.

Taking motivation from biological systems the overall objective of this work is to improve robot control design by understanding the contributions of feedback control and mechanics in the in the generation of stable and compliant responses to postural perturbation. Towards this objective, we investigated how to maintain compliant operation of our robot under changing geometrical configuration. More specifically, we investigated the effects of stance width and control variations on the stability and dynamics of standing balance during postural perturbation. We determined the changes that are required in a compliant controller in order to maintain standing balance as stance width changes. The results of this study may help provide insight and understanding to the methods of control for a task that bipeds and quadrupeds must accomplish on a frequent basis.

1.1 Background and Motivation

The goal of this work was to determine how mechanical configuration and active postural control mechanisms interact to maintain postural stability. The implications of this study may be used to direct studies aimed at gaining a better understanding of biological control of posture and to improve the control design of biomimetic robots and prosthetics. In this background section we present the established models and theories of biological control of posture and highlight the areas in which this research will add to this body of knowledge. Generally, this previous research has studied the control of specific models of standing posture, so the background that we are presenting will first describe the models of standing posture. Next, we will describe the different models of postural control and stabilization. We will then introduce some observations made in postural research that provide some motivation to the work presented in this dissertation. Finally, we will introduce robotic control, detailing its advantages and illustrate how a more bio-inspired control methodology could be beneficial in certain applications.

1.1.1 Models of Standing Posture

Standing posture is a complex task and researchers have developed many models to describe different aspects of it. To describe human postural stability in the *sagittal plane,* a single-link inverted pendulum is often used (He et al. 1991; Horak et al. 2005; Kuo 1995) (Winter et al. 1997). In this sagittal plane (anterior-posterior) model, the body is configured as a stick mass with the feet side-by-side and a common axis of ankle rotation. Motion occurs as rotation about the ankle axis and standing balance is maintained by exerting control torques about the ankle, which work to maintain an upright standing posture. As it pertains to our study, this model is limited because it has only a single degree of freedom which is the same control variable denoting postural disturbance. Because there is only this one variable to describe the state of the system, the system only

has a single mechanical configuration and mechanical stability cannot be varied or altered without changing components of the model. Therefore, this model of standing balance is not suitable for our study of the interaction between mechanical stability and control. However, this model is suitable and is often used for study and optimization of control for a single non-varying structure (Kuo 1995; Peterka 2003).

To describe human stability in the *frontal plane,* a two-legged tandem pendulum is used (Day et al. 1993; Gage et al. 2004; Prince et al. 1995; Rietdyk et al. 1999; Winter et al. 1996). The two-legged pendulum is also used to describe quadruped stability in both frontal and sagittal planes. The difference between each of these configurations is a matter of scaling the length and inertial properties of each component. In each configuration, standing balance is maintained by exerting control torques, about the hips and shoulders, which work to maintain an upright standing posture. The direction of torque exertion for each configuration is oriented within the appropriate plane of motion for the model configuration (e.g. abduction/adduction torques in the frontal plan for the frontal plane model).

In respect to this study, the advantage of the two-legged model is that, with its two legs, it is capable of changing its mechanical configuration and therefore changing its mechanical stability without changing any of its structural components. The result is that various levels of mechanical stability are possible with the same model.

1.1.2 Models of Biological Control

The models presented above are simplified descriptions of the structure of standing posture in humans and animals. However, in order to maintain balance in these standing postures and prevent falling, each of these models must be controlled against their inherent instability. The basic model used to describe postural control in humans and animals is the feedback model (Ishida et al. 1997; Kiemel et al. 2002; Kuo 1995; Park et al. 2004; van der Kooij et al. 1999). In the feedback control process, corrective

joint torques which stabilize the postural orientation against deviation and help to maintain standing balance are generated in proportion to input from selected sensory modalities. A number of control models present different transformations from sensory inputs to joint torque outputs. The most detailed models take into account the input from multiple sensory systems including visual, vestibular, proprioceptive, and tactile (Alexandrov et al. 2005; Horak et al. 1996; Macpherson and Fung 1999); (Winter et al. 1998). Such complex modeling approaches require intricate descriptions of the sensorimotor integration during the process of posture stabilization (Kiemel et al. 2002; Peterka 2002; van der Kooij et al. 1999; van der Kooij et al. 2001). In contrast, the simplest description of the control of posture is the linear viscoelastic model with a single feedback loop (Barin 1989; Morasso and Schieppati 1999; Park et al. 2004; Rietdyk et al. 1999). In this description, corrective torques are generated in proportion to joint angular displacement and velocity. The compromise between the different feedback models is the linear viscoelastic model, which is composed of two parallel feedback loops. These loops would both have a linear viscoelastic basis, but one would operate with a time delay and the other without (Peterka 2002). These loops were referred to as the delayed "active" and the non-delayed "intrinsic" loops.

The biological basis of the feedback model is that sensory information (tactile, proprioceptive, vestibular, and visual) regarding the body's position and orientation is used to generate torque responses to maintain postural orientation (Ishida et al. 1997; Kiemel et al. 2002; Kuo 1995; Park et al. 2004; van der Kooij et al. 1999). In these long latency "active" responses, somatosensory information is integrated in the spinal cord and higher brain centers to generate commands to motor neurons for the "active" response. Because time is required for the transmission, integration, and processing of the sensory information as well as the electromechanical process of force production in muscle, this active path operates with a latency that can be modeled as a time delay.

Intrinsic stiffness is a description of the elastic and viscous components of the muscles and connective tissue. However in the feedback model described above, the "intrinsic" component of the feedback loop is the result of intrinsic stiffness and the reflex response. Nichols et al. have shown that the short-range mechanical stiffness of muscle yields quickly during stretch, however the stretch reflex compensates for the mechanical yielding and increases the linearity of the response (Huyghues-Despointes et al. 2003a; b; Nichols and Houk 1976). The result is a response that can be modeled as a zero latency viscoelastic response. It has also been shown that the elastic modulus of intrinsic stiffness varies with muscle tension (Huyghues-Despointes et al. 2003a; Joyce and Rack 1969). This finding means that the modulus of intrinsic stiffness can be varied with muscle activation and the stiffness of a joint can be increased through co-activation of antagonistic muscles (Hogan 1984). These studies show that there are two methods of controlling the dynamics of the postural response available to the CNS. So the next step towards understanding postural control is to determine how these "active" and "intrinsic" paths are used.

1.1.3 Observations of Biological Control of Posture

As we have shown, postural control can be modeled as a feedback process with active and intrinsic components. However, studies have shown that the process is not constant and the parameters of the feedback loop can be altered in different situations. Studies by Peterka have shown that "sensory integration and postural regulation appear to be a linear process for a specific sensory condition and stimulus amplitude." However a shift in the source of sensory information occurred with changes in test condition (Peterka 2002). This shift implies an alteration of the gains of the feedback control mechanism. The notion of a feedback postural control scheme that relies on sensory re-weighting is further supported by a number of pathological conditions in which perception and sensory input is impaired (Jeka et al. 2004; Henry et al. 2001; Henry et al.

1998b; Park et al. 2004; Peterka 2002; Peterka and Loughlin 2004; van der Kooij et al. 1999). The studies showed that the elimination of certain sensory modalities caused changes in the resulting postural response strategies. The results suggest that postural response strategy changes could be accompanied by a continuous scaling of postural response feedback gains. In another study of postural responses to perturbation, Park et.al showed that feedback control gains exhibited a gradual scaling with perturbation magnitude and distance to edge of support (Park et al. 2004). The observed scaling of feedback gains with perturbation magnitude means that the CNS adjusts postural responses in accordance with biomechanical constraints (Horak and Nashner 1986). From these studies we see that postural adjustments can be described as feedback control with adjustable gains, and Specifically they show that gains scale to perturbation magnitude, but they leave open the possibility of gains scaling to other biomechanical constraints.

Changes in biomechanical constraints including postural orientation have been shown to cause changes in the parameters of postural control. For example, increasing stance width increases the available Base of Support (BoS) and increases the biomechanical stiffness of the musculoskeletal system (Day et al. 1993; Kirby et al. 1987). This increased stiffness was considered a passive mechanical stiffness and was not correlated to a change in intrinsic stiffness. However, in a study of postural response to perturbation under changing stance width, the magnitude of postural response to perturbation was shown to decrease with increasing stance width (Henry et al. 2001). The study suggested a shift in postural control from an active to passive strategy with increasing stance width, which was explained by an increase in the passive stability of the musculoskeletal system accompanied by a decrease in the active neural control needed to maintain equilibrium in response to horizontal displacement perturbation (Henry et al. 1998a). In other studies, investigators showed that the Central Nervous System (CNS) can modulate stiffness of the lower limbs, providing increased stiffness of the musculoskeletal system at wide stance (Horak and Nashner 1986; Winter et al. 1996).

They then claimed that reactive (active) control of quiet stance would not be required in this condition of wide stance with increased stiffness (Patla et al. 2002; Winter et al. 1998). These studies show that the passive and active properties of postural control can be modulated and that changing the biomechanical constraints alters the postural responses. However, they still do not explain an underlying reasoning for these changes. They also do not quantify any coordination between these properties or their modulation under changing conditions.

The studies conducted in the development of the models presented have provided great insight to the control of posture in different mechanical configurations, but the shortcoming of these studies is that they have not looked at postural control as an integrated process in which mechanics is considered as a variable that plays a role in postural control. So, the questions that we are trying to answer are “How are stance width, active control parameters, and intrinsic properties related?” and, “How is control strategy changed with stance width variations?”

1.1.4 Robot Control

In addition to developing a better understanding of the techniques of postural control in biology, the focus of this work was to transfer techniques of postural control from biology to robotics. In this section we introduce robotic control while detailing its advantages and disadvantages, and illustrating how a more bio-inspired approach would benefit certain applications.

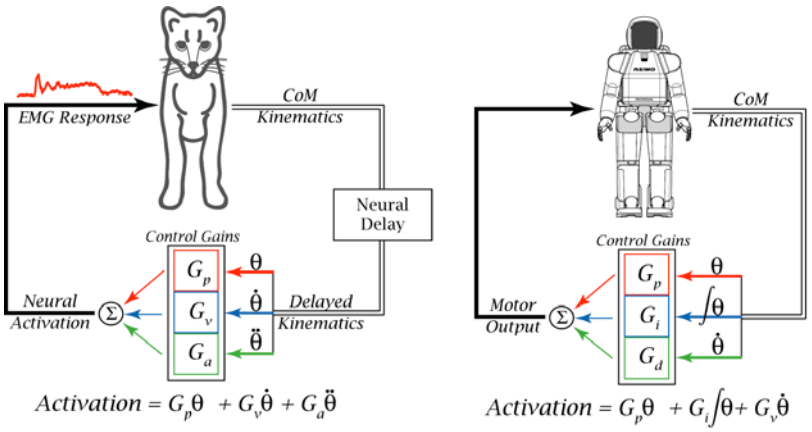

Figure 1.1 Feeedback Control describes for control of both biological posture and robotics. It has been shown that biological posture can be maintained through delayed feedback of joint kinematics. Muscle activation can be reconstructed from the gained sum of deviations of joint position, velocity, and acceleration. Robotic control is obtained by PID controllers in which motor output is a gained sum of deviations of position, position integral, and position derivative (velocity).

As we compare postural control in biology to robotic control, we see that they are similar in the sense that they are both described as feedback processes (Figure 1.1). However, we cannot ignore the fact that there are significant differences in the overall systems that distinguish biology from robots in each level of the control hierarchy. Previous research has shown three important considerations that are repeated here (Loeb et al. 1999).

- Biological muscles produce large, instantaneous changes in output force when kinematic conditions change, but respond only sluggishly when neural activation changes. In contrast, torque motors respond instantly only to changes in electric current.
- In biological feedback circuits, the signals from large numbers of noisy sensors of diverse physical variables converge with the signals from many command centers before they are routed to motorneurons. Motors have dedicated direct paths for feedback and control signals.

- Performance objectives also differ between biology and industrial robots in that animals usually find it more valuable to perform adequately in the widest possible range of circumstances rather than to perform optimally for limited conditions. Robots, on the other hand, are designed to a specific task very well.

Even with these differences, it is still possible to develop robots that emulate the qualities and dynamic characteristics of animal control. But in order to achieve this objective, these differences must be overcome. And the key to overcoming these differences lies in the characteristics of the feedback controller. As we examine feedback control in robotics, specifically robotic systems that emulate biological systems, we see that feedback falls into two major philosophies of control, high impedance control and passive dynamic control.

High impedance control is the most widely used control method used in industrial robots. High impedance trajectory tracking control provides a method of strictly controlling the trajectories of actuators regardless of the influence of the plant dynamics. It is used in the vast majority of today's robots, and its roots go back to the origins of controlled movements. This control philosophy is useful because it provides a means for precise movement and positioning. This quality is extremely important in industries such as manufacturing where tight dimensional tolerances are required. It is also useful in applications such as animatronics, weapons tracking, plotting, or any other application where precise trajectory control is important (Pratt 2002; Yamaguchi et al. 1999). Employed under the term "High gain trajectory tracking control", high impedance control is the control philosophy used in what is arguably today's most advanced, or at least most popular, bipedal walking robot, ASIMO. (Hirai et al. 1998) This device replicates walking movements obtained from motion capture of human locomotion. It uses a control strategy of Zero Moment Point (ZMP) control that requires it to maintain its center of mass (CoM) over the base of support (BoS) (Park and Chung 1999; Sorao et al. 1997; Vukobratovic and Juricic 1969). This is the control strategy used in most biped robot

designs. This strategy requires the robot to strictly control the position of the body while preventing position disturbance from external perturbation. This results in the exertion of high forces and high-energy consumption. High impedance and strict trajectory control also result in high forces when obstacles impede the desired trajectory. For this reason high impedance robots are too dangerous to interact with humans or in unknown environments. Other problems of high impedance control are that the motions of these systems must be explicitly scripted and their motions continue to look unnatural.

An alternative to high impedance control is the use of passive dynamics, which is a mode of operation in which the inherent passive properties of a device are exploited to obtain the desired motion. Characteristics of robots that take advantage of passive dynamics may be divided into three categories, passive postural stability (Rhex) (Koditschek et al. 2004), passive dynamics (walkers) (Mcgeer 1990) (McGeer 1990), and minimally actuated passive dynamic walkers (van der Linde 1999a) (Van Der Linde 1998) (Wisse et al. 2005).

Passive postural stability is the result of mechanical configuration and intrinsic stiffness and is a characteristic in which postural disturbances can be rejected by the spring and damping characteristics of the legs. Studies using hexapedal locomotion (cockroaches) have generated models that show neural or other detailed feedback is not necessary for stability. Essentially, stabilizing control algorithms can be embedded in the mechanics of the system. Control results from the information transferred through the mechanical structure that changes the motion, providing a mechanical feedback that alters the forces applied to the body (Figure 1.2) (Kubow and Full 1999; Ting et al. 1990). The understanding that has been gained through the study of hexapod locomotion has been applied to a number of robotic devices including RHex (Koditschek et al. 2004). The problem with these models is that they aim to stabilize a system that is essentially already stable. The height/width aspect ratio and the axial stiffness of the legs provide an intuitively stable structure, unlike the inverted pendulum structure of the human and cat

standing models. However, the notion of using the passive mechanical properties for postural stability is an interesting concept that we apply to bipedal postural stability.

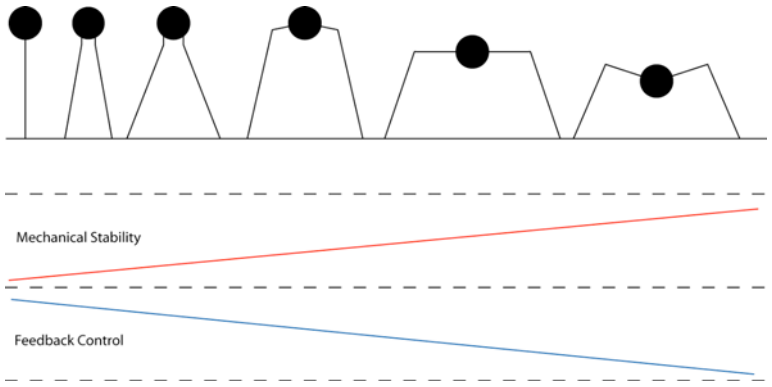

Figure 1.2 Feedback-Stability Transition: The inverted pendulum is an inherently unstable configuration that requires considerable feedback control to maintain posture. The configuration of a hexapod is just the opposite as a highly stable orientation requiring little feedback control to maintain posture. As a device transitions from a pendulum to a hexapod configuration, the level of inherent mechanical stability increases while the requirement for feedback control increases.

Pioneered by Tad McGeer and continued primarily by Andy Ruina, Steven Collins, Richard van der Linde, and Martijn Wisse, passive walkers have demonstrated that human-like locomotion can be obtained in a passive system walking down a slight incline (Collins et al. 2005; Collins et al. 2001; McGeer 1990; Mcgeer 1990; Ruina 1998; Ruina et al. 2005; van der Linde 1999b; Wisse et al. 2005). The idea was that the inherent dynamic mass properties of a system could be used to generate a desired movement. This concept utilized the basic principle of conservation of energy in cyclic motion through transference of kinetic and potential energy (McGeer 1993; van der Linde 1999a). The problem with these walkers is that their operation requires a very specific set of initial conditions and a particularly sloped walking surface. They are also sensitive to perturbation and have poor disturbance rejection.

Under-actuated systems were the next evolution of the passive dynamic walkers in which one or more of many joints were actuated to provide the energy input that was required to maintain stable gait cycles. (Collins et al. 2005; Donelan et al. 2004; Kuo et al. 2005; van der Linde 1999a) The research of passive dynamic walking and human walking has shown that the inherent physical properties of limbs are important to

locomotion and that a level of mechanical control exist that works in concert with active control to achieve natural biological movement. The problem with these passive systems is that the lack of actuation limits their functionality. Their operation is restricted to specific environments, and they require a specific set of initial conditions for their locomotive behavior. They are also not capable of initiating spontaneous movement or responding to perturbation.

The systems described in this section represented opposite ends of the spectrum of robotic control. We have seen the extremes of stiff control (high impedance), which is capable of controlling instable systems like inverted pendulums, and low gain passive control that is used in inherently stable systems. The robotics goal of our research was to take motivation from biology and gain an understanding of the relationship between active control and mechanical stability so that a controller could be developed that bridged the divide between passive dynamics and high gain control and enables robotic devices to move with compliant motion that mimics the dynamic characteristics of biological motion.

1.2 Investigation Approach

Although there are many paths that could be taken to reach our stated objective, we chose a modeling path that was divided into three projects. First, we designed and built model systems that were used to study the interactions of stance width and control of lateral balance. We then characterized the interaction between mechanics and control considering only delayed active feedback control and we developed a gain-adjustment function that facilitates consistent postural performance under stance width variations. Finally we evaluated the mechanics and control interaction in a system with intrinsic properties similar to those inherent in biological systems. A further description of each project is provided below.

Postural Model System

Our first project was to implement an electromechanical model of a standing animal for the analysis of stance stability under perturbation. We created a two-legged robotic device with a frontal plane configuration similar to a cat for the study standing balance. The device is capable of standing in a variety of stance widths and replicating the movements of yielding when subjected to lateral displacement perturbations. The design of the controller was based on established concepts of robotic and biological postural control. Specifically, it is a closed-loop design with feedback for position, velocity, and acceleration. The controller incorporates feedback loops for delayed active and non-delayed passive responses. The active loops have independent control of feedback delay for position, velocity, and acceleration. Each of the legs is capable of an independent response. We also created a numerical model of this system that allowed us to determine the properties of a large number of theoretical gain values and configurations. By using these models to study stance and posture, we had full access to control parameters while incorporating the physics of real world interactions. This work is shown in Chapter 2.

Interactions of Active Control and Stance Width Variations

We quantified the effect of stance width on the dynamics of the postural response with active-delayed feedback control. The standing model uses delayed feedback control to maintain balance. For delayed feedback systems, gains must be properly tuned for the mechanics of the system or its behavior may be unstable. Changing stance width changes the mechanics of the standing model and therefore changes the control gain requirements. We evaluated the system to determine the range of feedback gains that facilitate stable response to perturbation. We then determined how stance variation alters the dynamics of the postural response. Lastly, we formulated a function of stance-dependent gain adjustment that facilitates consistent postural response across different stance widths. These results are shown and discussed Chapter 3.

Effects of Increased Intrinsic Stiffness

We evaluated system responses with additional intrinsic stiffness (with both stiffness and damping components) to determine its effects on the postural stability and the dynamics of the postural response. These results are shown in Chapter 4.

CHAPTER 2

MODEL SYSTEM DESIGN

Investigating the interactions between mechanical stability and postural control requires a biologically relevant model of posture that is capable of a range of postural configurations with varying levels of static stability and dynamic properties. Bipedal upright standing models meet these criteria and allow for variable mechanics and stability with changing stance width. A particular advantage of this model is that it offers biological relevance by emulating humans and animals in both anatomical form and control function.

For our investigation, we designed a bipedal standing model to the size of cat. At this scale results can be compared to a large amount of preexisting biological data, and it is small enough to be operated by a single researcher. We choose the medio-lateral (M/L) model over the anterior/posterior (A/P) model because the (M/L) model enables a wider range of stance variation. Furthermore, the M/L model also has more applicability to human studies because of the proportions of the stance configuration.

In this section we describe the design and construction of our system. We also detail a series of initial tests that validate the biological relevance of the model and demonstrate its research potential.

2.1 System Design

We divided the development of the system into two primary elements; mechanical component design and feedback controller design. The development processes for these elements are detailed in the following sub-sections. The mechanical component design sub-section describes the development of the physical system that generates the desired motions and facilitates the application of the perturbation responses as precisely controlled hip torques. The controller design segment describes the postural controller

that generates the simulated neural responses, and that compensates for any undesired characteristics of the robotic implementation (e.g. friction and transmission losses). Additionally, we developed a motion platform to apply lateral displacement perturbations similar to those used in human and cat experiments (Brown et al. 2001; Henry et al. 1998b; Horak et al. 2005; Macpherson and Fung 1999; Torres-Oviedo et al. 2006).

2.1.1 Mechanical Component Design

We assumed that the motion of a cat subjected to lateral displacement perturbation is primarily limited to the frontal plane. We also assumed that the feet do not move and the leg lengths remain constant throughout the response. These assumptions were verified by evaluating the kinematic data of cats subjected to such perturbations (Torres-Oviedo et al. 2006). Analysis of the cat response shows that CoM displacement in the lateral direction is highly correlated with the perturbation while motion in the A/P direction is uncorrelated (Figure 2.1a,b). Analysis also shows minimal displacement of the feet and consistent leg length throughout the response (Figure 2.1c,d).

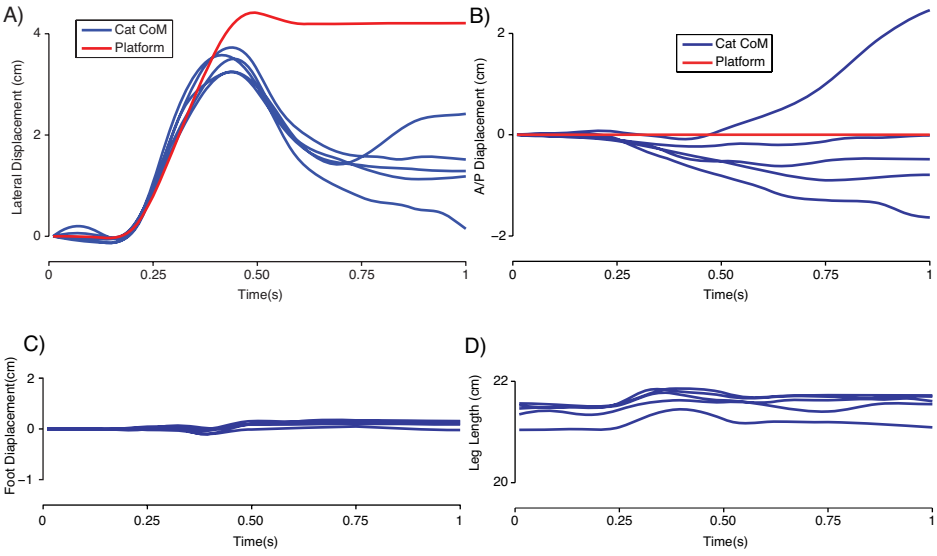

Figure 2.1 Cat postural responses to perturbation. (Data from Torres-Oviedo et al., 2006) Kinematic analysis of the response to lateral displacement perturbation reveals that (A) lateral motion of the cat correlates with the platform movement, (B) A/P motion is uncorrelated with the perturbation, (C) the feet do not move, and (D) legs maintain a consistent length through the perturbation response.

The resulting motions of a cat subjected to a lateral platform displacement perturbation are essentially the equivalent of a four-bar linkage (Figure 2.2a). The active force responses to the perturbation are abduction/adduction torques in the hip and shoulder joints. It has also been observed in the cat that the anterior and posterior parts of the body displace together during lateral perturbation. Therefore, when considering planar movement, the motion of the torso and a single pair of limbs can be used to represent the response of the entire body, making it equivalent to a biped.

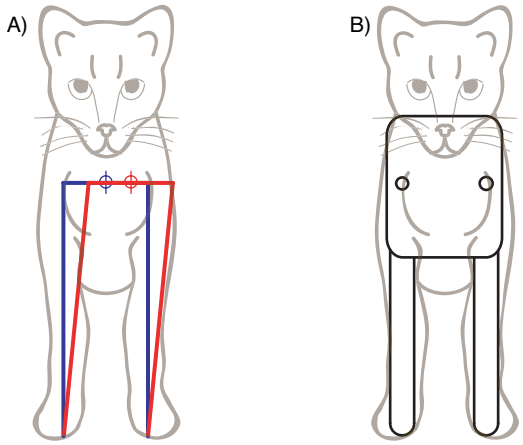

Figure 2.2: Robotic model concept. Our robot, "Floppy", is designed to replicate the motion of a cat subjected to lateral displacement perturbation. A) When the feet do not slip, this motion is essentially that of a four bar linkage (the ground is the fourth link). B) The system has three segments representing rigid torso mass and independently controlled legs.

We built a system that provided the four-bar motion and enabled the variation of stance width between trials (Figure 2.3). The mechanical structure of our device is designed with size and weight characteristics similar to a cat (Figure 2.2b). The distance between hip joints and between the hip joint and the ground are sized to match the pelvis width and leg length. Structural components were designed to minimize mass. However additional brass components were added to give the system a final mass of 2 kg, which represents $\approx 50\%$ of the weight of a young adult cat. To give the robot stability perpendicular to the frontal plane, legs were designed with a depth of 65mm. This depth provides sagittal plane stability and room to house the motors inside of the body resulting

in a robust compact structure. Final model dimensions and inertias of the robot are listed in Table 2.1and illustrated in Figure 2.4.

Table 2.1: Mechanical Properties

Symbol	Quantity	Value
P	Hip width	4.4cm
H	CoM position	1.9cm
θ_P,	Pelvis Angle	0° (initial)
θ_A, θ_C	Stance Angle	0° - 30°(initial)
SW	Stance width	4.4 - 8.9cm
L	Leg length	14 cm
M	Mass	2 kg
I_T	Torso Inertia	2.19e-3 kg m^2
I_L	Leg Inertia	3.38e-4 kg m^2

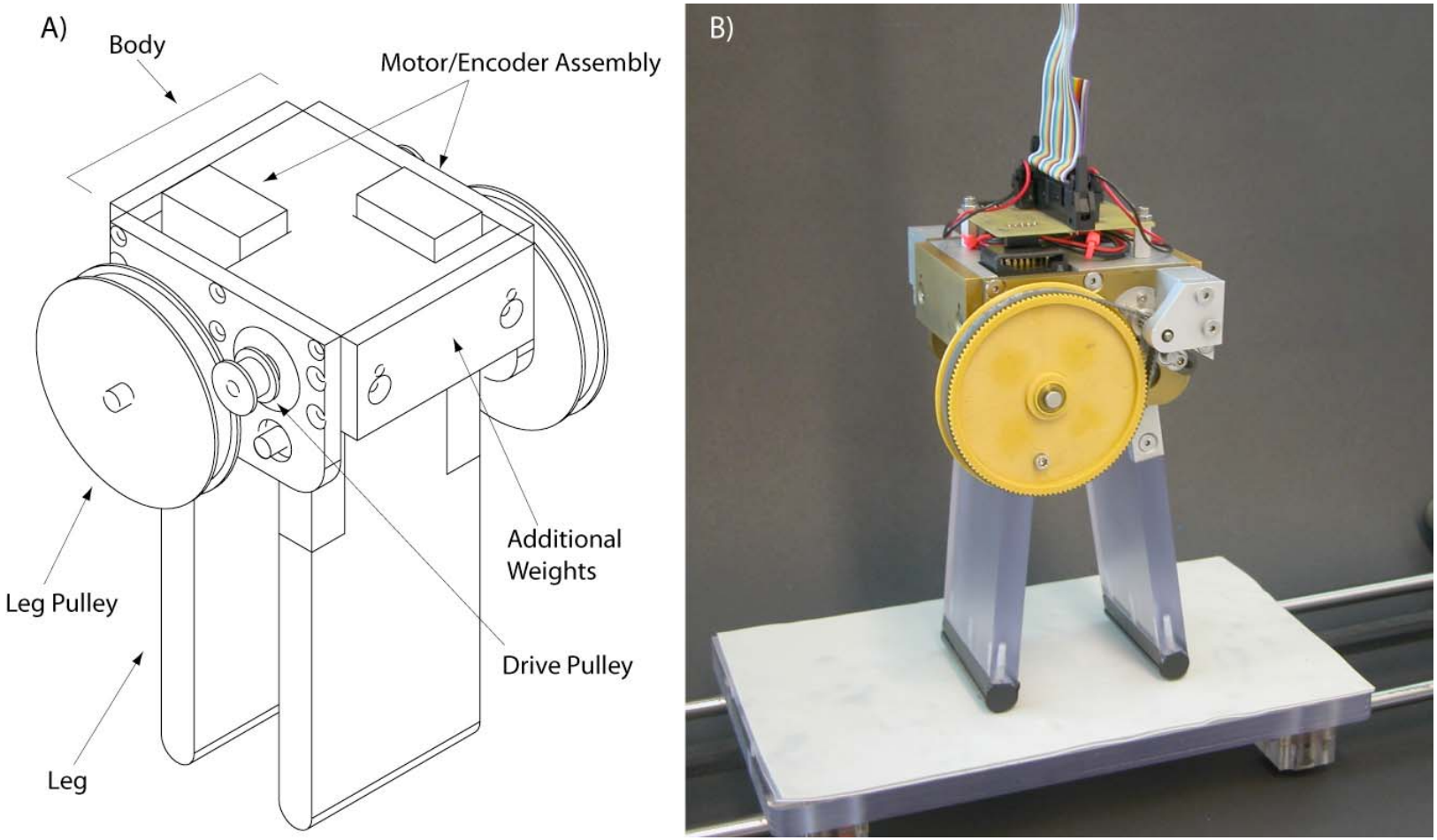

Figure 2.3: Robot Schematic. Each hip joint is driven by a coreless DC motor through a timing belt/pulley system with a 12:1 gear ratio. Position feedback is obtained via rotary encoders coupled to the motors. Additional weights were added to achieve cat dimensions.

Since our robot is designed to replicate biological stance, the feet are not pinned to the surface and the device can actually "step" under perturbation. This quality of function required the design of appropriate feet for ground contact. The ends of the legs were covered with silicone foam (McMaster-Carr 86235K132), to replicate the compliance of a cat footpad. This compliance provides a small amount of shear compliance (>1mm), supports the maintenance of traction, and absorbs the impact of a step, thereby eliminating bounce movements. The surface of the platform was also covered with a 1.6mm layer of silicone rubber (McMaster-Carr 86465K34) to provide a high traction surface.

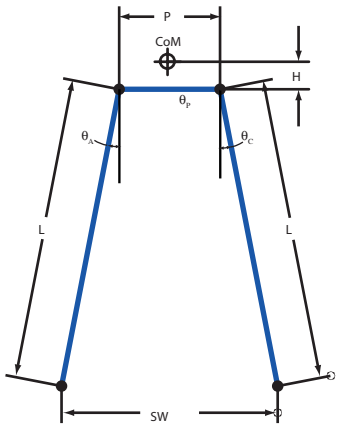

Figure 2.4: Robot dimensions and kinematic variables. The model is a 3-segment system with torque driven at the hips through θ_A and θ_C. Basic parameters of the system are detailed in table 1

The torque requirements for each joint were derived from the performance assumption that the hip motors should be capable of generating sufficient torque to maintain posture during a 1 *g* lateral acceleration in upright stance. This requirement may be excessive and the system will not undergo an acceleration of this magnitude due to limited friction and probable slippage. However, we wanted to ensure the motors ability to exert any commanded torque.

$$\text{Maximum Torque Specification} = 1\text{kg} \times 9.81 \,{}^{\text{m}}\!/_{\text{s}^2} \times .14\,\text{m} = 1.37\,\text{Nm} \qquad (2.1)$$

Each hip joint has one rotational degree of freedom driven by a coreless DC micromotor (Faulhaber 2342-024CR). The legs are driven through a timing belt and pulley (SDP-SI

MXL) with a 12:1 drive ratio. While direct drive of each leg would minimize transmission losses and rotational inertia, the torque requirements for a direct drive would require a larger motor that would not fit within our desired design envelope. Additionally, the 90° working angle of the leg would be destructive to the motor. The transmission system we used adds minimal weight to the robot, provides high transmission efficiency through a one-stage design, and enables the use of the smaller motor that can operate through multiple revolutions. The motor for each leg is controlled by a PWM current driver (Advanced Motion Controls Z6A6DDC). Current drivers are used because motor torque is a function of current and the objective of our controller is to specify the torque applied to each joint. With these drivers, joint torque can be explicitly specified, independent of joint velocity, enabling us to specifically control position and velocity feedback gains.

The mechanical components of "Floppy" were designed to have minimal mechanical losses and minimally impact the dynamics of the system. To compensate for the dynamic loss incurred due to non-optimal components, we designed an active compensation component into the controller that uses positive feedback to reduce the effects of viscous damping in the transmission system. The gain of this term is tuned experimentally to eliminate the damping of the freely swinging leg. By including this term in our controller, we ensure that the dynamic response of the system is the result of the passive dynamics of the mechanical configuration and the controlled active and intrinsic responses. This compensation will be described in detail in the next section.

The robot is electrically interfaced through custom fabricated PC boards and a single suspended ribbon cable. Ribbon cable offers a high degree of flexibility and minimizes the effect of the cable on robot dynamics. This interface cable provides current to the motors and joint position feedback to the controller. Joint position is measured using an optical rotary encoder attached directly to the motor. Working through the drive transmission, the encoders give a final joint resolution of 0.007 radians.

2.1.2 Controller Design

The control of standing posture is described as a feedback process with delayed *active* and non-delayed *intrinsic* components (He et al. 1991; Horak et al. 2005; Kuo 1995). In our robotic implementation of standing balance, the active component of the postural response was designed as a delayed feedback process using the deviation of joint kinematics as control variables (Figure 2.5). Some studies of postural control use Center of Mass (CoM) kinematics as feedback variables. (Lockhart 2005). However, using CoM kinematics provides only one control signal and will not drive two legs independently. Also, in upright standing postural configurations, joint angle displacements are proportional to CoM displacement. Therefore, we use joint kinematics to obtain control signals that are specific to each leg and can drive each leg independently. Joint positions are measured using the optical encoders. Derivatives of these signals are taken and filtered to obtain joint velocities and accelerations. These kinematic variables are then time delayed to replicate neuromuscular transmission and activation delays before being multiplied by feedback gain values and summed to give the active postural response. These feedback gain values are independently modulated to vary the magnitude of the active response.

In animals, the intrinsic component of the postural response is a result of the viscoelastic properties of the musculoskeletal system and these properties can be scaled by muscle activation. In our implementation, this response is a feedback process that also uses the deviation of joint kinematics as control variables. The intrinsic response acts without a time delay and the passive stiffness and damping properties of the muscle are simulated with the position and velocity feedback gains. These gains are co-modulated to simulate the variation of the intrinsic muscle properties that occurs with tonic muscle activation. With this method of modulation, the damping ratio of the intrinsic response is constant and a single variable is used to change the magnitude of the response.

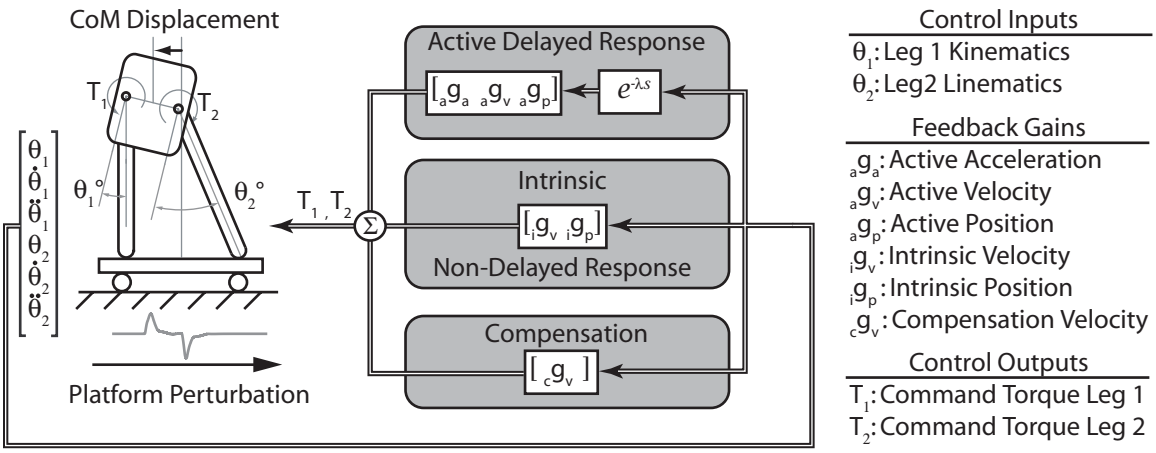

Figure 2.5: Schematic illustration of the control system. To achieve independently variable reflexive and intrinsic responses, we used a parallel model of control. The intrinsic response is controlled by a linear feedback pathway with elastic, viscous, and inertial properties. The active response is controlled by a pathway with a delay in series with elastic, viscous, and inertial elements. A third component (compensation) was added to compensate for the mechanical losses of our drive system.

With the active and intrinsic components acting independently, the postural controller is similar to the parallel cascade model of postural responses (Kearney et al. 1997; Mirbagheri et al. 2000) and other models that describe independent active and intrinsic components of a postural response to perturbation. In our model a third compensation component is added to our controller. As mentioned in section 2.1.1, this component is used to negate the effects of friction and transmission losses of the mechanical structure. It is effectively a positive feedback term that enables the leg to maintain a constant velocity when perturbed. The magnitude of the feedback term is determined experimentally by mounting the robot in a horizontal configuration and applying an impulse perturbation that imparts an initial velocity to each leg. The feedback gain magnitude is adjusted until the leg maintains a constant velocity throughout its range of motion. Inclusion of this term enables the hips to act like frictionless pin joints allowing us to have precise control of the forces in the joints and modulation of all components of the system response to perturbation. Without compensation, the losses of the mechanical system affect system dynamics, stabilizing the system in conditions in which active control and the natural dynamics would produce an unstable response.

Our control model was created in Simulink™ (MathWorks Inc.) and implemented on a dSPACE DS1103 real time processor running at a 5.0kHz sampling rate (dSPACE Inc.). The dSPACE controller provides the computational resources for control independent of the PC's CPU and operating system. The robot is interfaced through a custom MATLAB GUI (Graphical User Interface)that enables the setting of stance and control parameters and records 3.0 s time traces of joint kinematics, command torques, and command output for each component of the control loop

2.1.3 Simulation

In addition to the mechanical system, and to further validate our system and to establish a reference for performance analysis, we created a computational model of our system. The equations of motion for this model were developed in the Autolev™ simulator for engineering analysis and the simulations were run in the C programming environment. The simulations were based on the physical and control parameters of the robot. Mass and inertial properties were taken from robot measurements. Joint torques and gravitational accelerations were described specified variables so that they could be modified to the specific parameters of each trial in the C environment. The model is an idealized system that does not include parasitic losses such as Coulomb friction and non-linear damping.

The output from Autolev™ was a C program that could be used to complete a single trial under one set of control parameters. This core C program is the set of equations of motion that describe our system. A wrapper program was created to run iterations of the simulation with different stance and control parameters. The perturbation was modeled as a horizontal acceleration pulse that was applied perpendicular to gravity. This acceleration was recorded from trial data so that the perturbation to the robot and simulation would be consistent.

2.1.4 Platform

Velocity step perturbations were applied to our system to maintain comparison to animal and human data. In this type of perturbation, the support surface is laterally displaced at a constant velocity for a specified distance. The velocity of the perturbation and displacement magnitude are dependent on the subjects and type of perturbation being studied. A number of perturbation studies use this type of perturbation on humans and cats to ensure a consistent perturbation between trials (Brown et al. 2001; Henry et al. 1998a; b; Macpherson et al. 1987; Maki and Ostrovski 1993). To provide controlled perturbations to our robot we created a single-axis motion platform. The displacement surface is a 25 x 15cm surface covered with a 1.6mm silicon membrane to increase friction between the robot feet and the surface. The surface rides on two linear rails and four Rulon™ coated linear bearings. It is driven by two ESCAP DC micro-motors with a custom PWM motor driver in velocity mode through a 9.7 mm pitch diameter pulley and timing belt. The system is capable of accelerating the robot mass at 600 cm/s^2 with a peak velocity of more than 100 cm/s and maximum platform displacement magnitude of 32 cm. Platform control is implemented as an independent component of the Simulink™ model. Platform control is not directly tied to the control of the robot except for the shared resources. The platform is operated under high gain PID feedback control. Platform control was configured to apply step velocity perturbations to the robot, with an uncontrolled acceleration profile. Alternatively we considered using a constant acceleration step as the perturbation, however the acceleration of this trace did not match the recorded data from the reference cat experiments. Velocity step perturbations were used to maintain similarity to the perturbations in animal and human experiments.

2.2 System Tuning and Calibration

We created a system that is composed of multiple numerically controlled electro-mechanical elements. Although we calculate conversion factors that convert our

numerical values to physical forces, we still need to determine the range and magnitude of gains that bring the system into the range of stable behavior. This section describes our methods for deriving appropriate gains for compensation. We determine the minimum value and step size of feedback gains that significantly affect the dynamics of the robot. Lastly, we compare the postural response of the robot to the simulation results to confirm accurate modeling and gain selection.

2.2.1 Gain Tuning

A functional range of gain magnitudes and step intervals was established by performing several series of perturbation simulations in which independent feedback gains were increased until a significant difference in CoM trajectory was obtained (Figure 2.6). We performed independent simulations for acceleration, velocity, and position feedback gains. For each series of trials, we eliminated all other control elements by setting their values to zero so that the only influence on the system would be the tested parameter. Kinematic responses for each gain step were compared to the uncontrolled response. We determined the minimum effective gain and step interval to be the one that produced a noticeably different kinematic response compared to the uncontrolled response.

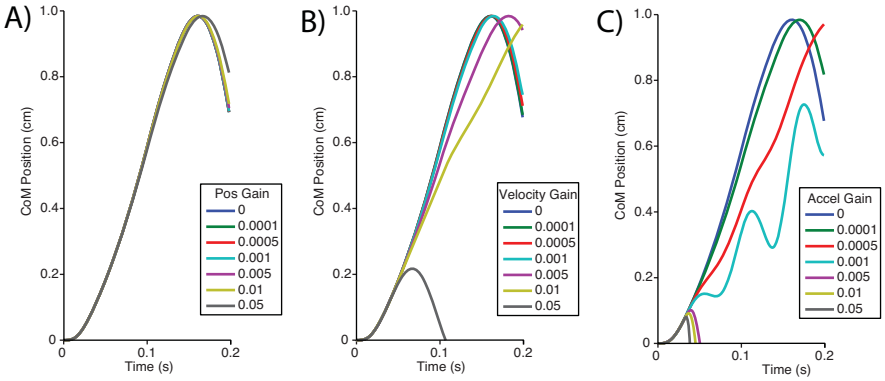

Figure 2.6: Functional gain increments. Functional gain increments were established by simulating free standing perturbations to the system while incrementing a series independent gains steps for a) position, b) velocity and c) acceleration feedback. Gain increments were determined by the magnitude that produced a significant difference from the uncontrolled trajectory.

Based on the result of these tests, the minimum effective gains and gain intervals were established as 0.01Nm/rad, 0.001Nms/rad, and 0.0001Nms^2/rad for G_P, G_V, and G_A respectively.

2.2.2 Compensation Tuning

We designed the compensation component of the controller to counteract the undesired mechanical losses in our physical implementation of a robot. Primarily, these losses arise from the belt (Figure 2.3), and they can be described as coulomb friction and viscous damping. Coulomb friction cannot be easily negated, but adding a positive velocity feedback term can negate the viscous damping. Thus, we added a negative damping term to reduce the effects of mechanical losses caused by the transmission system of each leg. To determine the magnitude of this term, we performed controlled impulse perturbations to impart an initial velocity the legs of the robot with all other feedback terms set to zero. For this tuning process the robot was mounted on a stand that held the body and allowed the swing horizontally to avoid the influence of gravity on swing dynamics. Each leg was stimulated with a torque impulse that imparted an initial velocity of 10 rad/s without any residual active torque. The legs were allowed to swing freely so that the effects of inherent damping could be observed. With viscous and damping losses, the velocity of the leg steadily decreases and comes to a stop. Perturbations were then repeated while incrementally increasing the positive feedback compensation term until the velocity of the perturbed leg remained constant through its range of motion (Figure 2.7). Once a gain value was reached that provided near constant velocity in both directions without any further velocity increase, that value was set as the compensation term. In the final tuning, compensation had a negative damping coefficient of 0.004 Nms/rad.

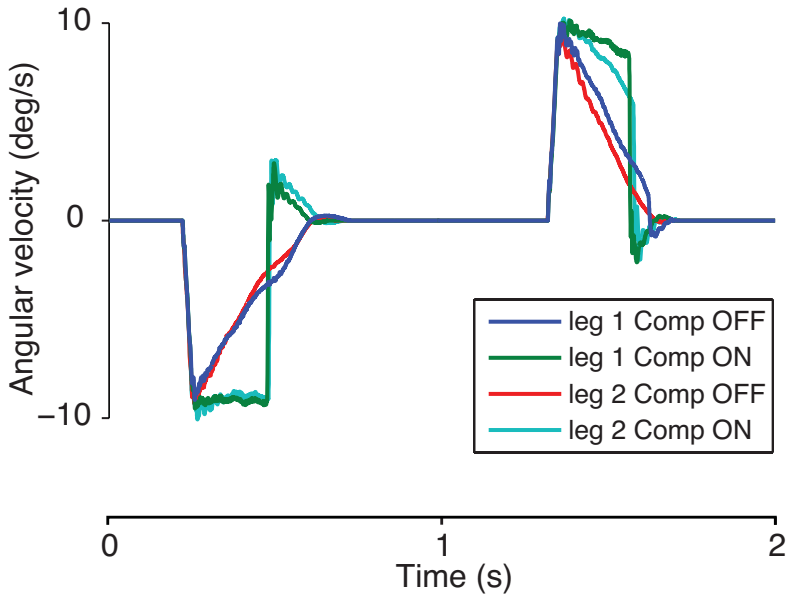

Figure 2.7: Bi-directional compensation effects. The perturbed unloaded leg has an inherent tendency for a rapidly declining angular velocity due to parasitic losses. Compensation adds negative damping to counteract these losses in the mechanical system so that leg velocity is maintained. The figure shows leg velocity with and without compensation following the application of a torque pulse that imparts an initial velocity of 10cm/s. Compensation had a final value of 0.004 Nms/rad and resulted in a near constant velocity for both legs in both directions.

2.2.3 Simulation/Robot Comparison

Postural performance of the robot was evaluated by comparing a series of perturbation responses to simulation results. The purpose of the evaluation was to validate proper function and establish the dynamic effects of compensation through comparison of postural responses. Postural perturbations were applied to the robot under a series of gains representing “low, “medium”, and “high” levels of feedback. These gains produce simulation responses that are described as unstable “falling over”, stable “under-damped”, and unstable “increasingly oscillatory” responses respectively. This gain series was applied to the robot with compensation active and inactive. CoM trajectories for the robot and simulation responses were then evaluated and compared.

Results show that parasitic losses add some stability to the system when parameters are set near the edge of stability and compensation has the effect of removing that added extra stability (Figure 2.8). With high gains and no compensation, the robot

exhibits stable responses. In contrast, simulation and robot responses with high gain and compensation are unstable with increasing oscillations. When the low gain values are used, all responses are unstable and the systems fall over. However, the simulated CoM trajectory falls between the compensated and uncompensated robot and the dynamics characteristics of the response more closely resembles the compensated response. With mid level gains, the compensated and uncompensated responses closely resemble each other and are slightly more damped than the simulation response. This difference is expected and is characteristic of the difference between systems with different levels of friction losses. Overall, compensation does not greatly alter the dynamic responses of our system.

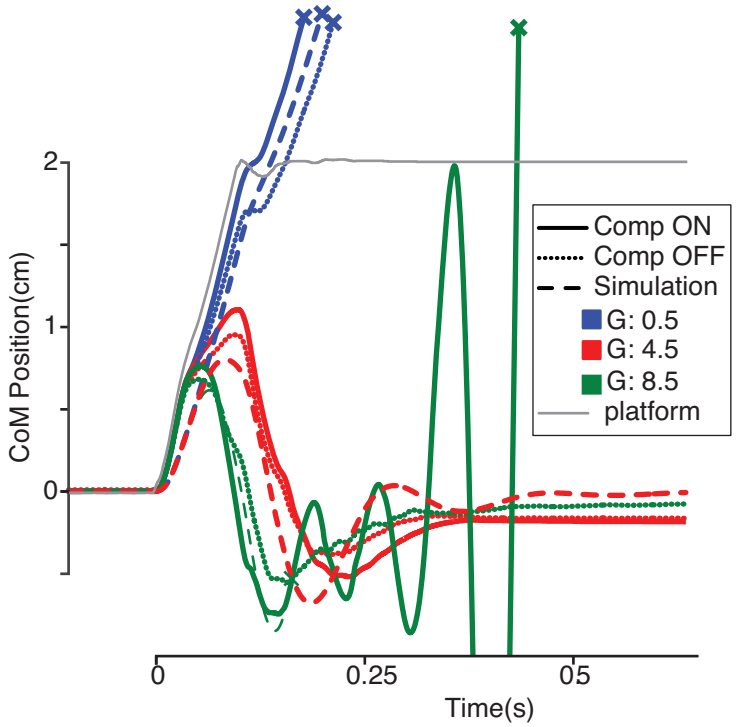

Figure 2.8: Simulation/robot comparison. Comparing the robot responses to simulation results shows that the responses are very similar. The robot has inherent losses due to friction and viscosity in the drive path. To compensate for these losses we apply a first order positive velocity feedback to approximate the measured loss. When this compensation is applied, the response approximates the unstable response of the simulation. The remaining difference is due to friction.

Simulation results were found to be in correlation with the robot data with only a small degree of variation. The slight variation between the systems was consistent with the results of un-modeled parasitic mechanical losses in the robot system. The addition of compensation in the robot system reduced the effects of parasitic losses, causing the robot responses to more closely resemble the simulation responses.

2.3 System Validation

After assessment of the initial working parameters and their subsequent tuning, we tested robot *Floppy* to validate its research function. We performed a series of tests to determine a functional range of feedback gains and demonstrate that it could mimic the kinematic response of a cat subjected to postural perturbation. We also performed a series of tests to verify that the system's response is critically dependent on both feedback gains and stance configuration.

2.3.1 Procedures

We computed a functional range of feedback gains using a simulation of a four-bar mechanism. The results of these simulations were used to guide the gain variations in the other experiments. Initial functional gain values were estimated by calculating the approximate stiffness required in a narrow stance configuration to return the robot to an upright posture from a 4cm displacement. We also calculated a corresponding damping value that would make the system critically damped. The lower limit of functional gain values was established by performing controlled perturbations to the system while independently increasing feedback gain values until the kinematic response deviated from the uncontrolled response. These values were then used to establish the step size for exploring position and velocity feedback gains.

We used kinematic data from cat perturbation trials to tune the feedback gains of the robot to match the response of the cat. The kinematic data was from lateral

perturbation trials of cats (Macpherson 1994; 1988). We configured the robot to the nominal stance configuration in experimental conditions and applied a step velocity perturbation. We ran repeated perturbations while varying the feedback gains until the kinematic response of the robot resembled the kinematic response of the cat.

We tested the effects of changing stance width and feedback gain parameters by applying lateral step-velocity perturbations to the standing robot while independently varying stance width and feedback gains. Each series of trials compared the response of the system to a reference response. The perturbation used in these trials had a magnitude and duration of 20cm/s for 100ms This perturbation is faster than the one used to replicate the cat response, but equivalent to perturbations used on other cat trials (Macpherson 1994). This increased magnitude perturbation was used because the perturbation needed to be challenging enough to be able to make the system fall if a response was inappropriate.

2.3.2 Analysis

The overall dynamic response of the system is described by the CoM kinematics, which are dependent on both feedback gains and stance width. We characterized this response by performing a second order linear regression of CoM kinematics to obtain an effective stiffness (K_{eff}) and damping (B_{eff}). When perturbed, a stable postural system responds as a damped spring mass system. The dynamic behavior of generalized spring mass damper systems can be characterized by linear stiffness and damping coefficients. These measures quantify the response behavior, identifying systems with similar responses and specifying behavioral changes. Systems with similar effective stiffness values will have similar response characteristics as indicated by their oscillating frequency (damped natural frequency). Systems with higher effective stiffness values will have higher oscillating frequencies and ones with lower stiffness will have lower frequencies. Effective damping will indicate the rate of decay in the perturbation response. Regression was performed on CoM kinematics for each combination of stance and control

parameters to determine the effective stiffness and damping coefficients. In addition to these coefficients, we also measured the initial perturbed excursion amplitude. This measure is quantified as the peak initial displacement of the CoM following the onset of platform displacement.

As we stated previously, the overall response of the system is described by the CoM kinematics. However, the directly measured variables of the system are the independent leg angles. Since the system has the structure of a four bar linkage, geometric equations were used to calculate CoM kinematics from the independent leg angles (Eq. 2).

$$\begin{aligned} \Delta x &= P + L\sin(\theta_A) + L\sin(\theta_C) \\ \Delta y &= L\cos(\theta_A) - L\cos(\theta_C) \\ SW &= \sqrt{\Delta x^2 + \Delta y^2} \\ CoM_T &= P\cos(\theta_B) + L\sin(\theta_A - \theta_B) - \frac{SW}{2} - H\sin(\theta_B) \end{aligned} \quad \textbf{(2)}$$

2.4 Results

After calibrating the compensation component of our controller, we showed that our robot is capable of mimicking the kinematic response of a cat subjected to lateral displacement perturbation. We also showed that changes in either stance width or feedback gains can significantly modify the postural response.

2.4.1 Mimicking the Cat Response

Using data from lateral perturbations of a cat in preferred stance, we were able to mimic the cat response using combinations of active and intrinsic gains (Figure 2.9). The stance angle of the robot was set to 3° to match the cat stance, and the appropriate feedback gains for mimicking the cat response ranged from 0.4 to 0.6 Nm/rad and 0.04 to 0.06 Nms/rad for the position and velocity feedback gains respectively. The corresponding intrinsic gain had a magnitude of 0.05 Nm/rad and 0.005 Nms/rad for the position and velocity feedback respectively. The kinematic response of the robot qualitatively

resembled the duration and waveform characteristics of the cat response. However the magnitude of the robot displacement was less than that of the cat. This difference can be attributed to the fact that the legs of this particular cat were longer than those of the robot. The responses for both systems were over-damped displacements that did not return to the original position.

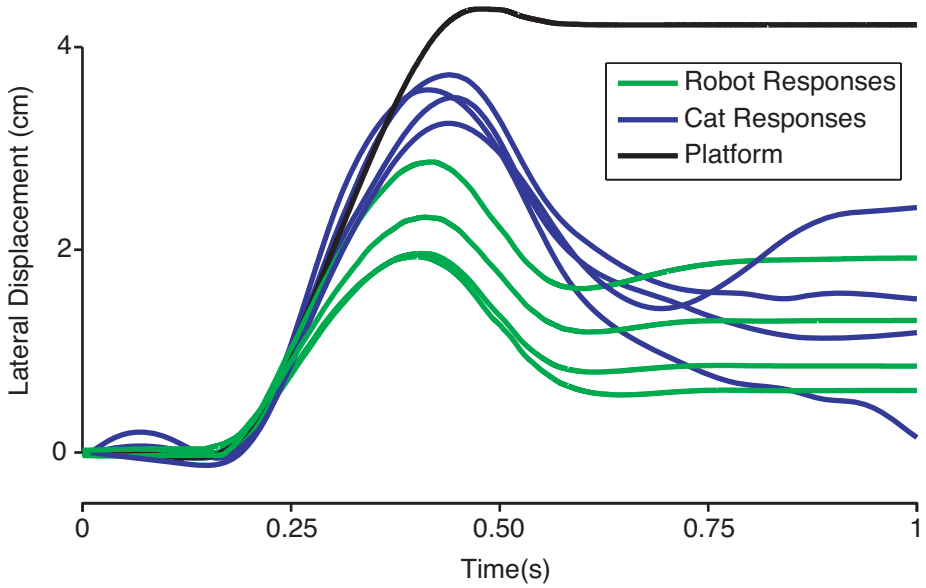

Figure 2.9: Cat/robot response comparison. When configured in an approximation of preferred cat stance, robot feedback gain can be tuned to mimic the cat response to lateral perturbation. The magnitude difference between the cat and the robot is an matter of scaling. The cat used in the experiments was slightly larger than the robot. It is important to note that the dynamic qualities of the responses for the cat and the robot are similar.

As we vary stance width and feedback gain, the responses of the robot can generally be described by one of four response types: insufficient unstable, stable damped, stable damped oscillation, and unstable oscillation response (Figure 2.10). Each of these response types were achieved by independent variation of either stance width or feedback gains. The insufficient unstable response occurs when the feedback gains are not of sufficient magnitude to compensate for the perturbation in the current mechanical configuration. The stable damped response is the most ideal response. It is described by gains that are appropriately matched to the mechanical configuration to enable a quick

recovery from the perturbation and its motion is either critically damped or over-damped. The stable oscillatory response also generates a sufficient response to recover from the perturbation, but it is described as under-damped with a short period of oscillation. The behavior of the excessive unstable responses is consistent with the behavior of a negatively damped (positive velocity feedback) system response with increasing oscillations.

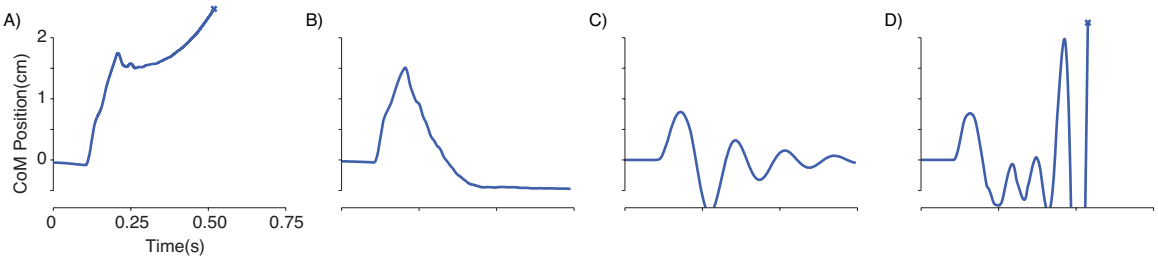

Figure 2.10: Typical response types. (A) Insufficient feedback gain results in an unstable response in which insufficient torque is generated and the robot falls over. When feedback gains are appropriate for the current stance width, the system exhibits a stable response that recovers from the perturbation. (B) The stable response can be critically damped or over damped. (C) The stable response can also be under-damped resulting in decreasing oscillations. (D) Excessive gain results in an unstable response that oscillates with increasing amplitude until the leg limits are reached, the system jumps off of the table, and the trial is stopped

We chose a set of parameters as a reference for examining the effects of independent parameter variations. This set represents the “middle of all parameters” and it enables the increase and decrease of each of the independent control parameters. This parameter set is referred to as the canonical parameters. The specific values of the canonical parameters are listed in Table 2.2. By independently varying the gains across their functional range we can measure their effect on overall system behavior. The kinematic response of the canonical set is shown as the thick red center trace in each of the trial series shown in Figures 2.11-2.15.

Table 2.2 Canonical Parameters

Variable	Value
Stance Angle	15°
Velocity Feedback Gain	0.045 Nms/rad
Position Feedback Gain	0.450 Nm/rad
Feedback Delay	30ms

2.4.2 Effects of Stance Width Variation

We examined the effects of varying stance width while keeping feedback gains constant. Qualitatively, increasing stance width results in a stiffer, more oscillatory system (Figure 2.11). Peak excursion decreases linearly with increased stance giving the appearance of a sturdier, more resistant system with increased stance (Figure 2.11c). However, oscillations increase with increased stance indicating an increasing instability. Decreasing stance width results in increased peak excursion and a smoother, more damped kinematic response. These changes were quantified by evaluation of the K_{eff} and B_{eff}. Increasing stance width from the canonical stance increases K_{eff} and decreases B_{eff}. Mechanically, this means that the system will have a higher oscillating frequency and slower decay rate (reduced damping ratio). In contrast, decreasing stance width from the canonical stance results in decreased K_{eff} and B_{eff}, resulting in a maximum B_{eff} at 15°. Also, at a narrow stance of 3°, the magnitude of the active postural response is not sufficient to compensate for the magnitude of the perturbation and the robot falls as a result of perturbation.

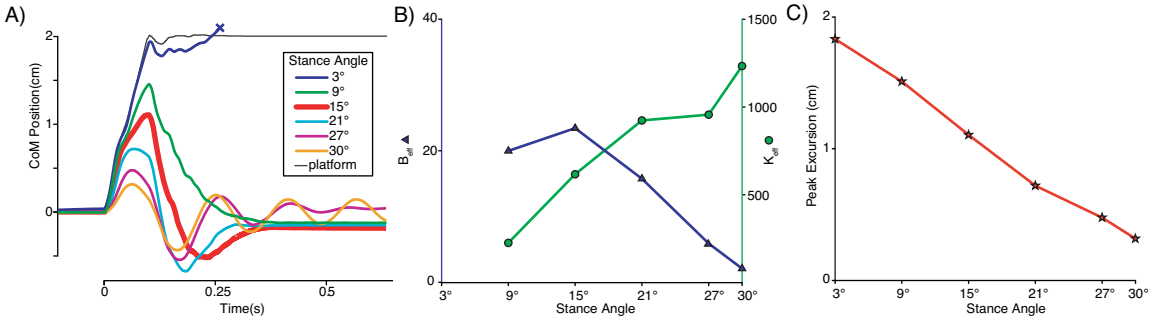

Figure 2.11: Varied stance responses. (A) With increased stance and identical control, the system exhibits an increasingly oscillatory response to perturbation. (B) Effective stiffness increases with stance while effective damping decreases. (C) Increased stance also increases the systems resistance to perturbation, decreasing the magnitude of initial excursion during displacement

2.4.3 Effects of Feedback Gain Variation

The effects of changing control gains were first examined by varying the feedback gains as a single parameter ($G_{collective}$). The gains were co-varied to determine the effects of a generalized increase in control. The corresponding position and velocity feedback gains maintained a constant 10:1 ratio. For simplicity, we internally scaled these gain values so that the range of effective velocity (G_v) and position (G_p) feedback gains would have the same order of magnitude. The resulting gains relate to controller values in the following manner:

$$g_v = G_v \times 0.01 \text{ Nms/rad} \text{ and } g_p = G_p \times 0.1 \text{ NM/rad} \quad (3)$$

For the collective gain variation:

$$G_v = G_p = G_{collective} \quad (4)$$

As we increase collective gain $G_{collective}$, we first notice a decrease in initial displacement amplitude, while the characteristics of the remainder of the response remain relatively unchanged (Figure 2.12). As gains are increased further we notice only a slight increase in the speed of the response. Generally, the responses become slightly faster with increased gain until $G_{collective}$ reaches a value of 8.5, where the response suddenly becomes unstable with excessive oscillations. As gains are decreased below the canonical values, the peak displacement grows and the response becomes weaker and eventually insufficient to recover from the perturbation. Interestingly, with $G_{collective}$= 2.5, the system recovers from the perturbation, but with a steady state error of 1cm. Quantification of effective stiffness and damping show that K_{eff} slowly increases with increased $G_{collective}$, while B_{eff} peaks at the canonical gain of $G_{collective}$ = 4.5 and decreases with deviations from that gain level. Peak initial displacement decreases with increased gain, but reaches a minimum displacement of 0.8cm at $G_{collective}$ = 7.0. At the gain of $G_{collective}$ = 8.5, the system becomes unstable with increasing oscillations and K_{eff} and B_{eff} are not measured.

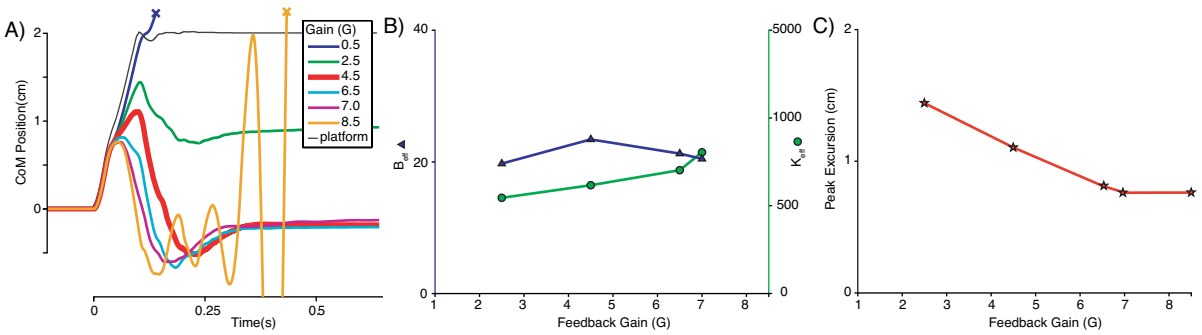

Figure 2.12: Uniform gain variation responses. (A) Uniform increases in feedback gain tighten the postural response, (C) reducing the amplitude of the initial excursion but maintaining the slightly underdamped dynamic characteristics of the response. (B) This maintenance of dynamic characteristics is indicated by the relatively constant nature of the effective stiffness and damping values.

In addition to varying $G_{collective}$, we also demonstrate the effects of independently varying the velocity (G_v) and position (G_p) feedback terms. Results showed that the system is differentially affected by changes in velocity feedback gain vs. position feedback gain. Independent variation of the velocity feedback gain, G_v, results in strangely non-linear behavior (Figure 2.13). As G_v is increased above the canonical value, the system begins to oscillate. However, this oscillation begins with a steady state displacement from the center position that decreases with time. As G_v is further increased the response becomes unstable with increasing oscillation. Decreasing G_v results in slower responses with increasing peak displacement amplitude. At the lowest gain of G_v =0.5, the response is sufficient to recover from the initial displacement, however, in its return, it overshoots the center and falls over. Quantitative evaluation of the response shows that both K_{eff} and B_{eff} increase with increased G_v, but K_{eff} increases at a much faster rate than B_{eff}. Mechanically, such a disproportionate increase results in an increasingly oscillatory system with increasing oscillation frequency.

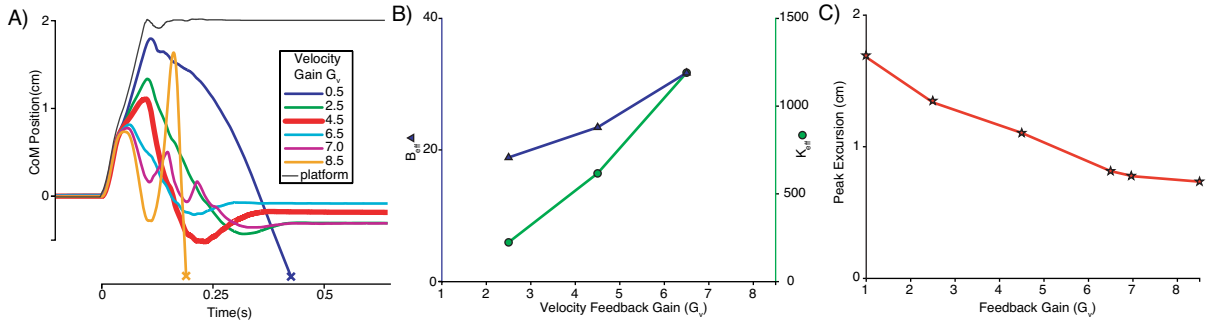

Figure 2.13: Varied velocity feedback responses. (A) Independent increases in velocity feedback gain results in an increasingly oscillatory response, quantified by (B) a large increase in effective stiffness and marginal increase in effective damping. (C) Increasing velocity feedback gain also results in reduced peak excursion, indicating increased resistance to perturbation.

Variation in G_p while holding G_v constant resulted in a single step reduction in peak displacement (Figure 2.14). Peak displacement was 1.1cm for the canonical G_p and the displacement increased with lower gain. For G_p greater than the canonical value, displacement was approximately 0.9cm. In contrast to the effects in increasing G_v, effective damping and stiffness both decreased with increased G_p, although this decrease reached a minimum plateau at G_p = 7 and above. Overall, increasing position feedback reduces the effective stiffness and damping resulting in increasing magnitudes of damped oscillation. At very low levels of position feedback, the system does not recover from the perturbation. Peak displacement is also minimally affected by position gain variation.

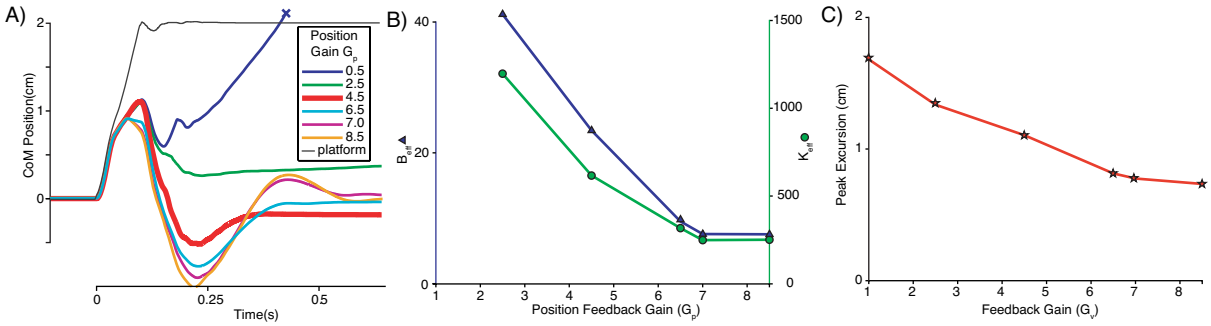

Figure 2.14: Varied position feedback responses. (C) In contrast to velocity feedback gain, position feedback has limited effect on the initial excursion magnitude as shown by the small step decrease that occurs at G_p>4.5. (B) However, increased G_p has significant effect on the dynamics of the later response, scaling both the effective stiffness and damping. (A) This scaling makes the system less stiff and more under-damped.

2.4.4 Effects of Feedback Delay Change

The apparent changes in postural performance that occurred with variations in feedback delay were fairly consistent (Figure 2.15). With no feedback delay, the system exhibits a stable over-damped response. As feedback delay increases, peak initial displacement increases and the system becomes less damped with increasing overshoot in the response. With a feedback delay of 45ms, response overshoot magnitude was approximately equal to the peak initial displacement. With a feedback delay of 60ms, the system has the highest measured peak initial displacement magnitude, but still exhibits sufficient response to return the system to the toward the center following the initial displacement. However, this return has a high velocity and results in an unstable overshoot. Quantitative evaluation shows that both K_{eff} and B_{eff} decrease slowly between 0 and 30ms delay. With a 45ms delay B_{eff} drops by 70% while K_{eff} drops by only 42%. Peak initial displacement shows a steady increase with increasing delay.

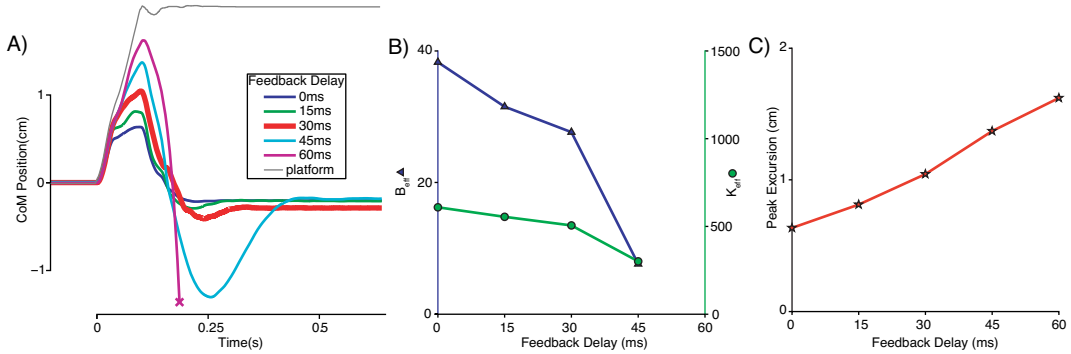

Figure 2.15: Varied feedback delay responses. Feedback delay has destabilizing effect on the dynamics of the system. As delay increases, perturbations have an increasing effect on the system causing greater displacement of the CoM. Delay also causes the response to increasingly overshoot the center, increasing oscillation and decreasing the effective stiffness and damping.

2.5 Summary and Discussion

The bipedal upright standing system was developed to demonstrate and evaluate the coordinated relationship between the mechanics of postural orientation and delayed feedback control. We have verified that our system is capable of generating postural responses that closely resemble the responses of a cat and that the dynamics of the response are dependent on the coordination of standing posture and feedback gain. The response of the system can be made unstable by independent variation of either factor and stability under stance width variation requires a coordinated variation of feedback gain. By demonstrating its ability to produce a wide range of stable and unstable responses, this system shows the relevance of further study to quantify a relationship between posture and control.

Modulation of control gain or stance width can invoke similar alterations of the dynamic response (Figure 2.16). For example increasing stance width while holding feedback gain constant has the effect of increasing the stiffness of the system while decreasing the peak initial displacement amplitude. Similarly, independently increasing feedback gain also increases the stiffness of the system but has a limited effect on peak displacement amplitude. The commonality of these effects on effective stiffness suggest that the dynamics of the postural response are linked to both parameters and that performance characteristics can be maintained through coordinated alteration of both parameters. This linked effect emphasizes the association of the two factors and the importance of coordinated co-modulation of stance width and feedback gain.

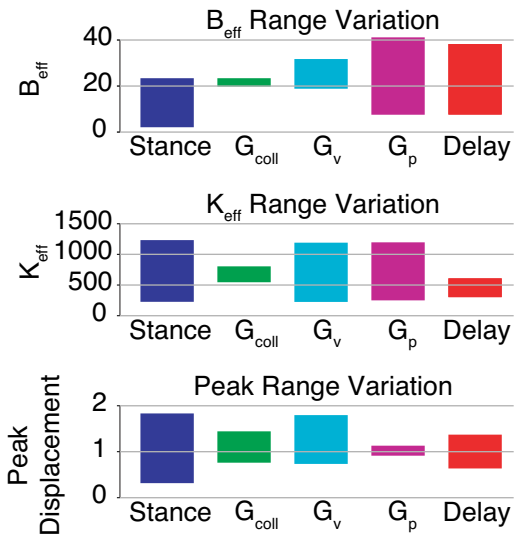

Figure 2.16: Range of performance variation by control parameter. Variations of each of the control parameters and stance width have different effects on the quality of the postural response. The range of each performance characteristic resulting from parameter variation is shown for each variable. Stance width variations have a significant effect on each of the characteristics, while collective gain variation has little effect on B_{eff} and considerable effect on peak displacement. Independent variation of the feedback gains results in greater variation of performance than the collective gain. Delay also has a significant effect on the system response, affecting all three measurement parameters.

This system enables the explicit modulation of mechanics and control, and this separation of factors may provide insight into the results of previous studies that could not isolate the differential effects of mechanics and control in biological systems. For example, our results support the experimental findings that observed decreased muscle response activation and consistent CoM displacement with increased stance during lateral displacement perturbations (Henry et al. 2001). The researchers attributed the decreased response to an increase in passive stiffness of the musculoskeletal system. However, they could not attribute the increased stiffness to changes in the passive properties of the muscles or postural configuration. With our system, we have demonstrated that increasing stance width with constant feedback gain results in increased active response and decreased CoM displacement. Also, decreasing feedback gains with consistent stance width has limited effect on peak displacement but significantly reduces the magnitude of the active response. Combining these two effects results in decreased activation with

consistent CoM displacement and could explain the previous observations of Henry et al. without an increase in passive properties of the muscles (Henry et al. 2001).

Our results also support the findings of studies that show velocity feedback to be most important in postural responses (Jeka et al. 2004). We found that the individual components of feedback have different effects on the kinematic response of the system. Velocity feedback has its highest relative effect on the magnitude of the initial displacement, whereas position feedback has little effect on the initial displacement but does determine how closely the system settles back to the original position. If one considers CoM displacement magnitude to be most important, then these results support the conclusion that velocity feedback is most important in a postural response.

We acknowledge that directly relating these results to the physiology of animals must be done with caution. There are a number of differences that distinguish this system from physiological systems. These differences have been detailed in Section 1.1.4. Furthermore certain modeling assumptions were made in the design of this system including the use of gain magnitudes based on metric variables and the use of lumped torso mass. Since our system uses gains based on engineering terms, the gain magnitudes of the device will not correlate with physiological gains. However, our studies and physiological studies primarily examine the scaling of gains with physical parameters and responses. Therefore, gain changes of this robotic system may parallel gains changes in physiological systems. Also, this system has a single rigid body mass as a torso and hip. This configuration contrasts with the human torso, which can flex and arc laterally. However, the rigid configuration is commonly used in models of lateral standing posture (Full and Koditschek 1999; Henry et al. 1998b; Horak et al. 2005; Winter et al. 2003; Winter et al. 1996), while few others have used a flexible spine model (Rietdyk et al. 1999).

Even with these noted differences, this robotic system has a distinct ability to address questions about biological control of posture and the interaction of control and

mechanical stability. We demonstrated that the mechanical stability, neural feedback control, and the interaction between these factors contribute to overall postural stability in our biomimetic model of standing posture. The analyses afforded by our device will allow us to more precisely quantify these important interactions. Ultimately, the knowledge gained in further studies will prove itself to be important as we make advances in rehabilitation, neural prosthetic design, and robotics.

CHAPTER 3

ACTIVE CONTROL WITH STANCE WIDTH VARIATIONS

One of our primary goals was to determine how stance width and active feedback control variations are coordinated when altering the postural dynamics of the system. We therefore analyzed the system to quantify the effects of stance variations. From this analysis we determined the gains that were required to maintain postural performance under varying stance widths. Our analysis methods for quantifying the effects of stance variations followed a four step process in which we:

- Quantified the dynamic response changes that result from stance variation,
- Analyzed and quantified the changing mechanics and structure of stance variation,
- Identified a link between stance changes and feedback control requirements,
- Developed and tested functions of feedback gain adjustments that facilitate consistent postural performance under varying stance widths.

3.1 Dynamic Effects of Stance Width Variations

The dynamic response of the system is a function of both stance width and feedback gains. In order to quantify the response changes that result from stance variations, we evaluated multiple responses for the full range of stances and feedback gains. Since our initial analysis revealed that overall stability is dependent on the combination of stance and feedback gain parameters, we first identified the region in parameter space that result in stable responses. After establishing the range of stable parameters, we evaluated the dynamic responses and quantified stance change dependent performance variation.

3.1.1 Identification of Stabilizing Gain Regions

We identified stabilizing parameter combinations (stance and active feedback gain) by subjecting the system to postural perturbations while measuring the postural response. The evaluated stances ranged from 0 to 30° stance angle (θ_s) with 3° increments. Velocity and position feedback gain values were evaluated for the ranges of 0 to 0.1 Nms/° and 0 to 1.0 Nm/° respectively. Throughout this analysis we use dimensionless scaled magnitudes of these gain values. Velocity feedback was scaled by 1000 rad/Nms so a gain of 0.035 Nms/rad is described as $G_v = 3.5$. Position gain is scaled by 100 rad/Nm, so a gain of 0.45 Nm/rad is described as $G_p = 4.5$.

For both the robot and the simulation, we determined the stability of each parameter combination (θ_s, G_v, and G_p) by observing and quantifying the post-perturbation displacement of the CoM (X_{CoM}). For the simulation responses, we defined a response to be stable if $|X_{CoM}| < 0.5\,\text{cm}$ for $t_{pert} > 1.5\,\text{s}$. Due to friction, the robotic system sometimes came to rest while standing with a substantial displacement, $|X_{CoM}| >> 0.0\,\text{cm}$. Because of this potential resting displacement, we qualified a robot trial as stable if the robot maintained a standing posture following perturbation and response.

We performed parameter sweeps to identify stable gain parameter combinations for each stance. For each stance, the stable gain combinations formed a region in the two-dimensional parameter space. An example of a stability map is shown in Figure 3.1. Together, the ensemble of these two-dimensional stable gain-regions constitute the stability map for the entire parameter space.

While performing each parameter sweep, we observed that the systems (simulation and robot) exhibited two modes of instability. When the gains were too low, the systems (simulation and robot) did not return to an upright stance following the initial displacement from the perturbation. Instead, the systems continued to fall in the initial displacement direction. When the gains were too high, both systems exhibited behaviors

with unstable oscillations following a perturbation. In the simulations, high gain unstable responses were oscillatory with increasing amplitude. During unstable trials, the robot oscillated and fell.

Our initial data showed that the upper of the stable gain regions for each stance were significantly higher for the simulation than they were for the robot trials. This discrepancy arose because the robot was standing unconstrained on the perturbation platform and the simulation was virtually "pinned" to the ground. Virtual pinning enabled unrealistic vertical forces to be exerted at the foot/ground interface. To correct this error in stability classification, simulations resulting in lifting force were considered unstable (Figure 3.1). After reevaluating the simulation results, the upper bound in the stability maps for simulation and robot trials corresponded (Figure 3.2).

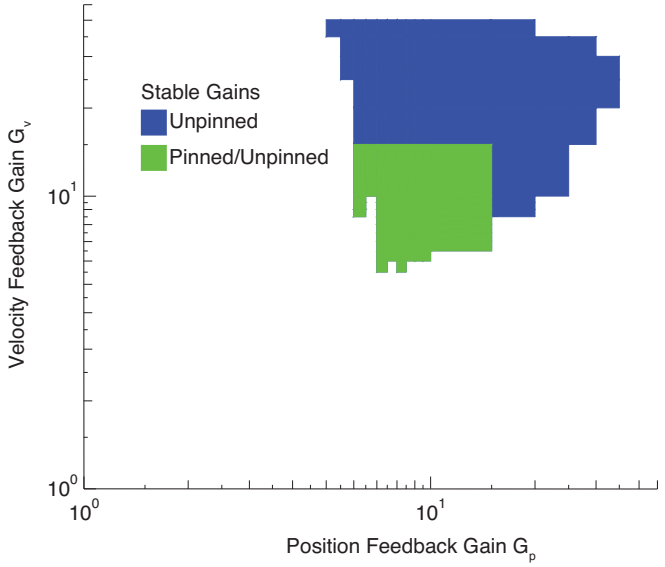

Figure 3.1: Sample Simulation Stable Gain Region with and without Pinning. When the constraints of the simulation are not considered, the system appears to have a large stability region as indicated by the combination of the blue and yellow regions. When pinning of the simulation is taken into consideration and responses are considered unstable if the leg exerts a lifting force, the stable gain region is reduced. No gain combinations produce stable responses when pinned and unstable responses without pinning.

The lower bounds for the simulation and robot trials also displayed some differences. As compared to the simulation, the robot remained stable when using lower magnitudes of velocity feedback than the simulation. This discrepancy was due to the

influence of friction in the system. Although compensation (as described in Section 2.2.2) was successful in reducing the effects of mechanical losses, it did not completely eliminate the effects of friction. The discrepancy was evident at low values of velocity feedback. We concluded that in these low-gain conditions, the simulation oscillated because the damping did not remove sufficient energy from the system; in contrast, the robotic system was stable due to friction losses. Friction stabilized the robot by removing kinetic energy that was not being removed by velocity feedback. This difference explains the discrepancy between the stable velocity feedback gains and the similarity of the position feedback gains at the lower bounds of stability.

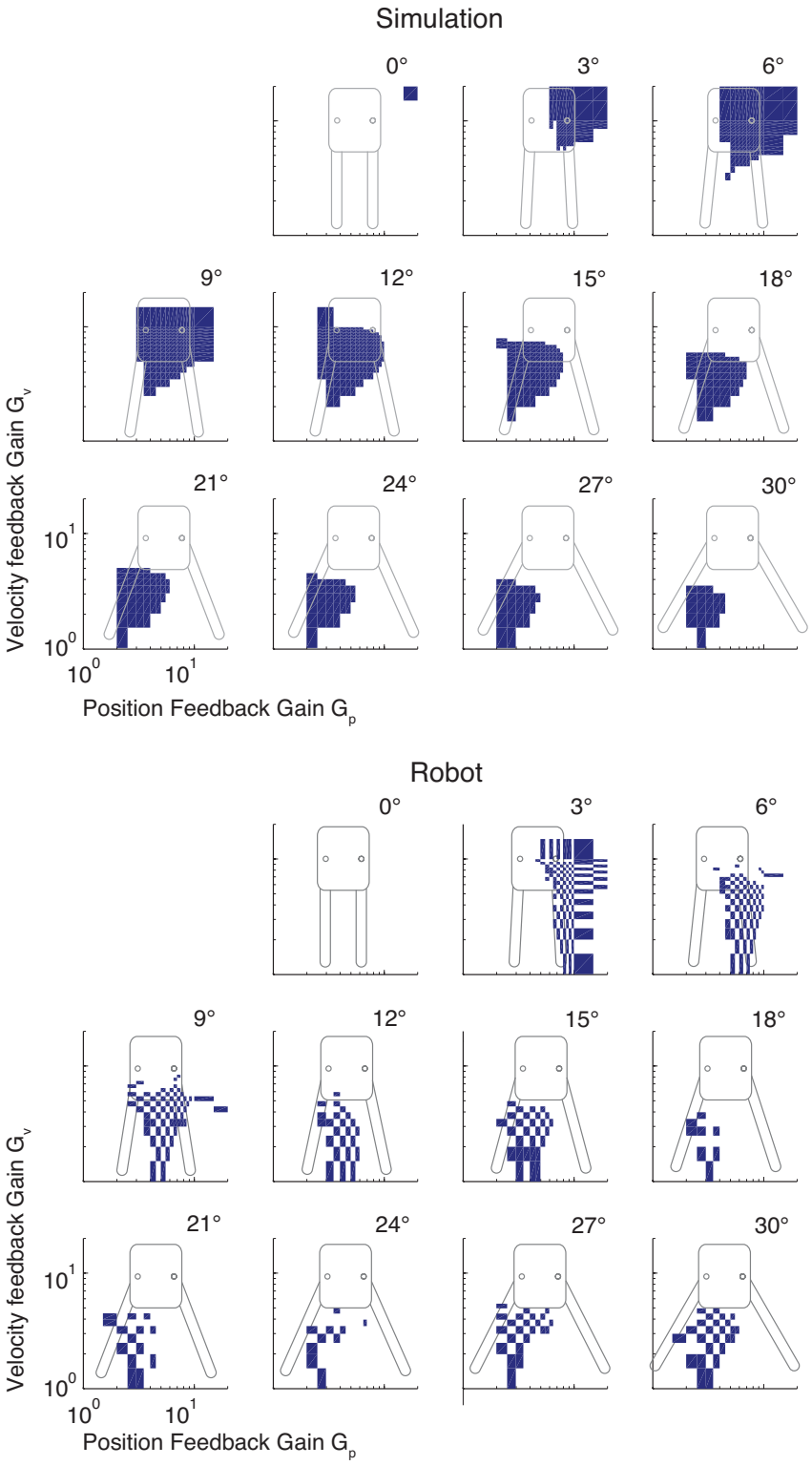

Figure 3.2: Stabilizing feedback gains. In each stance, only a limited range of feedback gains results in a stable postural response. In both the simulation results and the robot trials, the range of stabilizing gains decreases with increased stance width. The upper bounds of stability for the simulation and robot do coincide, but the robot was stable with lower velocity feedback gains. This difference can be attributed to the presence of friction in the robotic system, which has an effect similar to increased velocity gain.

The results of the parameter sweeps also showed that the magnitude of stabilizing feedback gain decreased with increased stance width. Interestingly, the stabilizing feedback gains for wide stance were not subsets of stabilizing gains for narrow stance widths. The regions of stabilizing feedback gains for narrow and wide stance were different in both simulation and robot trials (Figure 3.3).

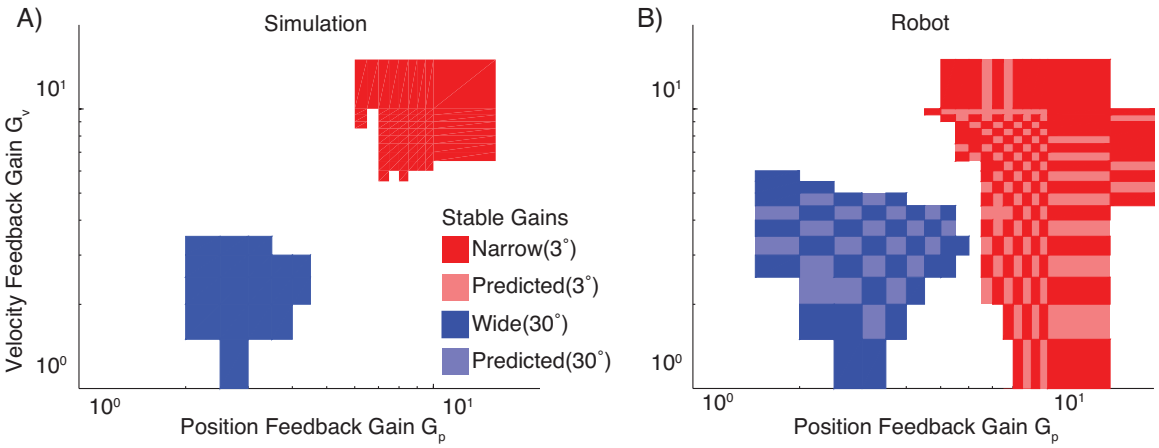

Figure 3.3: Narrow and wide stance stable gain comparison. Stabilizing gains for narrow stance and wide stance are disjoint sets. Thus, to remain stable feedback gains must be changed in accordance with changes in stance width. Robot parameters were evaluated on a spaced grid pattern, thereby leaving some parameter sets un-evaluated. To assist in the visualization of the stable regions we shaded un-evaluated parameter location that are predicted to be stable in a light red or blue for narrow and wide stance, respectively.

The disjoint nature of these gain-regions for different stances provided further indication of a link between stance and control requirements, and suggested that postural stability requires coordination between the parameters. Compared to wide stances, narrow stances system required higher magnitudes of feedback gain to resist the perturbation and remain standing. Since the maximum stable gains for the widest stances were lower than the lower bounds for the narrow stances, we predicted that a mechanical change occurs with increasing stance width that amplifies the effects of feedback gains, making the system unstable due to excessive gain. To evaluate this potential effect of stance variation, we analyzed the changing dynamic characteristics of the responses within the stable range of feedback gains and stance widths.

3.1.2 Analysis of Dynamic Responses

We quantified the characteristics of the dynamic responses by calculating the effective stiffness (K_{eff},) and damping (B_{eff},) values for stable responses. The measures were calculated by regression of post-perturbation X_{CoM} kinematics to a second-order system (Figure 3.4). The second-order system is used to describe the generalized motion of a spring-mass-damper system, and is governed by equation (3.1)

$$\ddot{x} = \frac{B}{m}\dot{x} + \frac{K}{m}x \tag{3.1}$$

Although our system used a delayed feedback controller, the motion resulting from perturbation could be approximated by the linear non-delayed model. The results of the regression are mass-normalized values with the units of $^{N}/_{kg\cdot m}$ and $^{Ns}/_{kg\cdot m}$ for K_{eff} and B_{eff}, respectively.

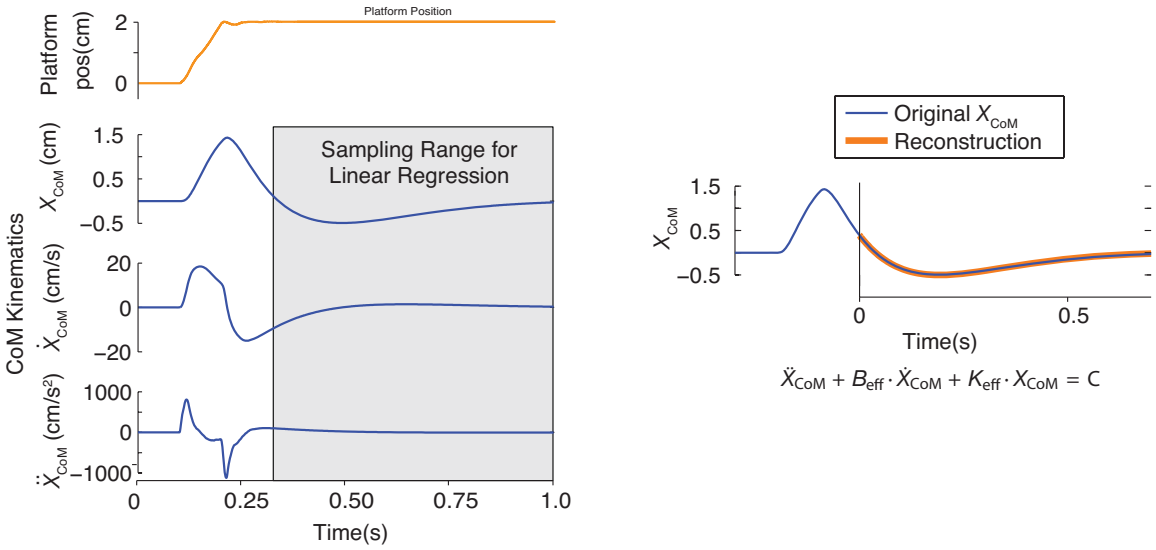

Figure 3.4: Regression Analysis of X_{CoM} kinematics. Postural responses were evaluated by performing a regression of CoM kinematics following displacement of the perturbation platform. The sampling range used for the regression is indicated by the shager region. The results produces effective stiffness and damping measures, K_{eff} and B_{eff}, of CoM displacement. These measures describe the dynamic characteristics of the CoM motion and can be used to reconstruct the motion profile from an initial displacement and velocity.

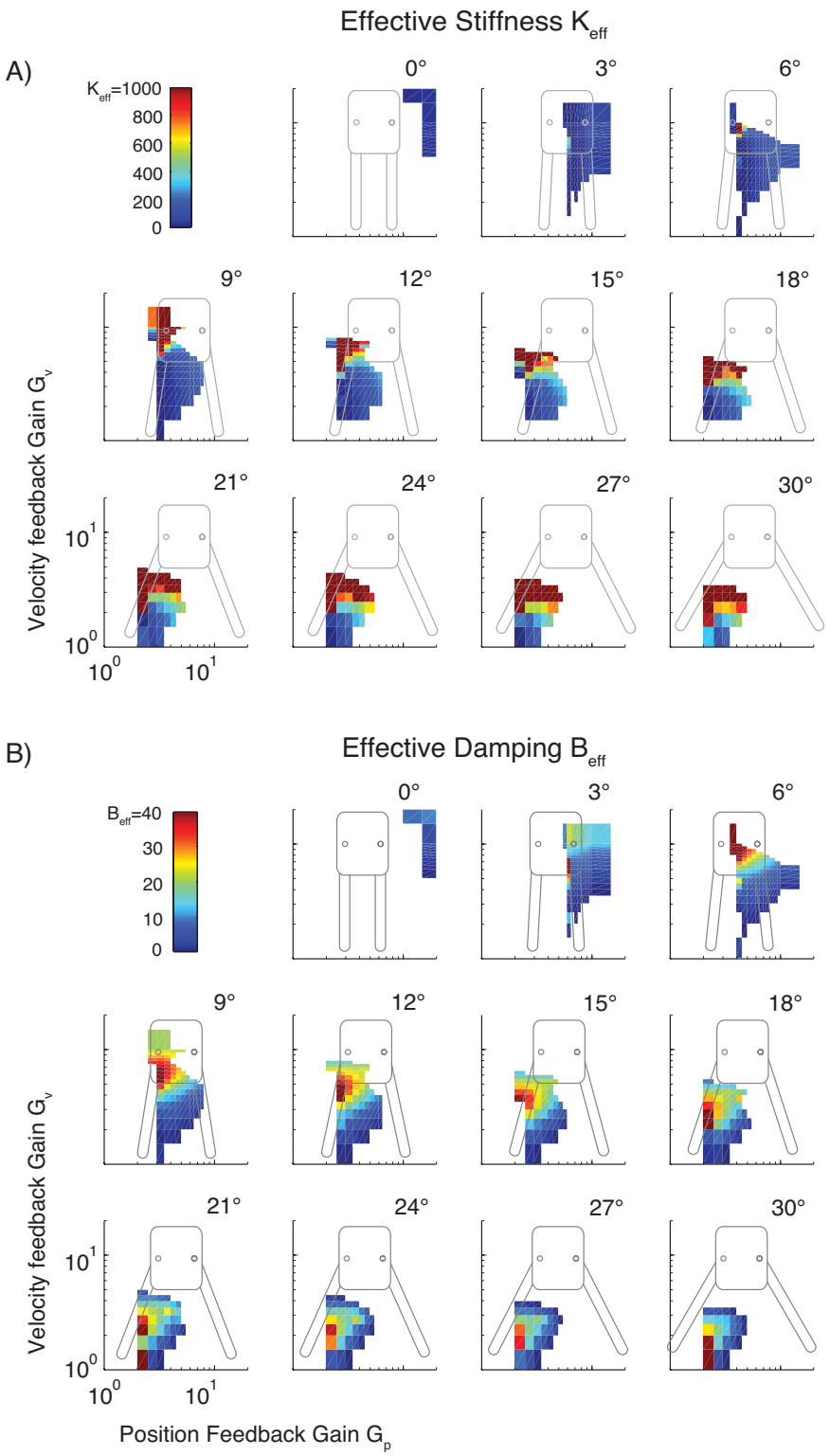

Figure 3.5: K_{eff} and B_{eff} Measures. Effective stiffness and damping was measured for the set of stable perturbation responses within the stance width and feedback gain parameter space. The measures show that stiffness increases with gain magnitude and stance width. Effective damping also increases with stance width and feedback gain. However, the magnitude of B_{eff} appears to peak before the edge of the stable gains region. The magnitude of B_{eff} then decreases slightly before the system becomes unstable.

We performed the regression over the full range of parameters evaluated in simulation. Although many parameter combinations were previously determined to be unstable, regression and calculation of K_{eff} and B_{eff} was still possible for some of these unstable responses. This resulted in K_{eff} and B_{eff} regions that were larger than the stable gain regions. These extra values are primarily with low-gains since wild oscillations and subsequent termination of the simulation prohibits analysis at high gains. The results of the regression analysis shown in Figure 3.5 illustrate the variation of K_{eff} and B_{eff}.

Evaluation of the postural responses within the stabilizing gain regions showed that effective stiffness and damping vary with G_v and G_p. Generally K_{eff} and B_{eff} increased with increasing G_v and decreased with increasing G_p. The maximum stable K_{eff} was observed to approximately 600 N/kgm. A limit of stable K_{eff} is a characteristic of the delayed system. A limit is realized because K_{eff}^2 is the natural frequency of the system, and the system has a 30ms delay. The phase of this delay increases with frequency. Moreover, at high frequencies, the phase delay is sufficient to cause instability.

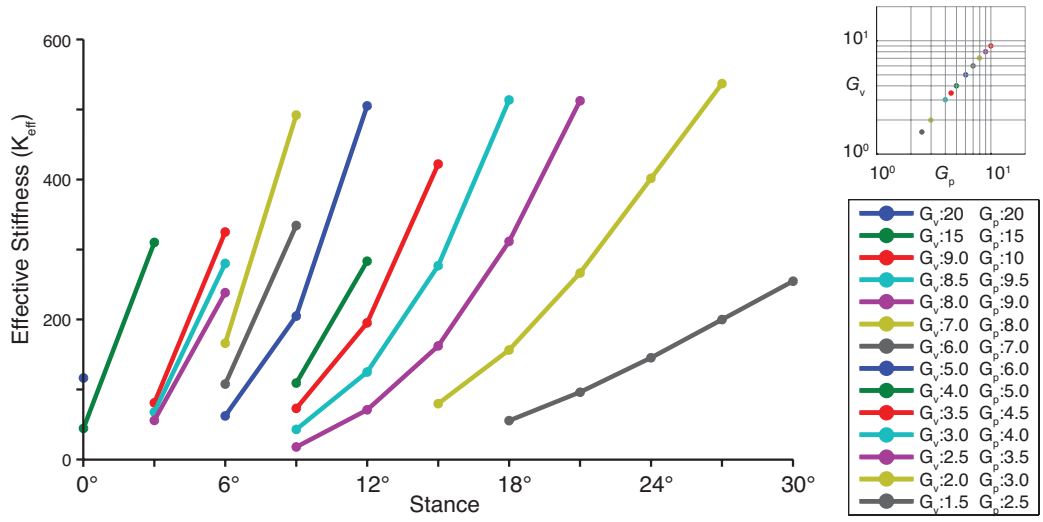

Figure 3.6: Effective stiffness measures with constant gain and varying stance width. To isolate the effects of stance width variation, K_{eff} measures were compiled for a series of constant feedback gains and varying stance widths. Each line of the figure represents a single combination of position and velocity feedback gains. The lines span the range of stance widths in which the gains produce a stable perturbation response. The results show that K_{eff} increases as a non linear function of stance width. The minimum stable measures of K_{eff} appear to be ~40Ns/kgm. Projection of a gain below this behavior results in unstable "falling over" behavior. The maximum stable measures appear to be ~600N/kgm. Projection of stance width and gain above this value results in unstable oscillatory behavior with increasing magnitude and frequency.

To evaluate the variation of effective stiffness, we compiled K_{eff} for multiple parameter combinations and organized the measures as functions of θ_s and gain sets (G_v and G_p) (Figure 3.6). The compiled data illustrates the stance-dependent variation of K_{eff}, for a number stable gain sets. Each line represents a single gain set and plots K_{eff} as a function of θ_s. The lines are plotted over the range of stances that have stable responses for the particular set of gains. These measures show that K_{eff} increases with stance width and constant feedback gains. For each gain combination, K_{eff} increased with stance from a near minimum stable value of approximately 30N/kgm to its maximum stable stiffness measure near the approximate limit of 600N/kgm. At stances beyond the upper limit of the illustrated curves responses were unstable with increasing oscillations. At stances below the limit of the illustrated curves the system was unable to recover from the perturbation.

The similarities of responses with similar effective stiffness and the dissimilarity of the responses with different K_{eff} indicate that effective stiffness is an appropriate measure of the dynamic behavior of the parameter set. Parameter combinations with similar values of K_{eff} have similar response dynamics. Evaluating a series of responses with $K_{eff} \approx 70$N/kg·m, we observed that they all have similar dynamic qualities even though responses are from different parameter combinations (Figure 3.7b). We also observed that the most dissimilar responses had the most dissimilar measures of K_{eff} (Figure 3.7a,b). To emphasize the characteristics of different K_{eff} we highlighted a series of responses from the same stance, but with different measures of K_{eff} (Figure 3.7c). Each of these responses exhibits different dynamic characteristics. These differences include variations in settling time, overshoot, and number of oscillations. Overall, the systems with higher values of K_{eff} exhibit faster responses with higher natural frequencies.

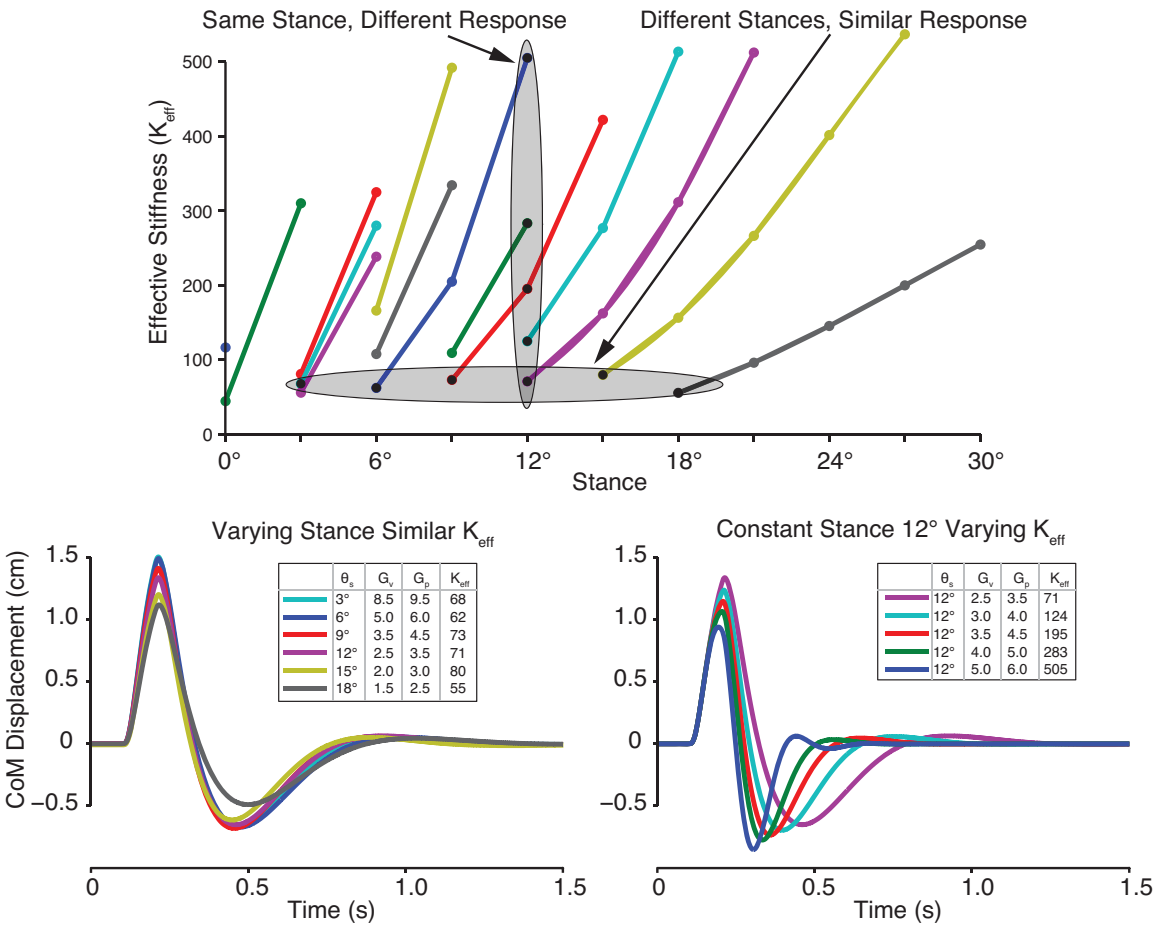

Figure 3.7: Quality of the effective stiffness measures. The use of K_{eff} as a measure of the dynamic characteristics of the postural response was verified by comparing responses of similar and dissimilar K_{eff}). Effective stiffness measures and their corresponding stances are shown. The series of postural responses with similar K_{eff} and different stances show qualitatively similar dynamic characteristics. Even within this group, responses that differ the most have the most dissimilar K_{eff}. The series of the same stance and different measures of K_{eff} show qualitatively different responses. The speed of the responses increases with K_{eff} thereby the second peak of the response oscillation and showing a correlation between the measurement of K_{eff} and the dynamic characteristics of the response.

In addition to K_{eff}, B_{eff} also provides some insight into the characteristics of the dynamic response. However, the change in B_{eff} is not well correlated with the changing behavior that occurs with stance variation. In contrast to the monotonic increase in effective stiffness that is observed with increasing stance, the change in effective damping is non-monotonic. With increasing stance, B_{eff} increases and then plateaus before the system becomes unstable (Figure 3.8). B_{eff} is apparently related to the

magnitude of effective stiffness rather than the change in stance. The measures K_{eff} and B_{eff} have maximum stable values in the observed parameter space. K_{eff} peaks at 600N/kg·m for the stable responses, but higher values are observed with unstable responses. In contrast, B_{eff} peaks approaches 20N/kg·m among stable responses and rapidly decreases to negative values with unstable responses. By correlating B_{eff} to K_{eff} we observed that B_{eff} approaches 20N/kg·m as K_{eff} increases to greater than 600N/kg·m and as K_{eff} increases further, B_{eff} decreases. These results suggest that B_{eff} provides an indication of the dynamic behavior of the system. However, the change in B_{eff} is not directly correlated to stance width variation.

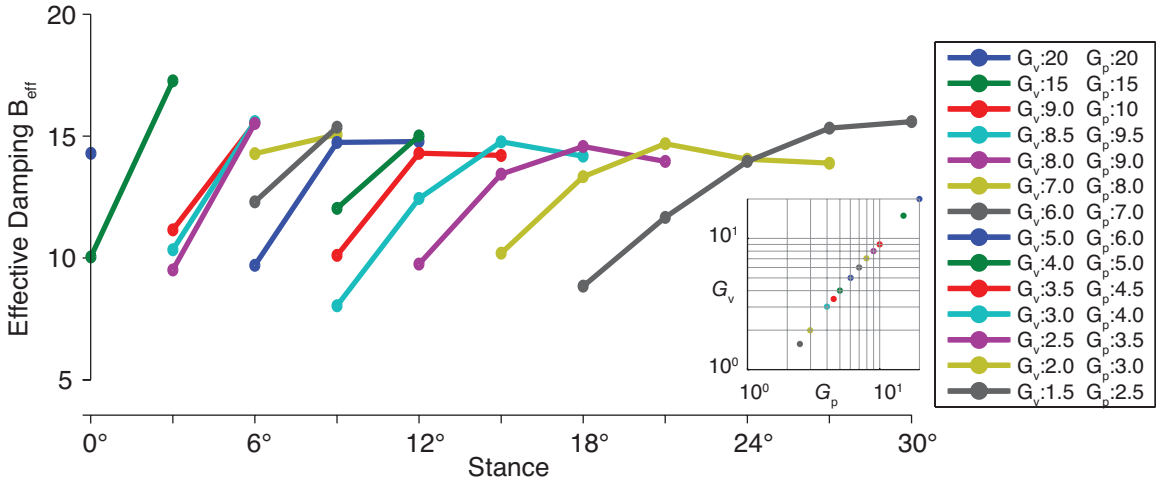

Figure 3.8: Effective damping (B_{eff}) increases non-monotonically with stance width. Near the limits of stability, max stable SW for the gain set, effective damping plateaus and undergoes a slight decrease before becoming unstable. In unstable configurations, B_{eff} has a negative value.

3.1.3 Evaluation of Performance Variation

Effective stiffness of the system response increases with stance. However, since no single set of gains produced a stable response at all stance angles, a complete correlation could not be made by direct calculation of stiffness change with stance variation. This fact hindered our ability to observe a continuous relation between increasing K_{eff} increasing stance. In order to conduct a complete evaluation of

performance change across the full stance range, we formulated a method of compiling the data into a continuous relation between stance and stiffness.

We hypothesized that the changing postural dynamics with increased stance was due to the changing mechanics that altered the dynamics of the system. These altered mechanics would then act as a gain on the system response. Therefore, since stance variation acts as a gain on the system, postural performance at different stance widths and consistent feedback (G_v and G_p) could be related by a consistent, stance dependent, multiplication factor. This multiplication factor would be effective through the range of stable stances for each set of feedback gains.

We evaluated K_{eff} from trials of different stance widths and constant feedback gains to determine if there was a consistent relation between effective stiffness and stance increases. We evaluated stiffness increase by calculating the ratio of K_{eff} for adjacent stances with common feedback gain. The resulting measure was the mechanical K_{eff} gain. We performed the study with 3° stance angle increments, and the resulting ratio calculation was the stiffness gain for a 3° stance increase. Evaluation of the K_{eff} gains showed that the value for multiple parameter sets (G_v and G_p) was consistent at each stance change, but decreased with increasing stance (Figure 3.9). The close proximity of the values for multiple parameters sets indicated that K_{eff} gain was not dependent on feedback parameters. Furthermore, the variation of gain values across stances indicated that K_{eff} gain is stance dependent.

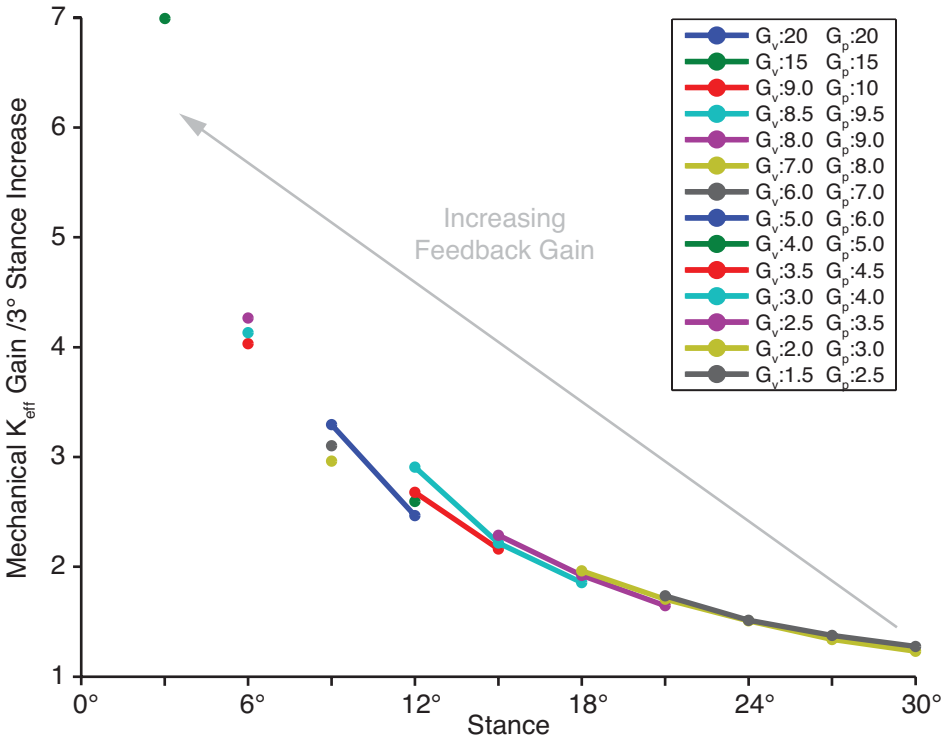

Figure 3.9: Effective stiffness change between stance angles. Increasing stance width consistently magnifies the measured effective stiffness of the response in a stance dependent manner. The relation between the effective stiffness of adjacent stance angles is quantified by the equation $G = K_{eff}$ (stance 2)/ K_{eff} (stance 1).

K_{eff} gain is the ratio of K_{eff} between adjacent stances with identical feedback gains. This ratio quantifies the effect of stance width variation on the response behavior, and shows that effective stiffness change is dependent on stance width and not dependent on the magnitude of feedback gain within the stable region. The variation of this ratio shows that the gain decreases with increasing stance, indicating that stance width changes have the greatest effect at narrow stances.

To generalize the K_{eff} gain results, we extrapolated a stiffness curve as a function of K_{eff} gain and θ_s. This extrapolation illustrates a scaled version of effective stiffness measures that would have been observed if a single set of gains were stable at all stances (Figure 3.10). The extrapolated stiffness curve was normalized to $\theta_s = 6°$. We normalized to this stance because a fewer number of parameter sets were stable at $\theta_s = 0°$ and $3°$. Also, the stance angle of 6° is representative of a normal preferred stance. The

normalized extrapolation facilitates the prediction of the K_{eff} for any stance angle given an original stiffness and stance angle. The formula for such predictions is as follows:

$$K_{\text{eff}}(\theta_s(2)) = K_{\text{eff}}(\theta_s(1)) \cdot \frac{K_{\text{projected}}(\theta_s(2))}{K_{\text{projected}}(\theta_s(1))} \tag{3.1}$$

The extrapolation also quantifies the stance dependent nature of the change in postural performance as a result of the changing mechanics that occurs as stance width increases. The following section focuses on this relation.

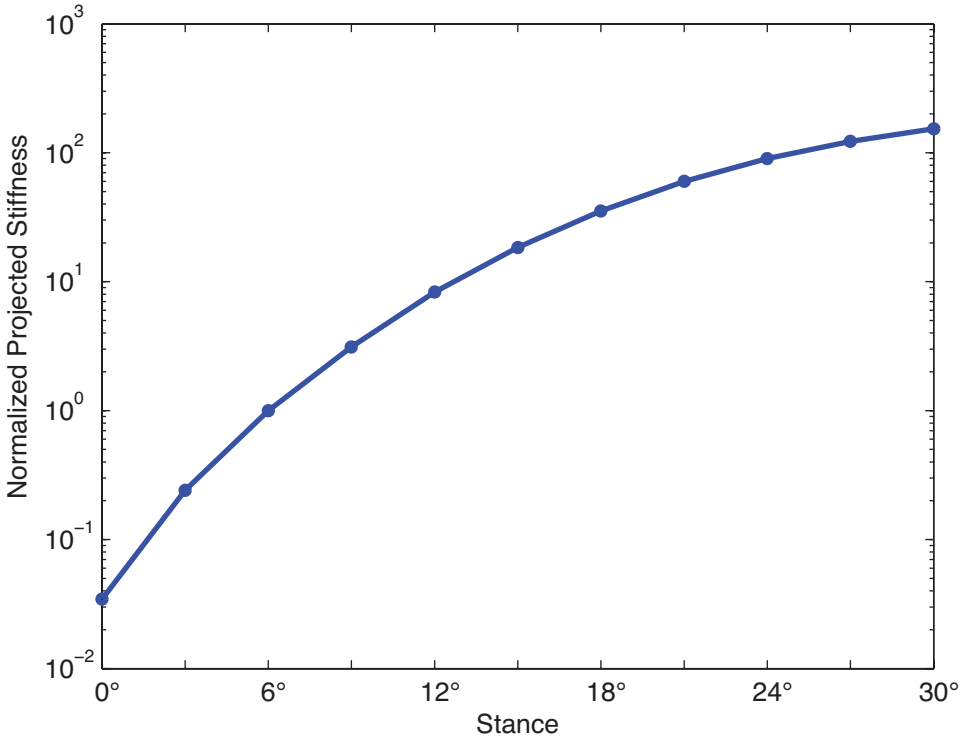

Figure 3.10: Normalized Projected Stiffness. This figure illustrates the theoretical effective stiffness of a single set of feedback gains across all stances. The curve is the projection of incremental increases measured from a series constant gain stance increases. The projection is normalized to a stance angle of 6°.

3.2 Mechanics of Stance Width Variations

Changing stance width changes the way the postural system responds to perturbations. The change in postural response occurs for two reasons:

- Stance width variations change the mechanical transfer impedance of the system resulting in different displacements at different stance widths.

- Stance width variations change the dynamics of the controlled mechanical system resulting in altered CoM motion (e.g. Joint torque → CoM motion).

Although changing mechanical impedance is usually considered the primary result of stance width changes, the changing dynamics of the controlled mechanical system is most influential in changing the motion of the CoM. Our purpose for the mechanical analysis is to determine how the changing mechanics (stance width) affects the dynamics of the controlled mechanical system and the resulting motion of the CoM.

In response to a displacement, torque is generated at the hip by the postural controller. This torque accelerates the CoM, resulting in the observed dynamic CoM motion. Changing stance width changes the torque that is generated for a given displacement and it also changes the acceleration of the CoM for a given torque. With stance width variation, the changes in the relationships between displacement and torque, and between torque and acceleration, result in changes in dynamic behavior of the system. We examined these relationships and calculated their effect on the system dynamics. As with previous measures, we calculated the value of these properties across the range of stance widths as well as the variation of these properties as stance dependent gains.

3.2.1 Effective Inertia:

The effective inertia of the system is the ratio between the torque applied at the hip and the acceleration of the CoM (Equation 3.2). Increasing stance width decreases the effective inertia, thereby increasing the acceleration for the same applied torque

$$\frac{1}{\text{Effective Inertia}} = \frac{\ddot{X}_{\text{CoM}}}{T_{\text{Hip}}} \tag{3.2}$$

The lateral motion of a bipedal system is internally controlled by hip abduction/adduction torque (T_{Hip}). The result of such torque is the acceleration of the CoM ($\ddot{X}_{\text{CoM}}$). As stance is varied, the magnitude of $\ddot{X}_{\text{CoM}}$ due to T_{Hip} also varies.

Increasing stance width generally results in increased $\ddot{X}_{\mathrm{CoM}}$ for a given $\ddot{X}_{\mathrm{CoM}}$, signifying a decrease in the effective inertia of the system relative to T_{Hip}. We calculated the effective inertia by calculating the instantaneous $\ddot{X}_{\mathrm{CoM}}/T_{\mathrm{Hip}}$. The calculation assumes an upright stance and constant hip torque (see Appendix B).

$$\begin{aligned}\frac{\ddot{X}_{\mathrm{CoM}}}{T_{\mathrm{Hip}}} &= (-0.00200*\mathrm{Cos}(2*\theta_A) - 0.05238*\mathrm{Cos}(\theta_A - \theta_B) - 0.02991*\mathrm{Cos}(2*(\theta_A - \theta_B)) + 0.18964*\mathrm{Cos}(\theta_B) - \\ &0.01746*\mathrm{Cos}(\theta_A+\theta_B) - 0.03492*\mathrm{Cos}(\theta_A - \theta_B - 2*\theta_C) - 0.03492*\mathrm{Cos}(2*\theta_A - \theta_B - \theta_C) - 0.01746*\mathrm{Cos}(\theta_B - \theta_C) + \\ &0.00200*\mathrm{Cos}(2*\theta_C) - 0.01495*\mathrm{Cos}(2*(\theta_A - \theta_B + \theta_C)) - 0.01746*\mathrm{Cos}(2*\theta_A - \theta_B + \theta_C) - \\ &0.05238*\mathrm{Cos}(\theta_B + \theta_C) + 0.02991*\mathrm{Cos}(2*(\theta_B + \theta_C)) + 0.01495*\mathrm{Cos}(2*(\theta_A + \theta_B + \theta_C)) - \\ &0.01746*\mathrm{Cos}(2*\theta_A+\theta_B+\theta_C) - 0.01746*\mathrm{Cos}(\theta_A - \theta_B+2*\theta_C) - 0.0948244*\mathrm{Cos}(2*\theta_A - \theta_B+2*\theta_C) - \\ &0.017465*\mathrm{Cos}(\theta_A + \theta_B + 2*\theta_C) - 0.09482*\mathrm{Cos}(2*\theta_A + qB + 2*v) + 0.01508*\mathrm{Sin}(\theta_A - \theta_B) - \\ &0.03694*\mathrm{Sin}(2*(\theta_A - \theta_B)) - 0.21952*\mathrm{Sin}(2*\theta_A - \theta_B) + 0.06105*\mathrm{Cos}(\theta_B)*\mathrm{Sin}(\theta_B) + \\ &0.01508*\mathrm{Sin}(\theta_A + \theta_B) - 0.03694*\mathrm{Sin}(2*(\theta_A - \theta_B - \theta_C)) - 0.01508*\mathrm{Sin}(qB - \theta_C) - \\ &0.00320*\mathrm{Sin}(2*(\theta_A - \theta_B + qC)) + 0.01508*\mathrm{Sin}(2*\theta_A - \theta_B + \theta_C) + 0.01508*\mathrm{Sin}(\theta_B + \theta_C) + \\ &0.03694*\mathrm{Sin}(2*(\theta_B + \theta_C)) + 0.00320*\mathrm{Sin}(2*(\theta_A + \theta_B + \theta_C)) + 0.01508*\mathrm{Sin}(2*\theta_A + \theta_B + \theta_C) + \\ &0.01508*\mathrm{Sin}(\theta_A - \theta_B + 2*\theta_C) - 0.10976*\mathrm{Sin}(2*\theta_A - \theta_B + 2*\theta_C) - 0.21952*\mathrm{Sin}(\theta_B + 2*\theta_C) + \\ &0.01508*\mathrm{Sin}(\theta_A + \theta_B + 2*\theta_C) - 0.10976*\mathrm{Sin}(2*\theta_A + \theta_B + 2*\theta_C)) / \\ &(-0.02075 - 0.00728*\mathrm{Cos}(2*\theta_A) - 0.00728*\mathrm{Cos}(2*\theta_C) + 0.00617*\mathrm{Cos}(2*(\theta_A + \theta_C)) + \\ &0.01138*\mathrm{Cos}(\theta_A)*\mathrm{Sin}(\theta_A) + 0.01138*\mathrm{Cos}(\theta_C)*\mathrm{Sin}(\theta_C) + 0.00569*\mathrm{Sin}(2*(\theta_A + \theta_C)))\end{aligned} \tag{3.3}$$

3.2.2 Displacement Ratio:

Active and intrinsic hip torques are the result of the stiffness and damping coefficients of the hip and are thus proportional to leg/hip displacement ($\Delta\theta_{\mathrm{Leg}}$). Increasing stance width increases the ratio $\Delta\theta_{\mathrm{Leg}}$ and ΔX_{CoM}. Therefore, assuming that feedback gains remain constant, increasing stance increases the magnitude of the torque generated for a given $X_{\mathrm{CoM}}$and $\dot{X}_{\mathrm{CoM}}$velocity ($\Delta X_{\mathrm{CoM}} = X_{\mathrm{CoM}}$).

We performed a kinematic analysis of the system to quantify the changing relation between $X_{\mathrm{CoM}}$and $\Delta\theta_{\mathrm{Leg}}$under varying stance width. We measured the variation of this ratio by calculating the derivative of $\Delta\theta_{\mathrm{Leg}}$vs. X_{CoM}. The resulting relation is the stance-dependent displacement ratio for leg angle and CoM displacement (Equation 3.4).

$$\begin{aligned}
\text{DisplacementRatio} &= \frac{\Delta\theta_{Leg}}{\Delta X_{\text{CoM}}} = \frac{\dot{\theta}_{\text{Leg}}}{\dot{X}_{\text{CoM}}} \\
\dot{X}_{\text{CoM}} &= 0.1397\cos(\theta_{\text{s}}) \times (\dot{\theta}_{\text{Leg}} - \dot{\theta}_{\text{pelvis}}) - 0.0192\,\dot{\theta}_{\text{pelvis}} \\
\dot{\theta}_{\text{pelvis}} &= \frac{3.142857\sin(2\theta_{\text{s}})}{3.142857\sin(\theta_{\text{s}})\cos(\theta_{\text{s}}) + \cos(\theta_{\text{s}})[1 + 3.142857\sin(\theta_{\text{s}})]}\dot{\theta}_{\text{Leg}}
\end{aligned} \quad (3.4)$$

3.3 Effects of Stance Mechanics on the Active Dynamic Response

We normalized the mechanical measures of effective inertia and displacement ratio to the variation of their magnitude with stance. These normalized values were combined to a resulting measure of the overall mechanical effect of stance variation on the response of the system. This measure was compared to the observed stance dependent change in response dynamics and subjected to further analysis.

3.3.1 Resultant Mechanics of Stance Variation

The displacement ratio (multiplied by the hip stiffness constant) scales the torque produced for a given X_{CoM}, and the inverse effective inertia scales $\ddot{X}_{CoM}$ when subjected to hip torque. These effects combine to scale $\ddot{X}_{CoM}$ for a given displacement. Because our interest is the change in behavior due to stance width variations, we normalized the calculations for effective inertia and displacement ratio to their value at a nominal stance (6°) and their *product* characterizes the effect of stance width variation (Figure 3.11). This normalized product of effective inertia and displacement ratio is the mechanical leverage gain for stance variations.

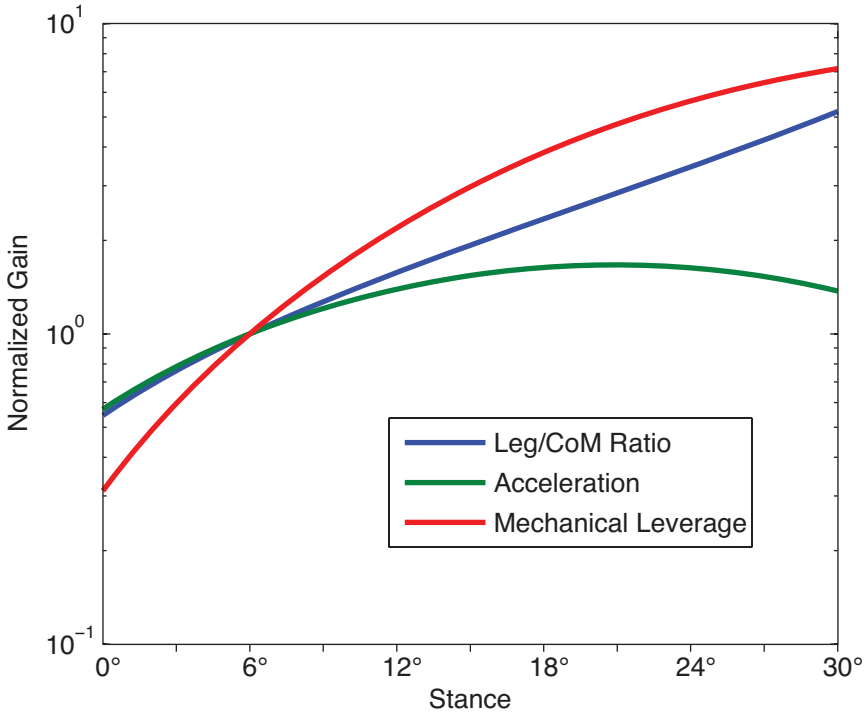

Figure 3.11: Mechanical Leverage. Stance width variations affect the kinematic relations between the components of the bipedal structure. These changing relations affect the ratio between Leg angle and CoM excursion as well as the acceleration of the CoM under constant torque. These two qualities combine to give the total leverage of the mechanical system under changing stance width.

We compared the normalized stiffness measures of the active system to the mechanical leverage gain of the system under stance variation (Figure 3.12). The results show that although both values increased with stance width, the rate of measured effective stiffness increase was considerably greater than the rate of mechanical leverage increase.

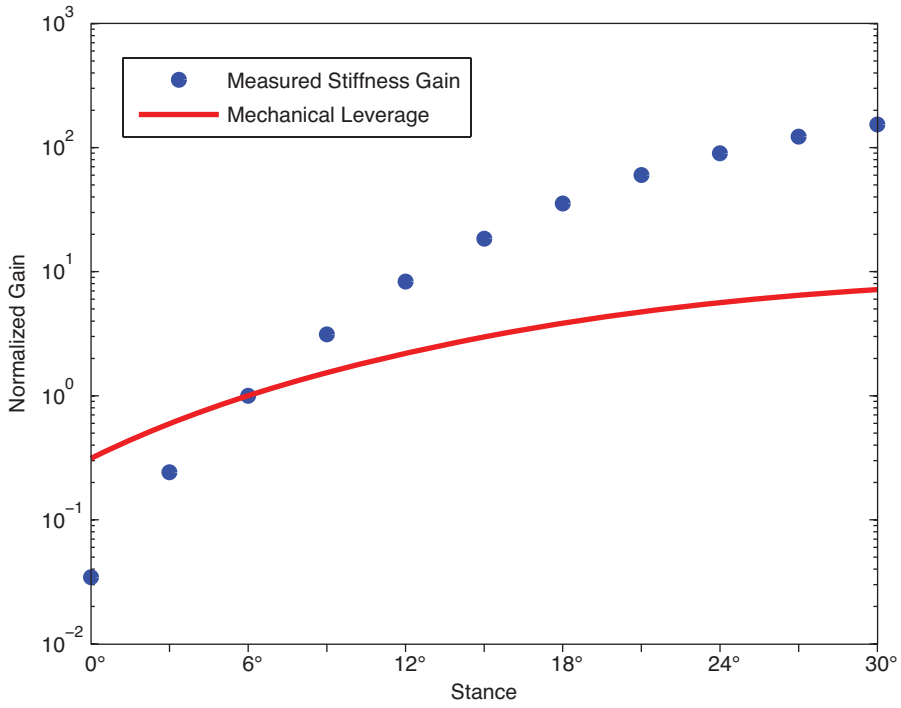

Figure 3.12: Comparison of Measured Effective Stiffness and Mechanical Leverage. Mechanical leverage matches the general trend of projected stiffness. The magnitude of projected stiffness is significantly higher than mechanical leverage. The matching trend indicates the mechanical leverage and projected stiffness may be related, but the difference in magnitude indicates that another factor is involved in the relation between leverage and projected stiffness.

3.3.2 Delay Effects

We hypothesized that the difference between the normalized magnitudes were the consequences of delay in the postural controller and the non-linear motion of the mechanical system. We then conducted an analysis of the delay effects to determine if the difference between the observed stiffness and mechanical leverage gain could be attributed to stiffness. We identified the changing mechanical leverage that occurs with stance width variations. Since the feedback loop contains a time delay, the changes in the kinematic response did not scale directly with the mechanical gain. Feedback delay was identified as a potential cause of the discrepancy between the change in mechanics and the change in response. To evaluate delay effects we examined the response of the system under a small perturbation and no feedback delay. The results showed that the observed effective stiffness gain matched mechanical leverage gain of the system (Figure 3.13)

This result verified our hypothesis that changing mechanical leverage causes a predictable change in the postural dynamics of non-delayed systems.

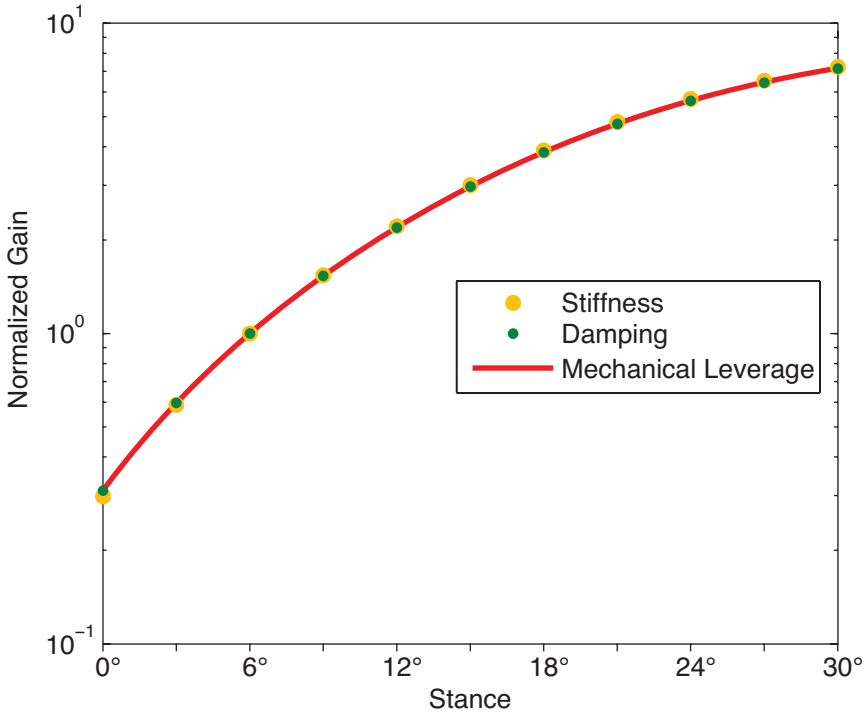

Figure 3.13: Effective Stiffness With Zero Feedback Delay Results. The change in postural response is equivalent to the change in mechanical leverage with small magnitude perturbation and without delay in the feedback loop**.**

We performed simulated perturbations to a simple spring-mass-damper system with a feedback time delay to further examine the effects of delay (Figure 3.14). This system was equipped with a mechanical gain that amplified the force response just as increasing stance width increases the mechanical leverage. We used feedback gains that resulted in K_{eff} and B_{eff} values that were similar to those measured in our system. Stiffness gain was examined by perturbing the system while varying the mechanical gain in the feedback loop and measuring the resulting response. Stiffness gain that we observed were the result of mechanical gain and delay. We quantified this gain by the ratio:

$$K_{eff}Gain = \frac{K_{eff(+mech\_gain)}}{K_{eff(-mech\_gain)}}$$

$$K_{eff(+mech\_gain)} \rightarrow \text{Effective Stiffness With Mechanical Gain} \qquad (3.5)$$

$$K_{eff(+mech\_gain)} \rightarrow \text{Effective Stiffness Without Mechanical Gain}$$

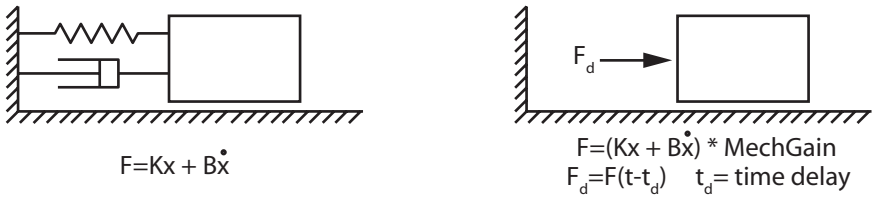

Figure 3.14: Simple Delayed Spring Mass Damper System. The delayed spring mass damper system is based on the common spring-mass-damper, but also incorporates a time delay and a mechanical gain to amplify the force of the spring and damper. Perturbations with such a system allow us to isolate and predict the amplification of effective stiffness that occurs with a mechanical gain in a time delayed system. Delay effects are measured by applying K and B values to the delayed system and measuring K_{eff}. Mechanical gain is then applied and the K_{eff} is re-measured. Delayed mechanical gain effects are evaluated by calculating effective stiffness gain as ratio of K_{eff}(mech gain)/K_{eff}. Without time delay, K_{eff} of the system with and without mechanical gain would be equal to K and K*(mech gain) respectively.

Results of the simple mechanical system tests verified the hypothesis that feedback delay alters the measured K_{eff} by increasing the measure to an magnitude that is significantly greater than the applied mechanical gain (Figure 3.15). The stiffness increase due to delay and mechanical gain is a non-linear result of the combined factors.

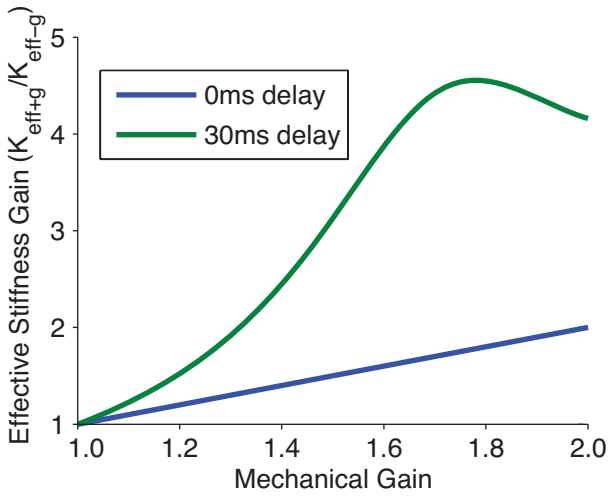

Figure 3.15: Effective Stiffness with Mechanical Gain and Delay. Without delay in the feedback loop, the change in effective stiffness is equivalent to change in mechanical leverage. With a 30ms feedback delay, the change in effective stiffness greatly exceeds change in applied mechanical gain.

We compared the delayed and non-delayed responses of this simple mechanical system to the responses of our bipedal system by coordinating mechanical gain to the change in mechanical leverage over the range of evaluated stance widths. The results showed that effective change is equivalent to the change in mechanical leverage for the simple and bipedal systems without feedback delay (Figure 3.16). The results also showed that, with feedback delay, effective stiffness change in the bipedal system is equivalent to the change in the simple system. This equivalence proves that the discrepancy between mechanical gain and stiffness gain is a result of feedback delay. It also proves that the stiffness increase observed with stance increases in the bipedal system were the combined effects of mechanical leverage gain and feedback delay.

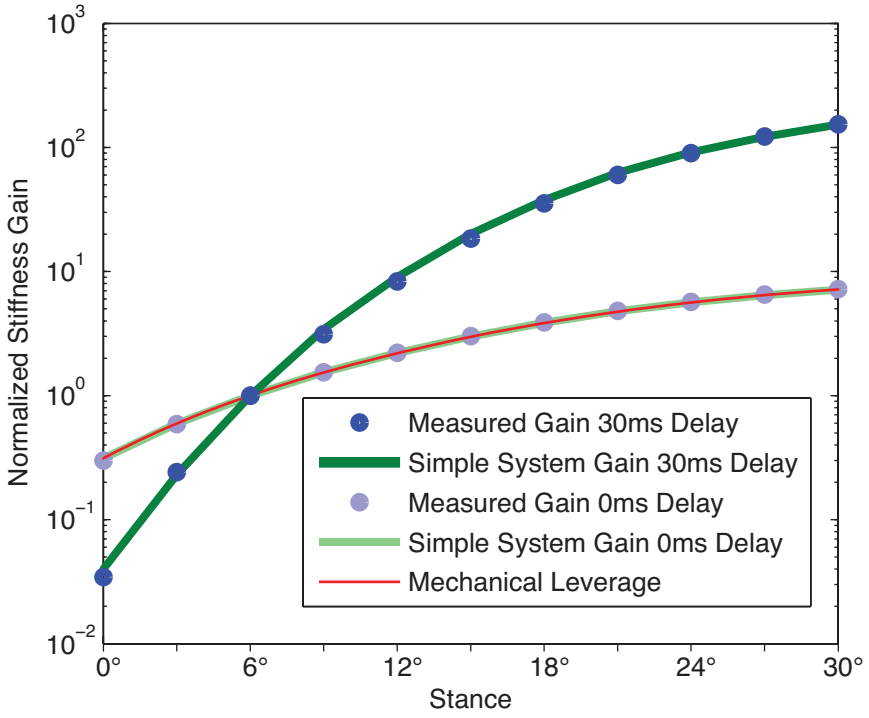

Figure 3.16: Normalized Stiffness Trends. Mechanical leverage varies with stance width. Changes in stance width can be correlated with a mechanical gain that is a result of the changing leverage. A mechanical gain that was equivalent to the normalized mechanical leverage for the range of stance widths was applied with the simple mechanical system. Using zero feedback delay, the normalized stiffness of the simple mechanical and bipedal systems follow the normalized mechanical leverage. Using a 30ms delay the effective stiffness of the simple mechanical and bipedal systems are equal and vary with a magnitude that is much higher than the mechanical leverage. The correlation between the simple mechanical and bipedal systems indicates that the changing behavior of the bipedal system is the result of the mechanical gain that occurs with stance width variation.

3.4 Predictive Response Scaling

We hypothesized that adjusting feedback gain to compensate for changing mechanical leverage would facilitate consistent postural performance under changing stance width. The reasoning behind this hypothesis was that the adjustments would result in no change in the overall gain of the feedback loop. With consistent loop gain, the overall system dynamics and effective stiffness would remain constant under changing stance. We developed a predictive scaling process that scales feedback gains with stance changes to produce consistent dynamic response characteristics. In this section we describe our scaling process and evaluate the results of stance-width-dependent scaling.

3.4.1 SWAG Factor

We added a gain adjusting scaling factor to the feedback loop to adjust active feedback gain under changing stance (Figure 3.17). This adjustment facilitated consistent postural performance under stance variations. Since our controller was linear and the scaling factor equally affects all feedback terms, scaling could be applied to either the feedback gains or the controller output. In our system the scaling factor was applied to the feedback gains rather than the output response (Figure 3.17). The magnitude of gain adjustment was determined by a pre-established function that we designated the Stance Width Adjustment of Gain function, or SWAG function. When implemented, the SWAG function scales the feedback gains to values that provide consistent postural performance between a reference stance and the current stance. The stance-dependent scaling value is the SWAG factor for the current stance. The SWAG factor scales the feedback gains, thereby adjusting the magnitude of the feedback response according to the changing mechanical leverage. The SWAG function is quantified as the reciprocal of the mechanical leverage gain.

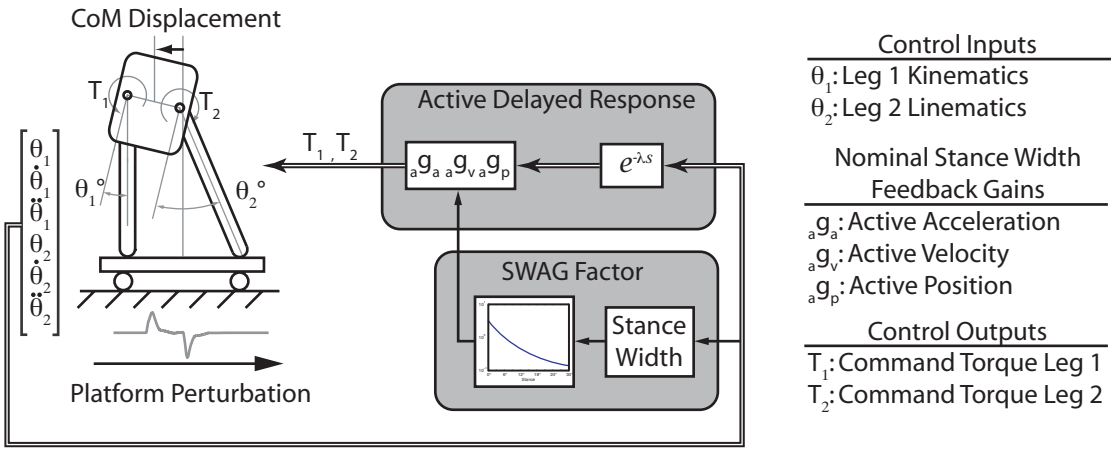

Figure 3.17: Feedback With SWAG Factor. SWAG Factor is a scaling factor that adjust the postural control feedback loop to provide consistent postural performance under varying stance. SWAG factor is formulated as the reciprocal of normalized mechanical leverage of stance.

As a preliminary test, we verified the effectiveness of the SWAG factor by reexamining data from trials with similar K_{eff} and varying stance width and comparing their stance dependent feedback gains with the SWAG function (Figure 3.18 using data from Figure 3.7). We also used trial data to predict feedback gains that would produce consistent dynamic responses at other stances, isometric-K_{eff} (iso-K) gains. Iso-K gains were predicted for several magnitudes of stiffness ranging from a relatively low stiffness value of $26\,{}^{N}\!/_{kg\cdot m}$ to a relatively high value of $422\,{}^{N}\!/_{kg\cdot m}$. Comparison of the observed and predicted values showed that observed gains aligned with the iso-K_v lines for narrow to mid-range stances. However, at wide stances, the observed gains were higher than the values predicted by the iso-K_v lines. These results showed that the SWAG scaling provided effective compensation for stance dependent mechanical leverage changes. However, further evaluation and direct implementation of the SWAG function was required to fully describe its effectiveness.

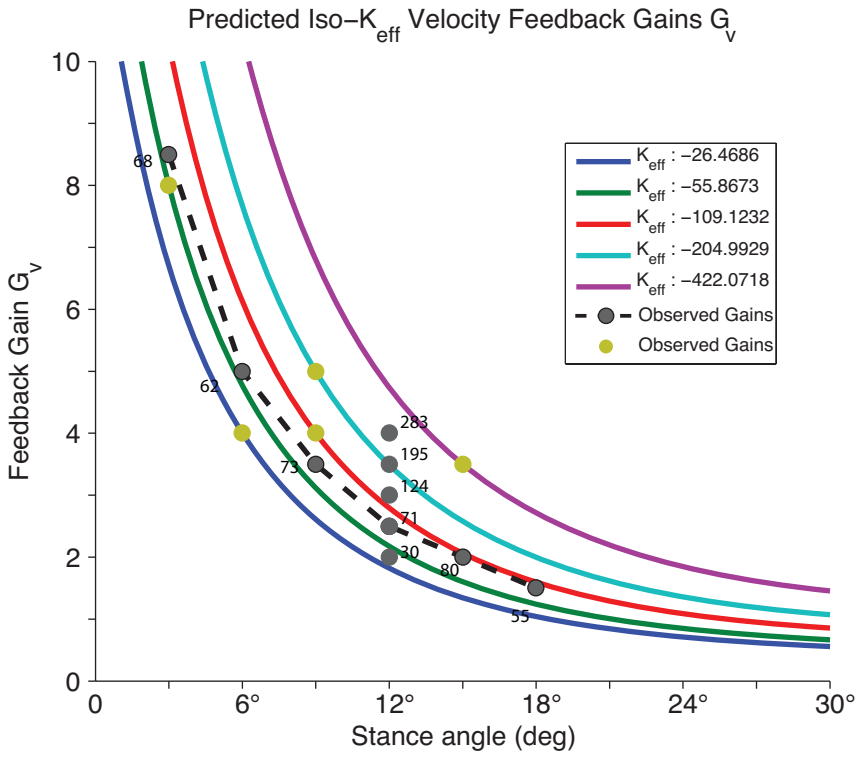

Figure 3.18: Iso-K_{eff} Lines. Each of the colored lines SWAG predicted feedback gains that provide consistent postural response (K_{eff}). Initial values used to predict the iso-K gains were taken from a number of random trials of varying K_{eff}. The initial for the series are shown in yellow. The dashed line indicates the gains for a series of trials with similar effective stiffness and various stance widths.

3.4.2 SWAG Implementation

Implementation of the SWAG factor requires the adjustment of both velocity and position feedback gains. Our initial hypothesis for SWAG implementation proposed that velocity and position feedback gains would be scaled equally. However, evaluation of simulation data for stable responses revealed that G_v and G_p were not generally of equal magnitude. Stability maps (Figure 3.1) showed that G_p values are higher than G_v within the stable gain sets. Based on this finding, we formulated G_v to scale directly with SWAG factor, and set G_p equal to G_v plus a constant offset (Eq. 3.6). Using this formulation, we implemented SWAG factor for a series of gain sets spanning low to high relative range for the reference stance condition.

$$G_{v(swag)} = G_{v(Ref)} \cdot SWAG\,\text{Factor}$$
$$G_{p(swag)} = G_{v(SWAG)} + 1 \qquad \textbf{(3.6)}$$

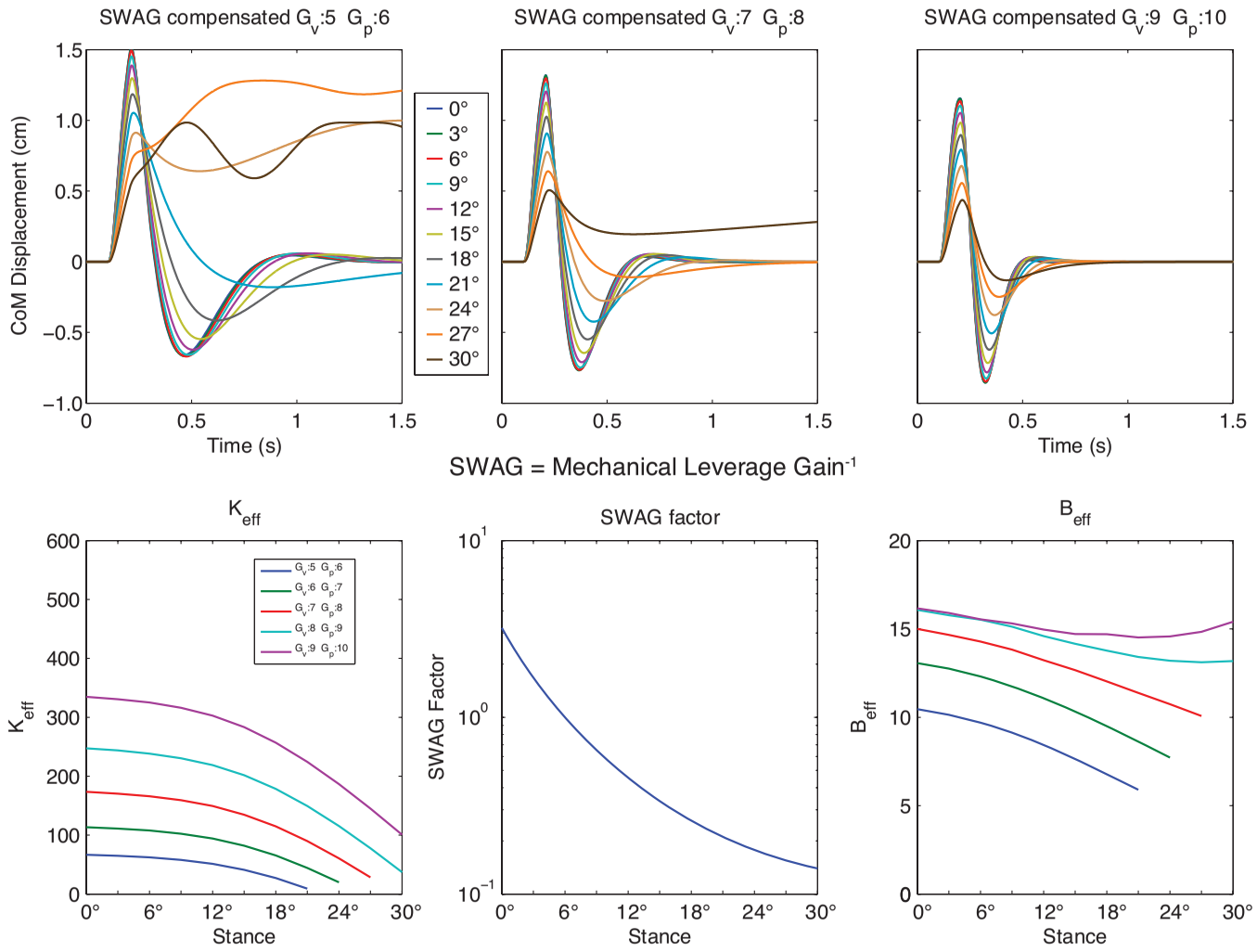

Figure 3.19: Perturbation responses with SWAG adjusted gains. Time traces are shown for the range of stance widths for A) low, B) medium, and C) high gain conditions. Effective stiffness, D), and damping, E), are conserved across the range of stance widths.

Qualitative evaluation of the response dynamics shows that SWAG implemented responses are generally stable and consistent for the majority of the stances (Figure 3.19 a,b,c). Beginning at θ_s=15°, the responses became progressively "slower". In the widest stances with the lowest gain magnitudes, the system did not recover from the perturbation. Dynamic analysis showed that effective stiffness and damping values were consistent at narrow stance widths but decreased at θ_s>15° (Figure 3.19 c,e). The stiffness decrease indicated that the SWAG factor (Figure 3.19 d) derived from instantaneous mechanical leverage values overcompensated for stance width changes, reducing feedback gain below the magnitude required for consistent performance.

Based on the observation that SWAG scaling was at least partially effective in stabilizing dynamic responses with stance width variations, we re-evaluated calculations of mechanical leverage to determine if X_{CoM} significantly alters the calculation of mechanical leverage. Our analysis showed that the mechanical factors contributing to mechanical leverage are not consistent and vary with CoM displacement (Figure 3.20a,b). This variation required the establishment of stance-dependent displacement magnitudes to which we would calculate displacement dependent SWAG factors. Since the magnitude of perturbed displacement was stance-dependent; the displacement magnitude for each stance was required to determine an appropriate SWAG function.

3.4.3 Mechanical Transfer Impedance

Perturbation impedance is a quality of the mechanical system to resist displacement when subjected to outside forces. It can be considered a measure of the stability of the mechanical configuration. The benefit of mechanical impedance is that it allows the system to be subjected to greater perturbations. This quality primarily affects the initial perturbation magnitude and does not have a major effect on the dynamics of the perturbation response. To measure perturbation impedance, we simulated a constant acceleration displacement to the system in each stance width. In each trial the system was

uncontrolled with all feedback gains set to zero. We then measured the CoM acceleration and compared it to the platform acceleration.

$$\text{Mechanical Transfer Impedance} = \frac{\int\int \ddot{X}_{\text{CoM}}}{\int\int \ddot{X}_{\text{Platform}}} = \frac{X_{\text{CoM}}}{\Delta X_{\text{Platform}}} \tag{3.7}$$

We integrated the acceleration of the system while subjected to the perturbation to determine total displacement magnitude. We evaluated several time points during the perturbation and calculated the displacement magnitude for all stances. These displacements were identified by the displacement magnitude for the 0°stance condition (Figure 3.20c). We then used these displacement magnitudes to calculate displaced mechanical leverage values (Figure 3.20d). After evaluating the postural responses in the reference stance, we determined that the stance-dependent displacement series corresponding to 1.7 cm displacement at 0° would provide the displacement magnitudes that matched the observed postural responses. This displacement series was then used to formulate a revised displacement-matched mechanical leverage and SWAG functions (Figure 3.20e). We then used the revised SWAG function to evaluate a new series of perturbations.

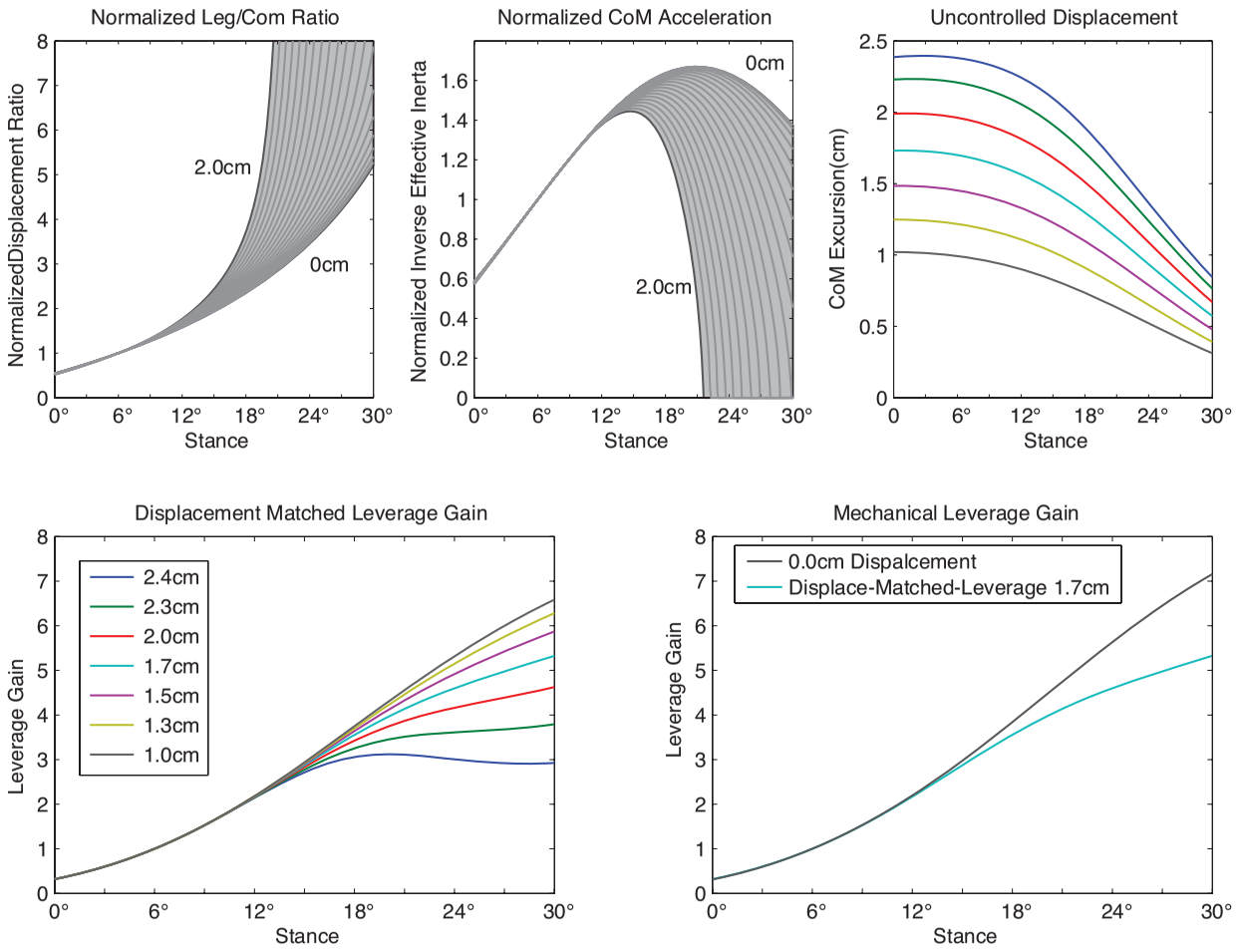

Figure 3.20: Perturbation Impedance. When the uncontrolled system is subjected to platform displacement perturbations, the acceleration of the CoM relative to the platform will proportional to the acceleration of the platform. The magnitude of this proportion is a measure of the impedance of the mechanical system. High impedance means that perturbations will not greatly effect the system. and impedance of 1 indicates the magnitude of the platform perturbation is equal to the perturbation experienced by the system

Application of the displacement-matched SWAG factor resulted in more consistent dynamic responses across stance widths. The responses were generally under-damped, exhibiting the same number of oscillations and nearly equivalent settling times. The most significant deviations in the responses occur above stance angles of 21°. Above this stance angle the response dynamics diverge with stiffness remaining consistent with mid level gains, increasing with high gains, and decreasing with low gains (Figure 3.21).

The variation of K_{eff} at wide stances was the combined result of different gain magnitudes used in the series and wide stance leverage sensitivity to displacement. Low gain magnitudes facilitate greater X_{CoM}, and the increased displacement reduces the mechanical leverage. Therefore, with low gains, mechanical leverage values are lower than the values for SWAG calculations and the resulting SWAG adjusted gains are lower than the required value to maintain postural responses. At high gain values, displacement is reduced and leverage is higher than the SWAG adjustment resulting in increased K_{eff} with increasing stance. SWAG values are set for a nominal expected displacement. Feedback gains that result in less displacement during the perturbation will result in increasing K_{eff} with increasing stance. Feedback gain resulting in more displacement will causes K_{eff} to decrease with slightly with increasing stance.

With the simulations confirming the expected performance of the SWAG function across stance widths, we implemented SWAG on the robot to observe conservation of postural performance (Figure 3.22). The robot trials confirmed the function of the SWAG factor. Application of the SWAG factor resulted in consistent perturbation responses across the stance range. The dynamics of the responses was characterized by the general form of an under-damped postural response with a single small overshoot during the perturbation recovery and similar settling times. The final settling positions of the responses varied and were the results of friction and other non-exact characteristics of real systems. Although the resting positions of the responses varied, the responses still

maintained similar qualitative features, thereby confirming consistent performance.

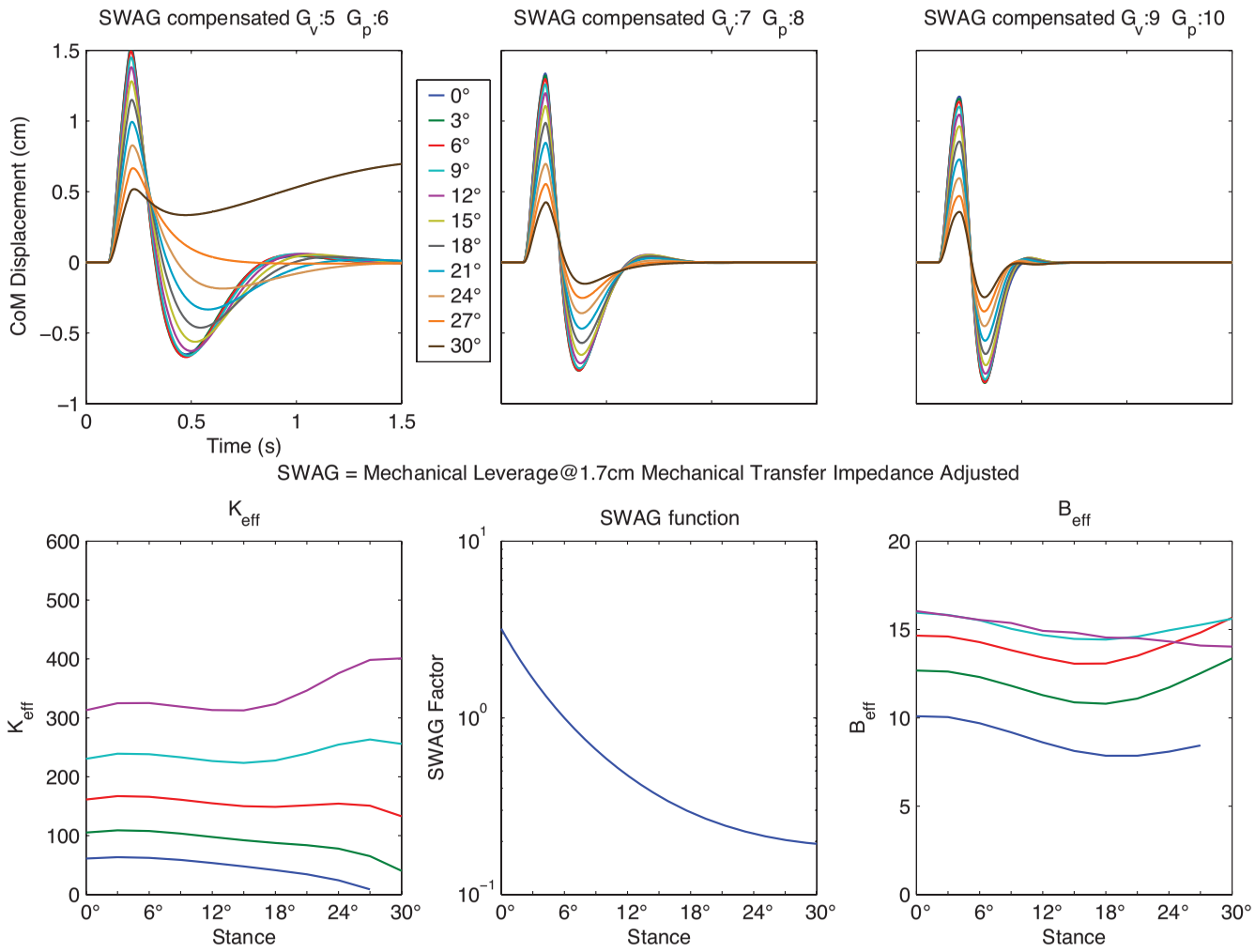

Figure 3.21: Perturbation responses with displacement adjusted SWAG function. Perturbation responses for A) low, B) medium, and C) high gain ns conditions when impedance adjusted SWAG factor is used. Effective stiffness, D), and damping, E), are conserved across the range stances

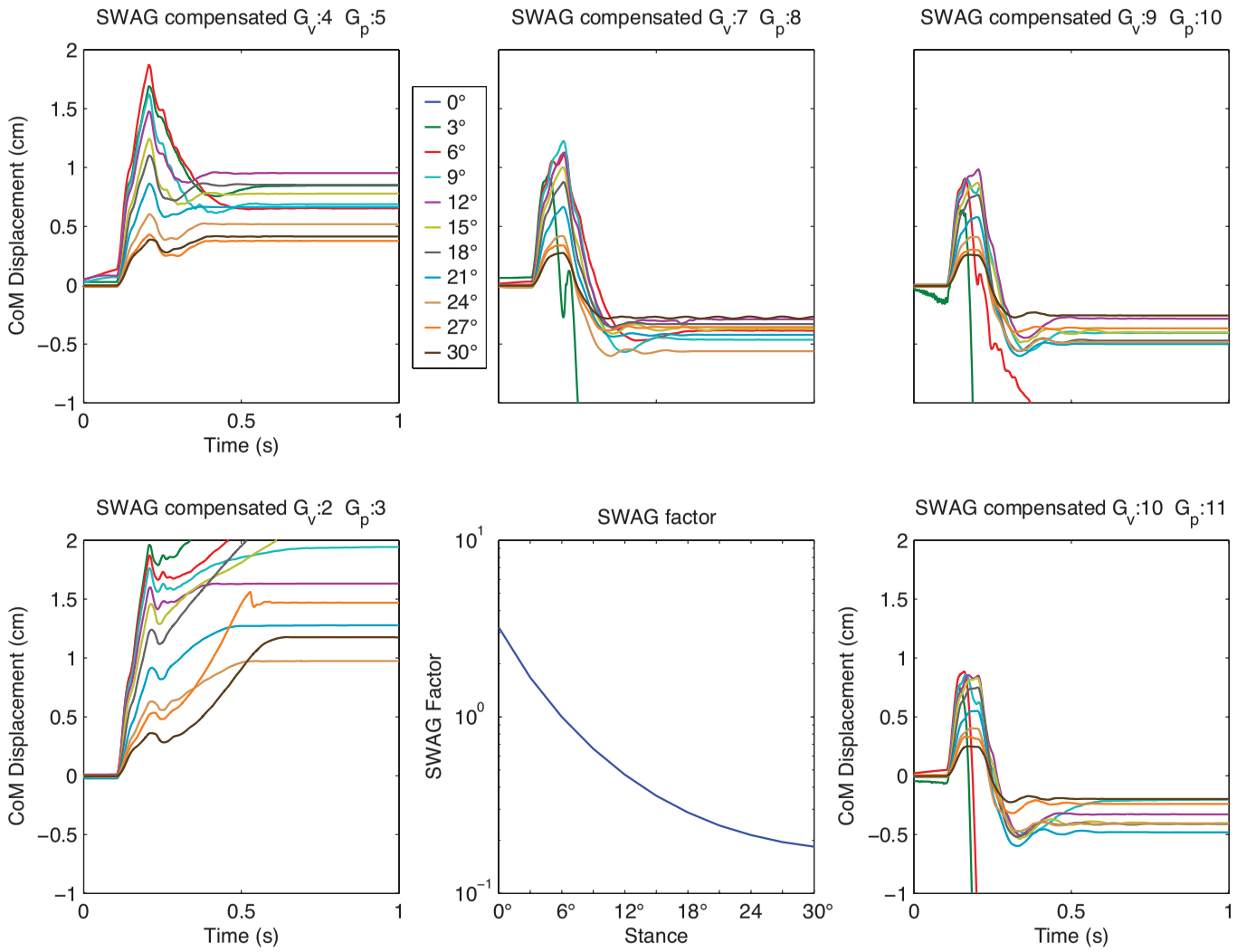

Figure 3.22: SWAG Adjusted Robot Trials: The robot trials illustrate consistent performance across the range of stance widths. For each gains series, the perturbation responses have the same general form for each of the stances, and the settling times are roughly the same.

3.5 Summary and Discussion

In Chapter 2 we showed that postural performance is the result of the combined effects of both stance width and feedback gain and that variation of either of these parameters results in changes in the postural performance and even postural instability. In this chapter, we quantified postural performance for stable combinations of stance width and feedback gain. For each stance only a limited range of feedback gains resulted in a stable behavior, and performance varied throughout that region of stable gains. By examining a invariant set of feedback gains across multiple stance widths, and measuring the resulting performance variation, we were able to isolate the effects of stance change on postural performance. We identified the source of the performance variation as the combined effect of mechanical changes with stance width variation and delay. Stance variation alters the kinematic relations between the leg joints and the CoM, essentially altering the mechanical leverage between the mass of the system and the joint actuators. Using kinematic analysis we quantified the mechanical leverage as a function of stance angle and generated a gain adjustment factor that scales feedback gain with stance so that the system maintains postural performance characteristics. The adjustment factor is calculated as the reciprocal of mechanical leverage and we have termed this adjustment the “SWAG” Factor (Stance Width Adjustment of Gain). We have demonstrated that the use of the SWAG factor results in postural responses that are qualitatively similar across stance widths. The responses exhibit similar response characteristics matching settling time and oscillations, as well as quantitative measures of effective stiffness and damping.

The variations in postural performance exhibited in the widest stance with SWAG adjustments are the results of variations in the components of mechanical leverage with CoM displacement. Our initial measures for mechanical leverage were derived from the upright stance with zero displacement. However, the measures of effective inertia and displacement ratio are sensitive to displacement at wide stances and their values decrease

with CoM excursion. Since the postural response involves displacement and the average $X_{CoM} \neq 0$, use of a SWAG function derived from center position results in decreased measures of effective stiffness at wide stances due to overcompensation by the SWAG factor. To compensate for this inconsistency, we derived a revised SWAG function from the stance-dependent displacements that result from the 2 cm perturbation. The result of this adjustment was a SWAG function that was most accurate for a perturbation and feedback gain combination that results in a 1cm of displacement and fairly accurate for other stable gain combinations. With lower gains and larger displacement, the average effective mechanical leverage gain is less than the average used for the SWAG. Therefore SWAG overcompensates the gain adjustment and effective stiffness decreases. With high level gain and small displacements effective average leverage is higher than the values calculated by the SWAG function and the system is therefore under-compensated resulting in increasing effective stiffness. The limitation of the SWAG function is that is it is a single variable scaling function for a non-linear system. Appropriate scaling for stance width requires additional terms to take CoM displacement into consideration. SWAG could use gain magnitude to adjust for CoM displacement magnitude, consequently this scaling would only be appropriate for a single magnitude of perturbation. Other perturbation magnitudes would result in similar effective stiffness deviations at wide stances. By generating our scale based on the displacements of the high magnitude perturbation used in this study, we have developed a SWAG factor that can provide reasonable responses across a wide range of gains and the full range of stances.

The key importance of the SWAG function is that the gain adjustments were derived from analysis of the kinematics of the mechanical system, not from observed responses. We detailed the changes that occur in the mechanical system with increased stance width. We then developed gain adjustments based on those changes. The result is a

postural system that allows desired characteristics of postural performance to be set and maintained through stance width variations.

Overall this study has shown that postural performance is dependent on the interrelation between postural orientation and feedback control. Variations of each of these parameters require variation of the other. We have shown that by calculating the variation of the mechanical leverage with stance width, we can develop a function of stance-dependent gain adjustments (SWAG function) that enables the conservation of postural response dynamics following a stance width change.

CHAPTER 4

INTRINSIC STIFFNESS EFFECTS

In Chapter 3 we investigated the relation between stance width and active delayed feedback gains, and we showed that stability requires a coordinated relation between stance width and feedback gains. To continue our investigation of the relation between stance and feedback control, we determine intrinsic stiffness (IS) to its effects on the dynamics of the postural response.

IS is a term that is used to describe the non-delayed stiffness and damping characteristics of the joint motion. In mechanical systems, IS may be the result of springs and dampers or other passive elements installed in the system. In biological systems, IS is a property of connective tissue and activated muscles. In the muscles, intrinsic properties can be modulated by controlling the level of muscle activation, thus IS is not considered passive. Regardless, the forces produced by IS are instantaneous as opposed to the delayed forces of the active response.

Because IS generates non-delayed reactive forces, we hypothesized that IS could enhance postural stability across stance widths and reduce the requirements of active control. We also wanted to determine how IS affects postural responses with the implementation of the SWAG function.

To verify our hypothesis, we conducted a three stage investigation. First we examined the effects of IS on the overall stability of the system. This stage was designed to evaluate the potential IS–dependent variation of the stabilizing gain ranges and determine if IS has different effects at different stances. Next, we examined the dynamics of postural responses with increasing magnitudes of IS to determine how IS alters the independent responses. Lastly, we evaluated the dynamics of IS responses with active gains that have been scaled by the SWAG function.

4.1 Stability Effects

To identify the stable regions, we performed a sweep over the parameter space (θ_s, G_v, G_p, and G_i) and determined the stability of each response. Our methods for identifying the stable combinations were the same as those described in section 3.3.1. Simulation responses were stable if $|X_{CoM}| < 0.5\,\text{cm}$ for $t_{pert} > 1.5\,\text{s}$. The sweep was performed over the entire parameter space, including intrinsic stiffness as a variable parameter. Intrinsic stiffness has both elastic and viscous components that provide stiffness and damping to the postural response. To reduce the number of parameters and the number of trials requires for this study, we scaled both the elastic and viscous components by a single variable. These components were set to a constant ratio of 10/1 (elastic/viscous). This ratio was comparable to the ratio of the stable gain values observed in Chapter 3. We evaluated IS with elastic coefficients ranging from 0 to 0.03 Nms/° and viscous coefficients ranging from 0 to 0.3 Nm/°. Similar to the methods used for the active delayed feedback gains, we used a dimensionless scaled magnitude of the intrinsic gain values throughout the investigation. An IS gain with a viscous coefficient of 0.025 Nms/rad and an elastic coefficient of 0.25 Nm/rad is identified as $G_i = 2.5$.

The results of the sweep were similar in form to the results from the sweep in Chapter 3, except for the fact that these results have the extra dimension of G_i. Therefore, for each θ_s, the sweep produced multiple stable regions in the two-dimensional space of G_v and G_p, one for each iteration of G_i. These results showed that the addition of intrinsic stiffness increased the range of stabilizing active feedback gains (Figure 4.1), facilitating stable postural responses with a wider range of active feedback gains. The magnitude of the range increase was dependent on stance and intrinsic gain magnitude. Narrow stance configurations were less sensitive to intrinsic stiffness, requiring high magnitudes of gain to create an observable difference in stability range. In wide stance configurations, intrinsic stiffness facilitated stable responses with lower feedback gain magnitudes.

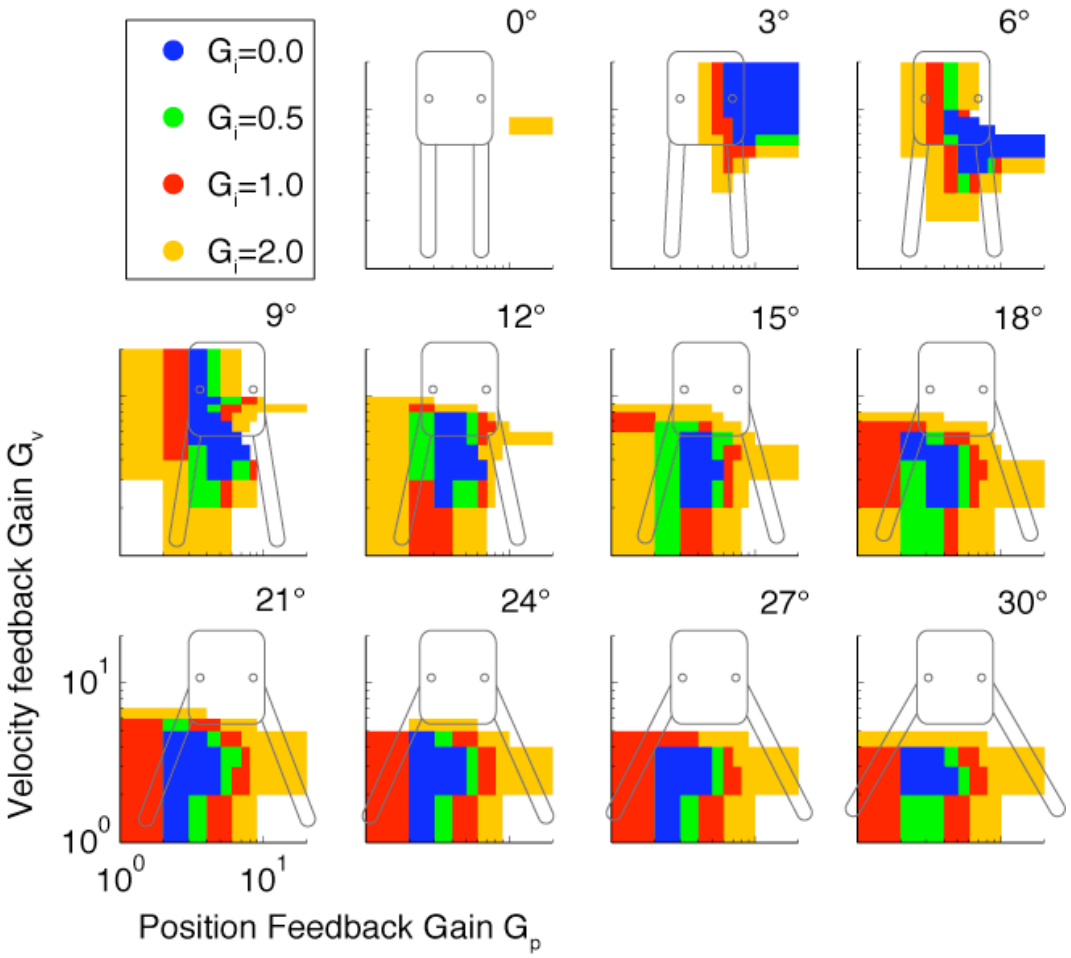

Figure 4.1: Stability Map with increasing G_i. The stability map illustrates the values of G_v and G_p that produce a stable response for each stance and value of G_i. Each circle indicates a stable combination of gains. The different colors represent the evaluated values of G_i. The smallest stable regions occur for G_i=0 (blue) and grow with increasing G_i. The largest regions shown, G_i=2.0 (orange), encompass the stable values of all lower magnitudes of G_i.

Initially we considered the possibility that G_i would simply complement G_v and G_p, thereby shifting the stable region and their respective gain values. However, results of the parameter sweep showed that the addition of IS increased the range of stable active gains rather than shifting the range by supplementing the active gain. If G_i were to simply supplement active gain, the range of stable G_v and G_p would shift, negatively, by the magnitude of the additional intrinsic gain. Such a shift would cause a decrease in the magnitude of the upper boundary as well as the lower boundary of stability. Instead we observed a decrease in the lower boundary and either no change or an increase in the

upper boundary (Figure 4.1,Figure 4.2). This result indicates a intrinsic stiffness dependent growth in the stability region for both higher and lower magnitudes of G_v and G_p.

As we examined the IS-dependent stable range increase more closely, we observed that the increase was not equal for both of G_v and G_p. The extension of the stabilizing range was greater for G_p than it was for G_v,. Intrinsic stiffness facilitates stable responses for substantial increases in of G_p, and the stable range of G_v experienced only a marginal increase. We highlight this result in Figure 4.2 by illustrating the changing stable gain region of a single stance. The figure shows that the growth of the stabilizing gain region in the positive G_v direction is on average less than the magnitude of the additional intrinsic stiffness magnitude. In contrast, the stable range increase in the positive G_p direction exceeds the magnitude of additional intrinsic stiffness. The reduction of the minimum stable magnitudes of both G_v and G_p are limited by the by zero gain.

The effects of IS on the stable regions of active feedback gain are consistent across stances affecting similar alterations of the regions for each stance. The forms of the range alterations are also similar for the incremental increases in intrinsic stiffness. The range grows similarly for each increment of IS. The major difference between all of the IS dependent variations is that in wide stances, IS can fully compensate for the perturbation without the need for any active feedback. This zero-active stability is due to mechanical leverage resulting in low gain requirements for wide stances.

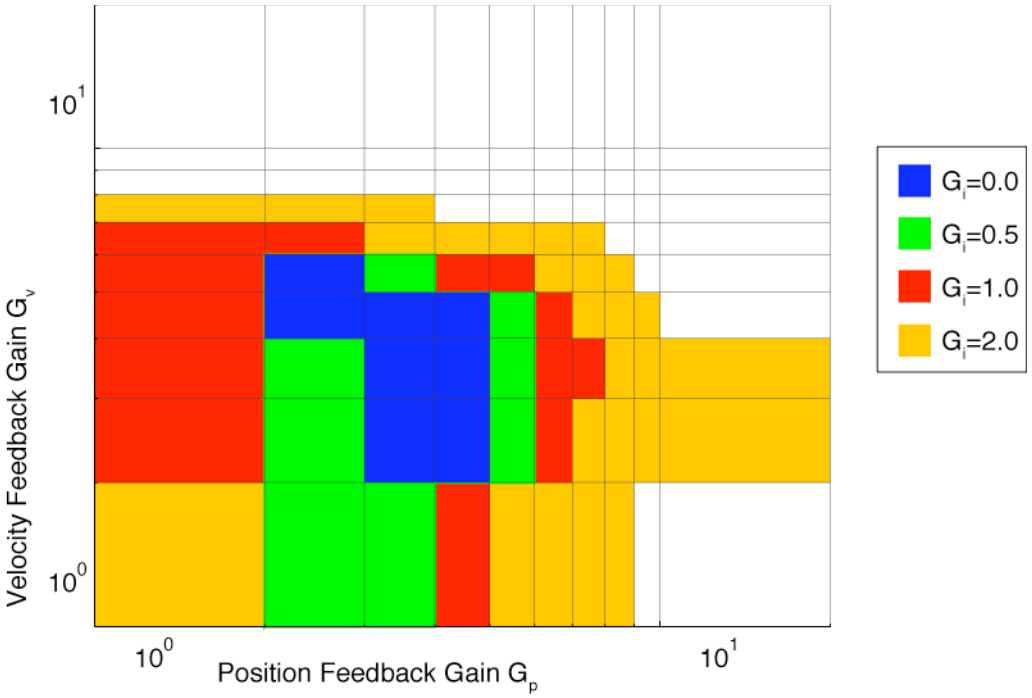

Figure 4.2: Stability with increasing G_i at θ_s=18°. We evaluated stability at θs=18° for increasing magnitudes of G_i. The range of stabilizing gains increases with increasing G_i. The stabilizing range is smallest when G_i =0 (blue region), and largest when G_i =2.0 (orange region). As G_i increases the stabilizing region increases. The stabilizing gain region for each magnitude of G_i includes the range for lower values.

The results of the single parameter intrinsic sweep (G_i) showed that stable range of G_v. and G_p were affected differently. To make sure that this was not an artifact of the proportion of stiffness to damping in our single parameter IS; we evaluated the postural responses with the individual addition of intrinsic components. We swept stiffness (G_{ip}) and damping (G_{iv}) independently for zero to three. The results showed that the individual components do have differential effects on the stable ranges (Figure 4.3). G_{ip} facilitates stability with lower magnitudes of G_p but does not facilitate increased stability for higher magnitudes of G_p or G_v. Increasing G_{iv} facilitates stability for higher both higher and lower magnitudes of G_v. It also facilitates stability for higher magnitudes of G_p. These results are understandable because instability in the lower gain ranges is the result of insufficient stiffness being unable to return to system to the upright position. Also, instability in the higher gain regions is the result of excessive oscillation, which can effectively be considered negative damping. Additional G_{ip} increases damping and

thereby removes the energy form the system and slows down oscillations. This means that higher active gains can be used without the negative effects of oscillation.

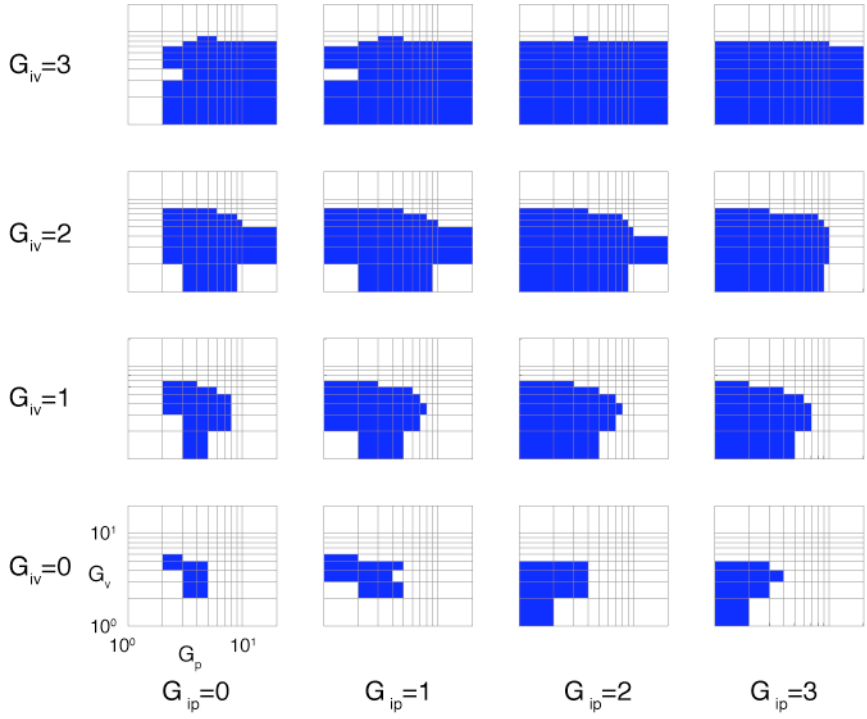

Figure 4.3: Stability Range with Independent G_{iv} and G_{ip} at θ_s=18°. When intrinsic stiff and damping are varied independently, we observe that increasing stiffness facilitates stability with lower magnitudes of gain and damping facilitates stability with higher magnitudes of gain.

4.2 Dynamic Effects

The results of our parameter sweep have shown that the addition of IS increases the range of stabilizing active gains, especially in the direction of lower active gains. This means that lower magnitudes of active gain can facilitate a stable response when IS is engaged. So, instead of only adding G_i to the system and quantifying the change in the response, we also decided to evaluate response changes as active gains are reduced while intrinsic gains are increased. Therefore, we evaluated the addition of IS in two methods. First we evaluated response changes while varying the magnitude of G_i and maintaining G_v and G_p constant. In this method, G_i was added to G_v and G_p.

$$G_{total} = G_{active} + G_i$$

Next we evaluated the effects of replacing active feedback with intrinsic stiffness. This method required a coordinated reduction of G_v and G_p with the addition of G_i of the same magnitude.

$$G_{active} + G_i = \text{Constant}$$

For each of these methods, we evaluated the effects of IS on the dynamics of postural responses for several gain combinations. In order to determine these effects over the full range of stances without evaluating each individual stance, we evaluated the stance angles of 6°, 18°, and 27°. θ_s =6° is our previous reference stance, and it also a representative example of a narrow stance. The other stances, θ_s=18° and 21°, are representative examples of a moderate wide stance, and very wide stance, respectively. For each stance we evaluated low, medium, and high magnitude active feedback gains relative to the stable range for the stance, without intrinsic stiffness (Table 4.1, Figure 4.4) .

Table 4.1. Evaluated Stance and Gain Parameters (G_v, G_p)

θ_s	Low	Medium	High
6°	4,5	6,7	8,9
18°	2,3	3,4	4,5
27°	1,2	2,3	3,4

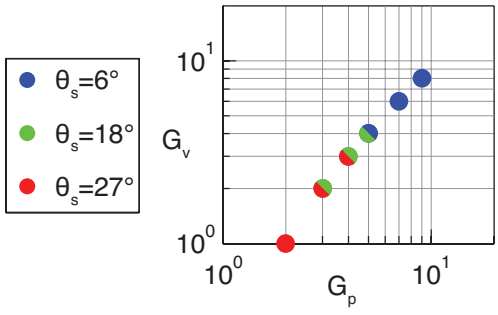

Figure 4.4: Evaluated Gain Parameters. We evaluated the dynamic responses for a series of stance and gain parameters. The parameters are listed in Table 4.1. This figure presents a visual illustration of active gain parameters for reference to the stabilizing gain range figures

4.2.1 Addition of intrinsic stiffness

We performed the series of trials as indicated for the series with added G_i and active gain. Figure 4.5-Figure 4.7 show the resulting data from these trials for stance $\theta_s = [6° \; 18° \; 27°]$, respectively. For each series, subplots A, B, and C, show the results for the low medium and high gains, respectively. The time traces in subplots A, B and C, show that CoM motion, X_{CoM}, for different magnitudes of intrinsic stiffness. As we predicted, the addition of intrinsic stiffness has a stabilizing effect. By calling the effects stabilizing, we mean that increasing G_i results in decreased decrease in peak initial displacement, decreased settling time, and decreased oscillations. In each of these series, we observed that the addition of intrinsic stiffness progressively reduced the magnitude of the peak initial displacement and decreased oscillations.

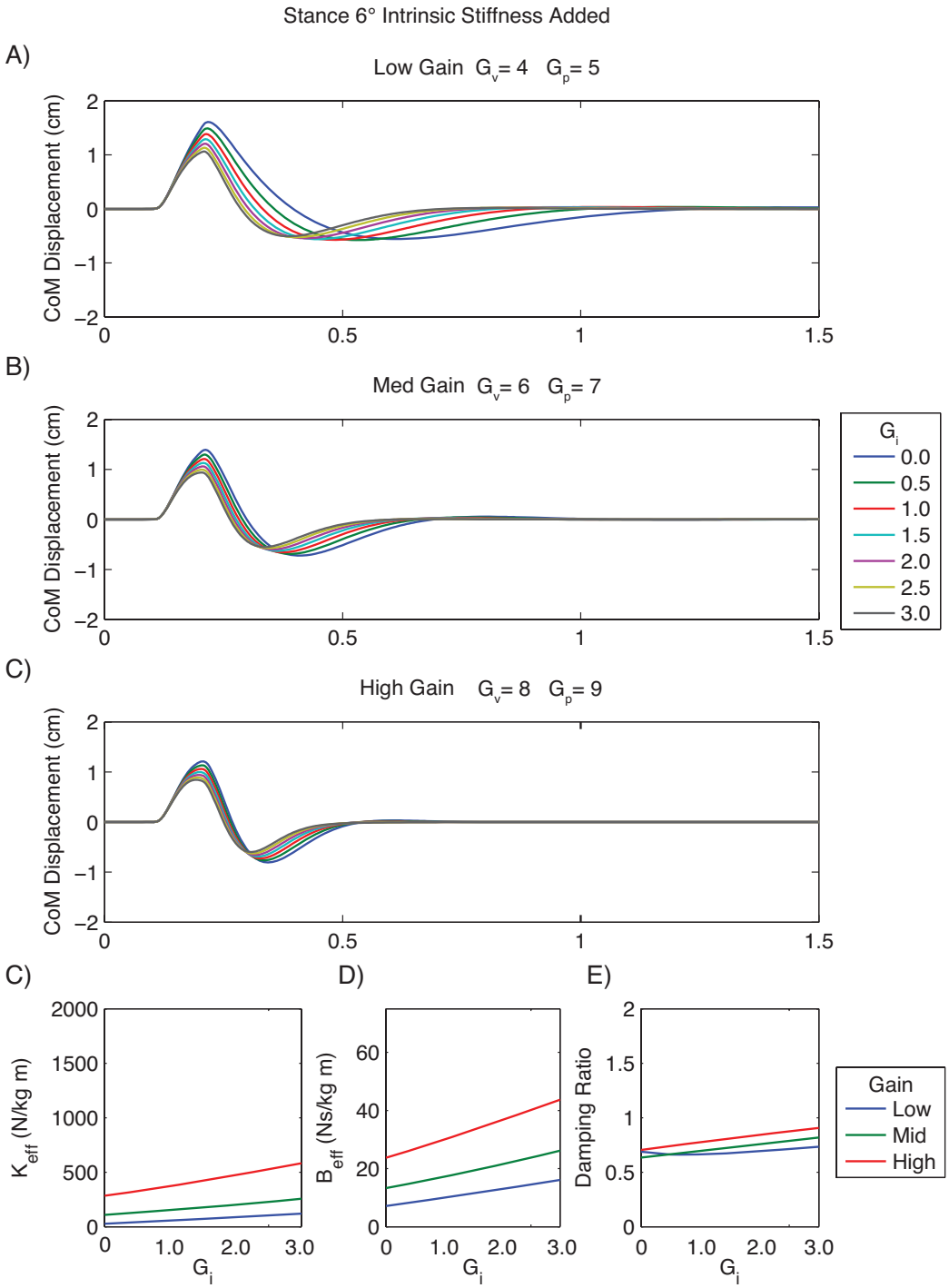

Figure 4.5: Postural Responses with increasing G_i, θ_s=6°. When $\theta_s = 18°$, the form of the postural responses with increasing G_i are similar except for decreasing displacement magnitude. This relative consistency is also evident the relative consistency of the damping ratio and uniform variation of K_{eff} and B_{eff}. The consistency of the responses is a result of the low relative magnitude of Gi compared to the active gains, G_v and G_p. G_i Has the effect of reducing the displacement magnitude, but the dynamics of the response are dominated by active gains.

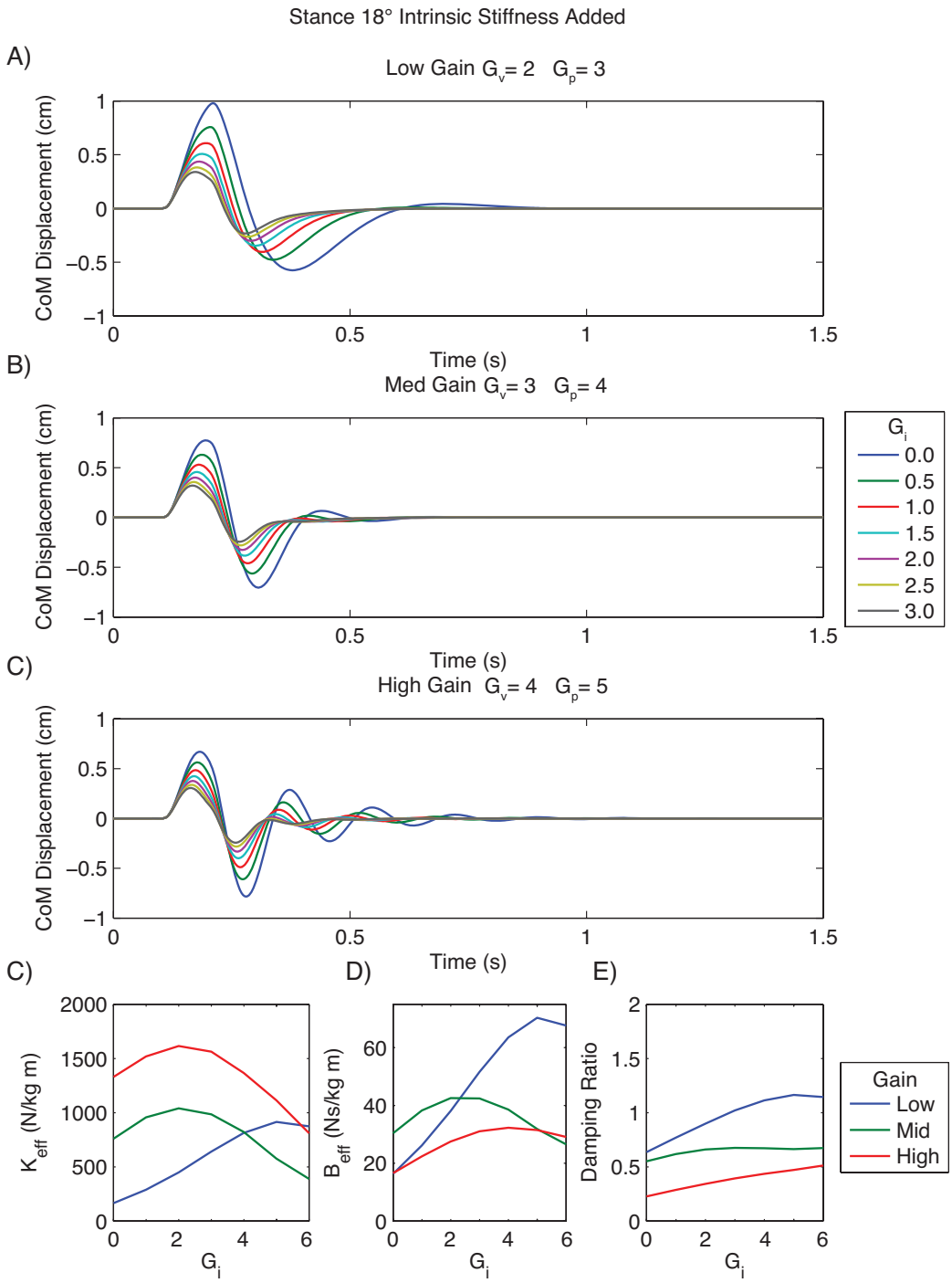

Figure 4.6: Postural Responses with increasing G_i, θ_s=18°. With increasing G_i, the initial displacement of the postural response is greatly reduced. The magnitude of the reduction is proportional to the ratio of $G_i / G_v, G_p$. As active gain is increased (B,C), there is less reduction of the initial displacement. However there is less displacement with G_i =0. The ppostural responses for G_i =3.0 for each set of active gains (grey trace in subplots A, B, and C) all have similar displacement magnitude and gross shape of the postural response. The difference between these =3.0 responses is that the oscillations of the responses increase with active gain. With high active gain and G_i =3.0, there is a slight oscillation that is the result of the active gains.

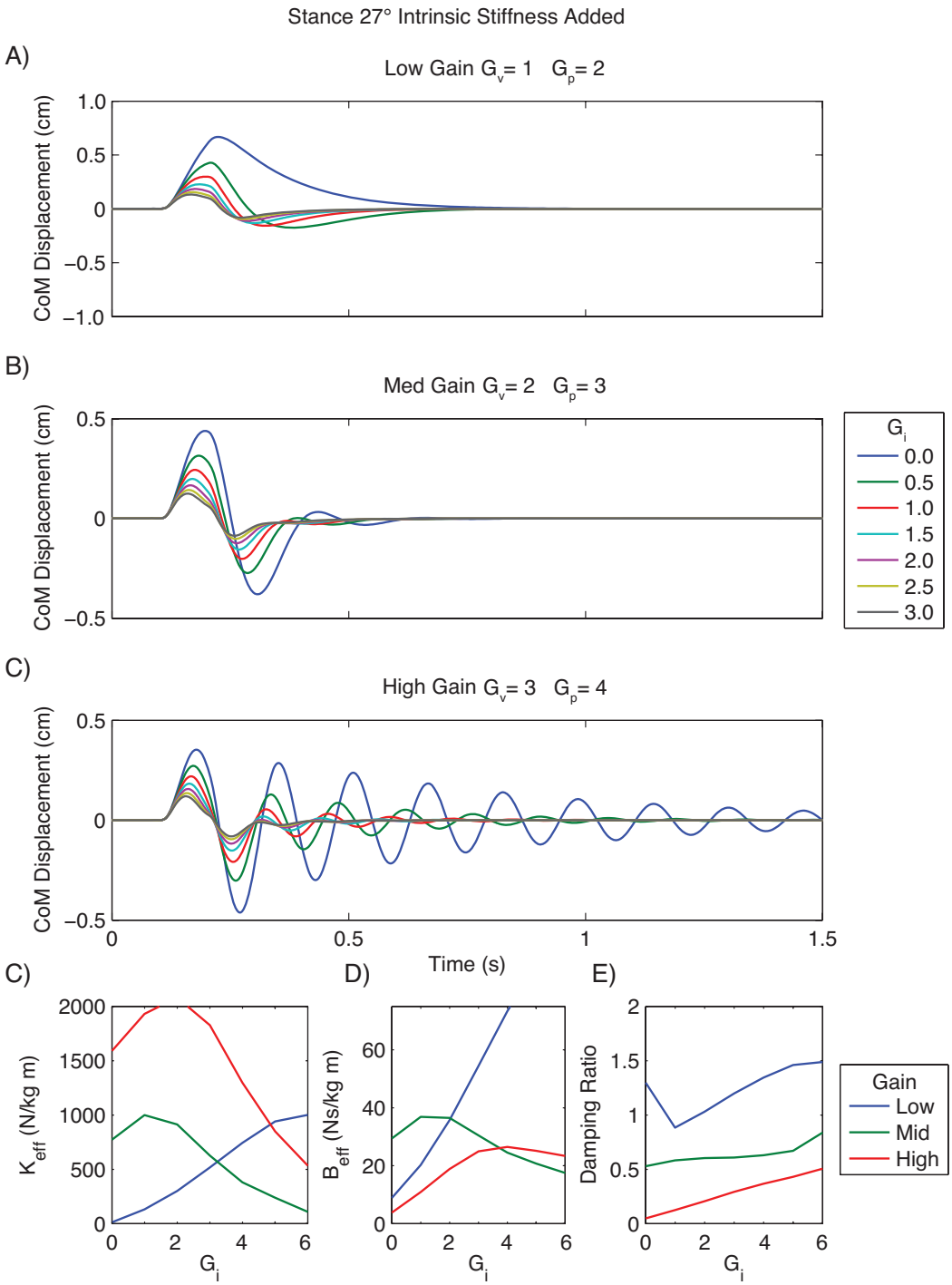

Figure 4.7: Postural Responses with increasing G_i, θ_s=27°. In the low gain condition with G_i =0, the active response is barely able to stabilize the system after the perturbation. This effect is evident by the very long time constant of the response and the large initial displacement with a slow return. As G_i is increased, the response becomes stable and we see a gradual variation of the response with increasing G_i. Also, because of the low magnitude of the stable gains at this wide stance, the magnitudes of G_i are high relative to the active gains and there is a large variation of the responses with increasing G_i. The result the active response is increased oscillation. This characteristic is illustrated by comparing high intrinsic, low active response (grey trace subplot a) to the high active low intrinsic response (green trace subplot c).

There are two reasons for the reduction of initial displacement; the first reason is the addition of gain. Since we added gain, the magnitude of displacement should reduce since the more controller effort was exerted due to the higher gain. The second reason for the reduced displacement is because IS had a faster response to perturbation due to its lack of delay. For example in Figure 4.4a, the addition of G_i caused a divergence of the responses beginning at the start of the perturbation. This result contrast with the results observed with the addition of active gain where all responses for a given stance had the same initial trajectory. The delay of the active gain also caused a discontinuity in the response when the active efforts become effective. Without IS, this delayed effort initiates the return of the CoM toward the center position, resulting in a sharp direction change. However, IS exerts control effort from the beginning of the perturbation resulting in decreased total displacement with increased G_i.

IS reduced the oscillation of the system partly because the damping efforts (from the velocity component of G_i were in proportion to the actual velocity of the system. This contrast active delayed feedback where its velocity term generates control efforts that are proportional to a velocity measurement that was $30\,\text{ms}$ past. If the natural frequency (ϖ_N) of the system is slow enough, the current velocity and the present velocity will be similar and the effect of delay will be small. However, if the natural period of the system ($1/\varpi_N$) has a magnitude that is comparable to the delay, then the present velocity and the previous velocity could be in opposite directions and the delayed "damping" efforts would actually accelerate the system rather than decelerate the system. IS has no delay so the velocity dependent component of the stiffness decelerates the system and increasing IS increases the deceleration of the system.

Evaluation of K_{eff} and B_{eff} variations under increasing G_i shows that the effects of IS on K_{eff} are predictable, but not consistent (Figure 4.5-Figure 4.7d). In each stance and gain condition, K_{eff} initially increases with increasing G_i. However, with continued

increases in G_i, K_{eff} eventually begins to decrease. The point at which K_{eff} begins to decrease occurs at different magnitudes of both K_{eff} and G_i for each parameter set (θ_s. G_v, G_p). These characteristics also describe the variation of Beff. However, the variations of Beff are not the same foe each parameter set. For example, Figure 4.4c,d show the G_i dependent variations of K_{eff} and B_{eff} for θ_s=18°. K_{eff} for both medium and high gain initially increase then decrease with peak magnitudes occurring at $G_i = 2$. B_{eff} for medium and high gain also increase initially then decrease, the peaks for medium and high gains occur at $G_i = 2$and, $G_i = 4$, respectively. Since the variations of B_{eff} and K_{eff} are non-monotonic and their inflections points do not correlate with any observed parameters, we could not draw conclusions regarding the effect of IS from these independent parameters.

To establish a better understanding of these variations, we analyzed the damping ratio of the responses. Damping ratio (ζ), is a parameter that characterizes the frequency response of a second order ordinary differential equation. For a damped harmonic oscillator with mass, m, damping coefficient, b, and spring constant, k, the damping ratio is $\zeta = \frac{b}{2\sqrt{k \cdot m}}$. Since our measures use mass normalized values for K_{eff} and B_{eff}, damping ratio can be written as: $\zeta = \frac{B_{eff}}{2\sqrt{K_{eff}}}$

Evaluation of damping ratio shows that ζ generally increases with increasing G_i. One exception of this trend of increasing ζ is observed low-gain parameter set for $\theta_i = 27°$ (Figure 4.5e). ζ initially decreases with the first increase of G_i then increases with continued addition of G_i. This discontinuity is the result of borderline instability in the postural with that particular parameter set. With $G_i = 0.0$ the system is greatly displaced and almost fails to recover from the perturbation (Figure 4.7a). This is indicated by a very slow return to center position and a very low magnitude K_{eff}. As G_i is increased, the system generates a stronger response and the displacement is maintained well within the

limits of stability. With this anomaly explained by the borderline stability of the parameter set, we conclude that the addition of G_i increases the damping of the postural response as evident by increasing ζ with increasing G_i. This increased damping ratio increases the stability of the system, enabling a wider range of active gains and increases perturbation rejection (smaller initial displacements).

4.2.2 Replacement of active gain with intrinsic stiffness

In addition to adding G_i to continuous levels of active gain (G_v, G_p), we also evaluated the incremental replacement of active gain with intrinsic gain. The magnitudes of the velocity and displacement components of G_i are equal to the velocity and displacement components of G_v and G_p ($G_i = G_v + G_i$). Therefore, as we increase G_i, decreasing both G_v and G_p by the same magnitude would keep total feedback gain magnitude constant. We evaluated the responses for the previously listed parameter combinations (Table 4.1), with an incremental replacement of G_v and G_p with G_i. The replacements were conducted for G_i=0:1:3.0. Exceptions to this interval occurred when G_v, G_p < 3.0. In each of these cases, the series of trials was terminated when $G_v = 0.0$.

Results of the study show that K_{eff} consistently decreases with incremental replacement of G_v and G_p with G_i. This decreases occurred for all evaluated stances and gains, and it contrast the results of the experiments in section 4.2.1. Previously, increasing G_i caused a gradual decrease in settling time while the response behavior remained qualitatively similar. An example of this behavior in observed in Figure 4.9c, where the oscillations continue throughout the progression of G_i, even though the settling time decreases. When G_i replaces G_v and G_p, the oscillations are quickly eliminated with only small increases in G_i (Figure 4.9c) The system also shifts from being under-damped to over-damped as indicated by the increase in ζ (Figure 4.9f). The reason for this behavior difference is the reduction of the active gains. The delay of the active gains is

the primary cause of the observed oscillations in the responses. As active gain is reduced and replaced with the non-delayed, faster responding, non-oscillatory G_i, initial displacement and oscillation magnitude will decrease.

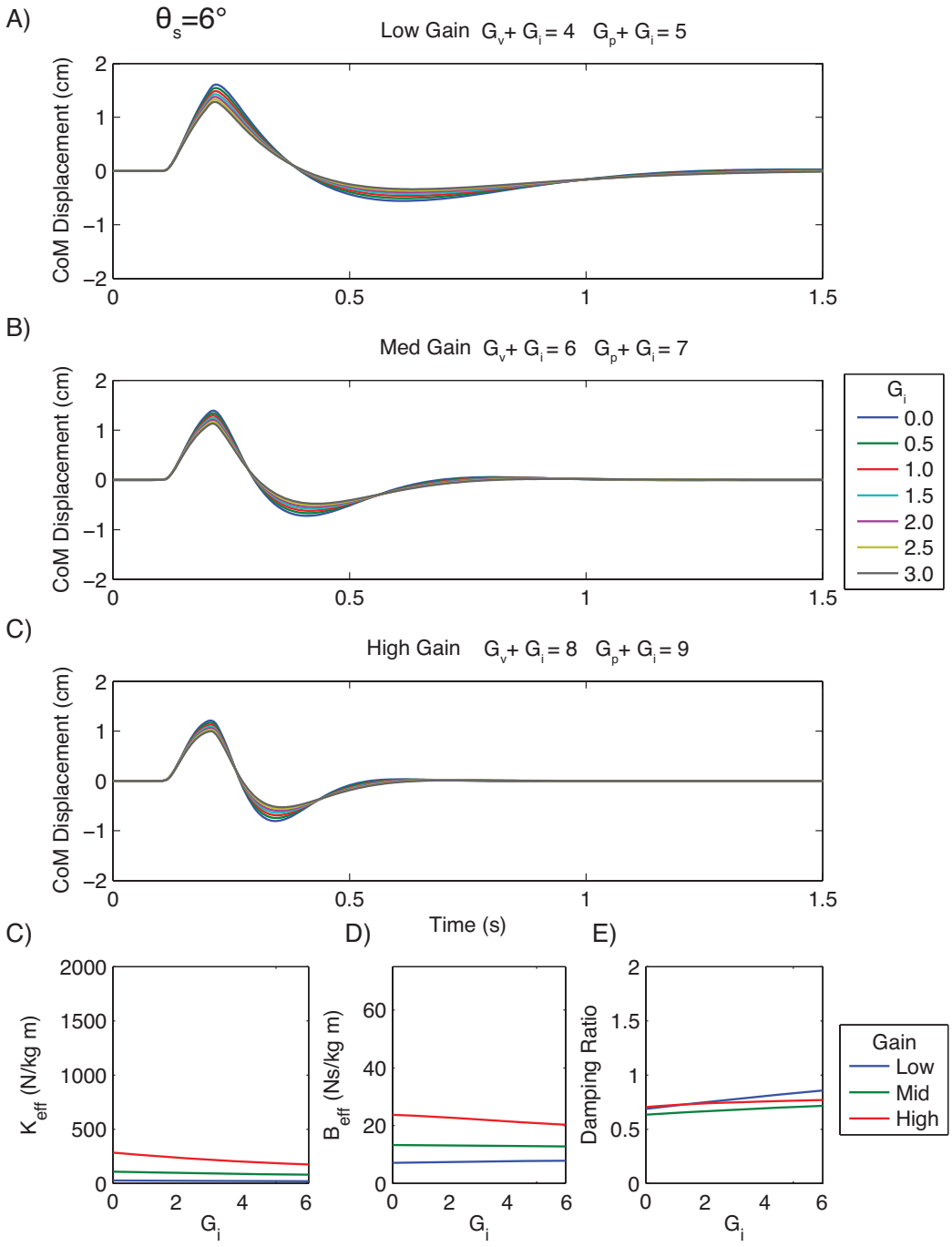

Figure 4.8: Postural Responses with G_i replacing G_v and G_p, θ_s=6°. Since the gain magnitude requirements of the narrow 6° stance are relatively high, the addition of relatively low magnitude intrinsic gain does not significantly alter the postural response. However the addition of G_i does slightly increase ζ, indicating that intrinsic stiffness does contribute to the stability of the response.

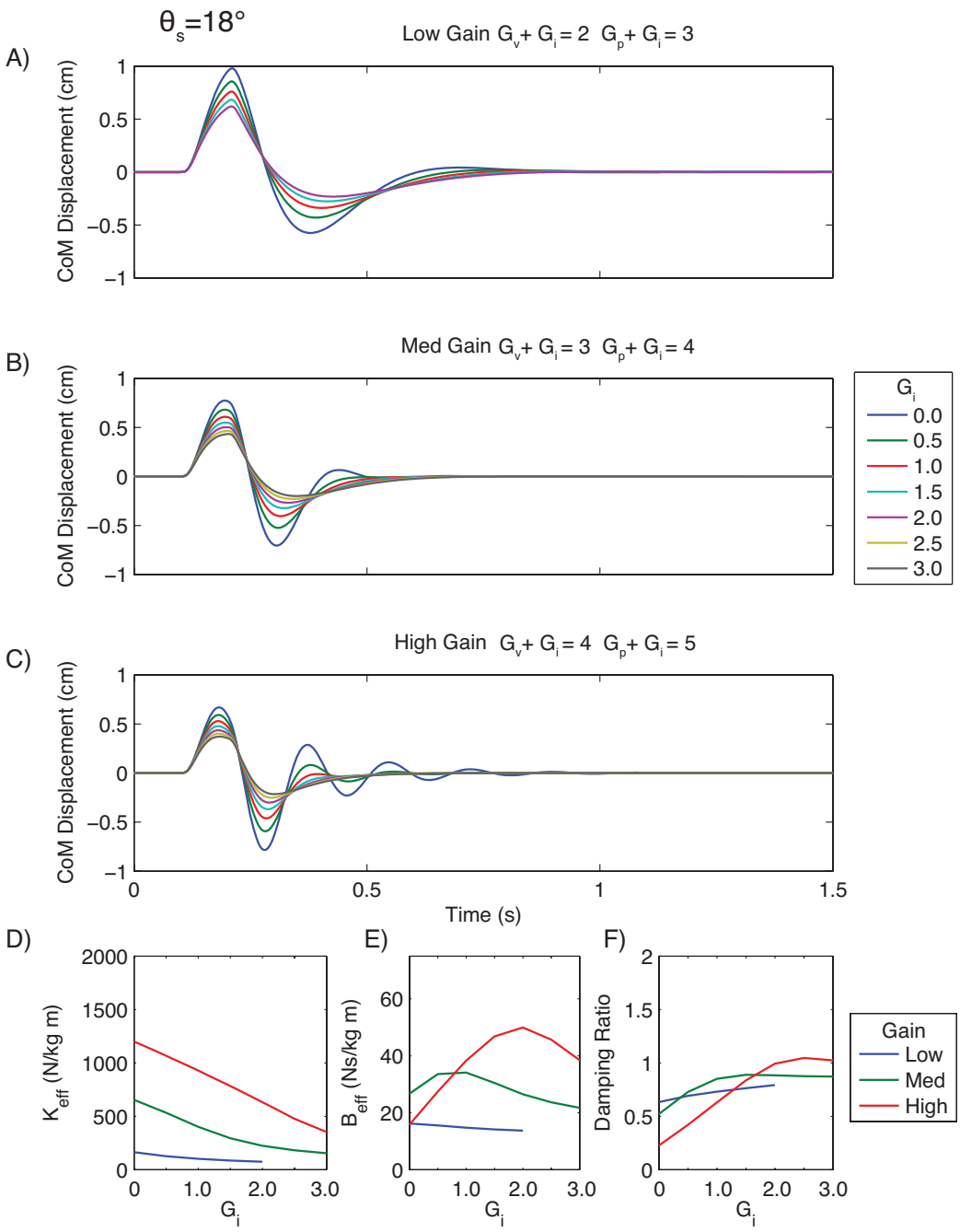

Figure 4.9: Postural Responses with G_i replacing G_v and G_p, θ_s=18°. In this stance, the total gain magnitude is low enough that replacement with G_i significantly altered the response. Using the middle gain parameter magnitude, G_i replacement immediately reduced oscillation, eliminating the second response overshoot (B red trace). Further gain replacement continued to increase the stability of the response and brought the system towards critical damping (ζ=1).

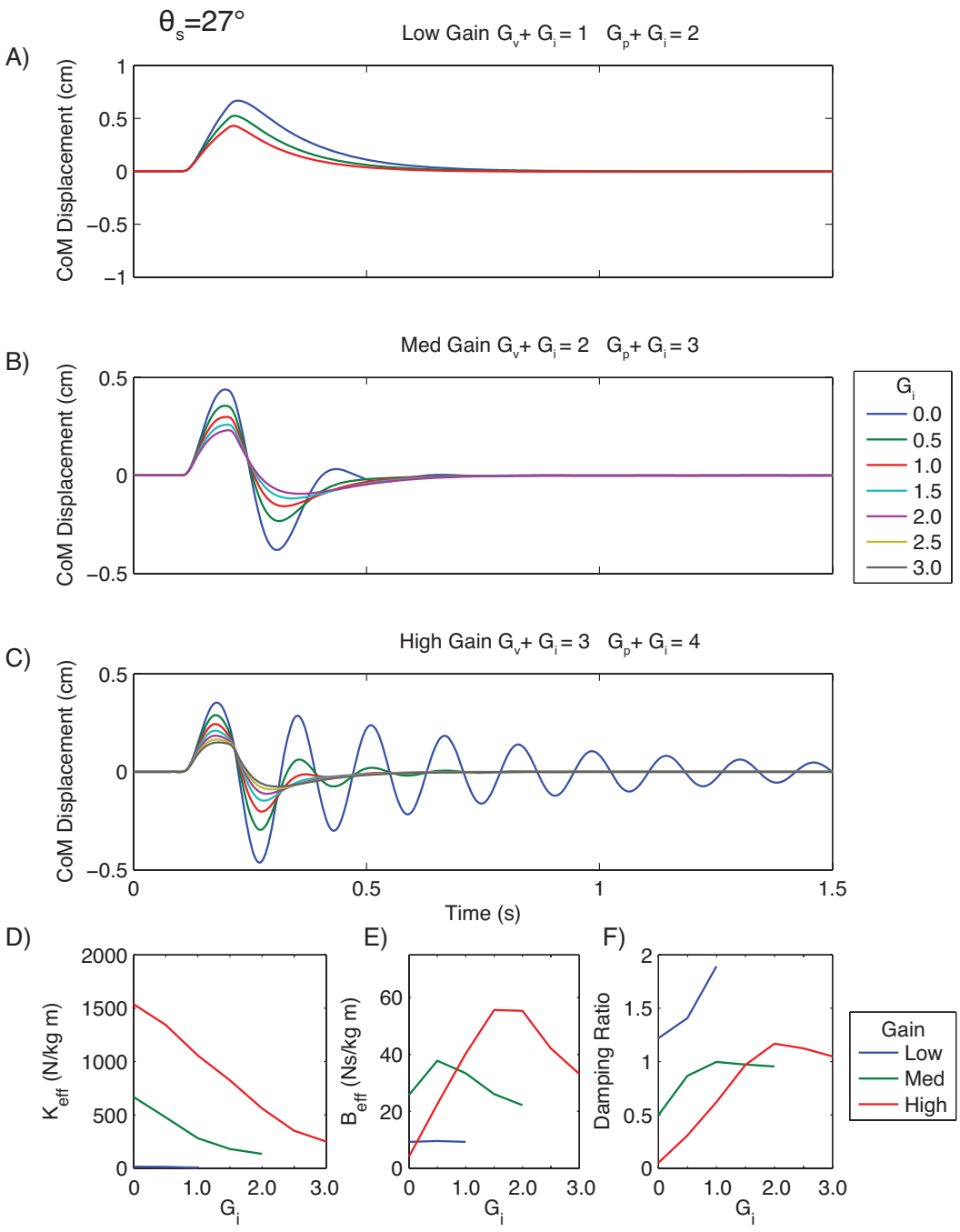

Figure 4.10: Postural Responses with G_i replacing G_v and G_p, θ_s=27°. This series is limited by the low magnitude of the active gains. Since we reduced active gain win increasing G_i, each series was limited by G_v =0. So the maximum magnitude of Gi for low and medium gains were G_i =1.0 and G_i =2.0, respectively. Replacement of active gains with intrinsic gain in these low gain conditions shows that intrinsic gain is more stable than active gain. In the high gain condition (subplot C) , the response with G_i=0.0 oscillates when active gain is dominant. However, when G_i is dominant, the response with G_i=3.0 is very stable with low displacement, no oscillation, and the response is slightly over-damped. In both the low and mid gain conditions, B_{eff} peaks then decreases with increasing Gi (D). The interesting point is that as this peak occurs, ζ>1.0 and with further G_i increase $\zeta \rightarrow 1.0$. This may indicate that the system is approaching critical damping.

4.3 Intrinsic with SWAG

We have shown that increasing G_i alters the dynamics of the postural response by decreasing the displacement magnitude resulting from the perturbation and increasing the damping ratio (ζ) of the response. The results of these alterations are reduced oscillations and settling time, and altered measures for K_{eff} and B_{eff}.. We have also shown that the use of the SWAG function is effective in maintaining consistent response dynamics under stance variations. In this chapter, we investigated the combination of these factors to determine the effects of intrinsic stiffness on SWAG scaled responses.

To determine the coupled effects of intrinsic stiffness and SWAG scaling, we evaluated postural responses for multiple parameter sets across the range of stances. We assessed the variation of K_{eff} and B_{eff} with increasing G_i, and calculated ζ. The results of these SWAG trials show that K_{eff} and B_{eff} do not remain consistent with increasing stance and SWAG when $G_i \neq 0$ (Figure 4.11,Figure 4.12). K_{eff} and B_{eff} generally increase with increasing θ_s and G_i. An exception to this trend occurs as $K_{eff} \rightarrow 1000\ {}^{N}/_{kg \cdot m}$ with increasing θ_s. As θ_s is further increased, both Keff and Beff begin to decrease, resulting in a slight decrease in ζ. We also observed that the magnitude of the initial displacement, settling time, and oscillations were all reduced considerably with increased stance.

Although K_{eff} increases considerably with increasing stance, the system does not become unstable with increasing oscillations. This result contrast the responses observed in Chapter 3 when only active gains were used. On those occasions, increasing θ_s (without the SWAG function) increased K_{eff} caused the system to become unstable when $K_{eff} \rightarrow 600\ {}^{N}/_{kg \cdot m}$. The addition of G_i with the SWAG function causes K_{eff} to increase with θs. However, even with the increased K_{eff}, oscillations decrease with in creased stance and the system displays increased stability with reduced displacement and settling times.

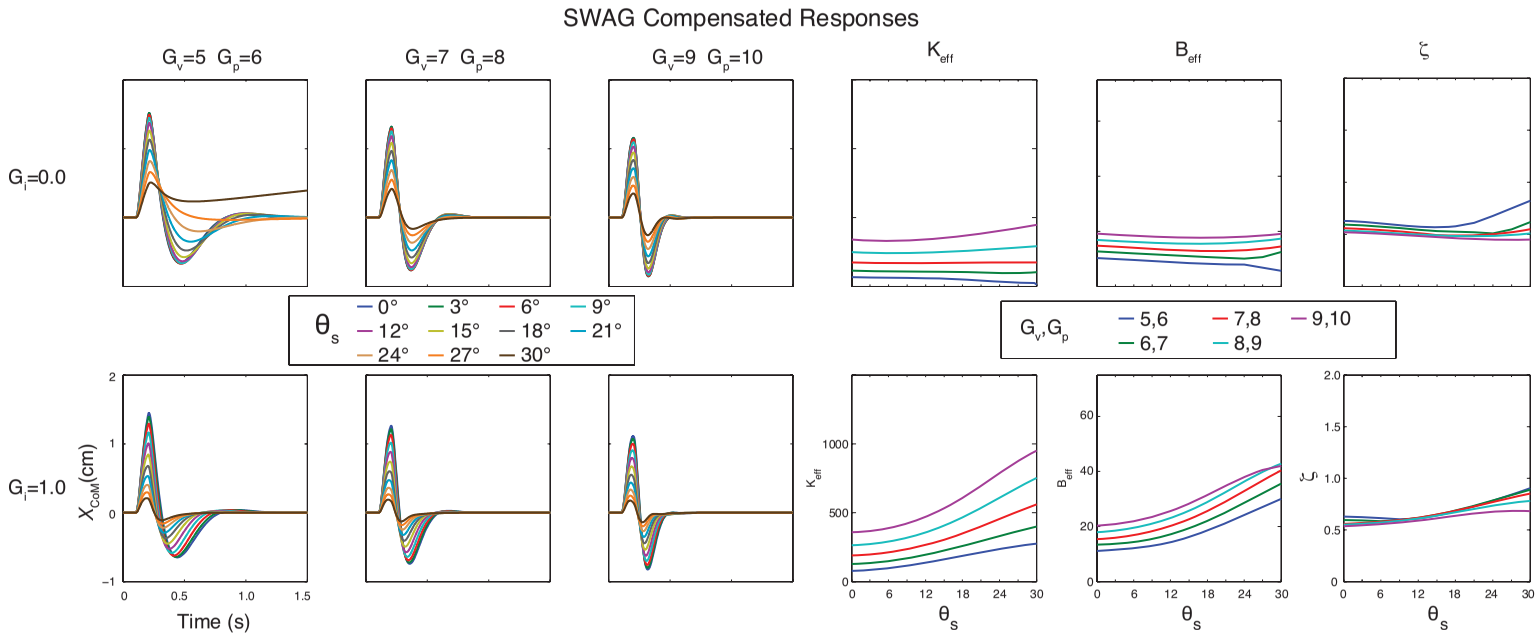

Figure 4.11: Postural responses with SWAG and Intrinsic Stiffness. The addition of IS results in increasing K_{eff} with stance increases and SWAG scaling This K_{eff} increase is the result of increased effectiveness of G_i with increasing stance and reduced displacement magnitude resulting in higher mechanical leverage at wide stances. This reduced displacement effect is evident when comparing the results of SWAG scaled responses with G_i =0. With the lowest gain parameters (G_v =5, G_p =6), the wide stance response is unstable because of low gain magnitude. When intrinsic stiffness is added, displacement is reduced so mechanical leverage is not reduced and all K_{eff} measures increase.

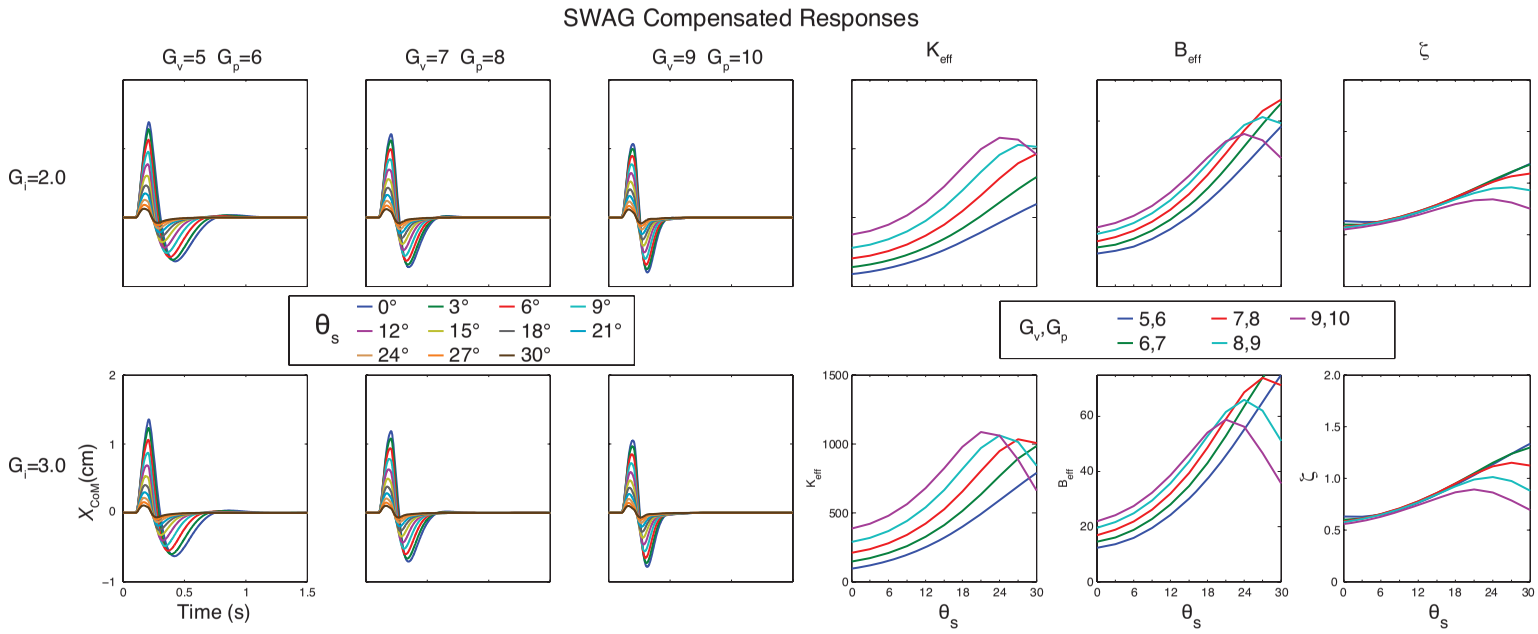

Figure 4.12: Postural Responses with SWAG and G_i=2.0,3.0. As higher magnitudes of G_i are used with SWAG scaling, initial displacement magnitudes at wider stances become similar for all magnitudes of active gain. This result indicates that G_i is dominating the displacement portion of the response. The slight variation in settling time and the difference between K_{eff} measures indicates that the remainder of the at wide stance responses are affected by the active gains.

4.4 Discussion

Our study of the effect of IS has shown that increasing G_i increases the stability of the system facilitating stable responses for a wider range of active feedback gains. This stabilizing effect increases with the magnitude of G_i and facilitates a proportionately wider stabilizing range for G_p than G_v.

Intrinsic stiffness affects the dynamics of the postural response by reducing the initial displacement of the system caused by the perturbation and it also reduces the magnitude and duration of post perturbation oscillations in the system response. The reduction in initial displacement is the result of a lack of delay in the in the intrinsic feedback loop. Without delay, the intrinsic response responds immediately at the start of the perturbation, generating postural restoring forces as the displacement begins. The immediate nature of this response contrast the response of the active gains which have a 30 ms feedback delay. Because of this delay, systems without intrinsic feedback are accelerated by the perturbation for 30 ms before active feedback generates a response. As a result, systems without IS each have a minimum displacement magnitude that is dependent on stance and the mechanical transfer impedance of that stance. With IS, perturbation response is immediate and displacement magnitude is reduced relative to the G_i =0 response displacement magnitude.

The dynamics of the postural response are also affected by intrinsic stiffness. Since there is no delay in the feedback loop, the velocity and displacement components of the response are proportional to the current state of the system. This temporal correlation between state and response enables the damping term of the intrinsic response to reduce the velocity of the system resulting in decreased oscillation and settling time.

Evaluations of SWAG scaling with intrinsic stiffness has shown that increasing G_i alters the stance dependent responses resulting in increased K_{eff} with increased stance. However since IS increases the stability of the system, the increased K_{eff} does not result in unstable

oscillations as previously observed. Instead the systems exhibit decreased displacement magnitude, settling time indicating an overall increase in stability. Overall increasing intrinsic stiffness increases the stability of the postural response.

CHAPTER 5

DISCUSSION

Compliant postural strategies employed by animal neuromuscular systems may provide robust solutions and inspiration for robotic and prosthetic design. However, variations in postural orientation can alter the response dynamics of such compliant systems. Furthermore, with delayed feedback control, these variations can cause unstable responses. In the bipedal model of standing balance, compliant postural controllers with feedback delay must coordinate control gain adjustments with changes in stance width. In this dissertation, we showed that increasing stance width requires a reduction in feedback control gain and that this reduction is directly inverse to the change in mechanical leverage that occurs within the structure.

5.1 Conclusions

Our investigation of the relation between stance width and postural control was conducted in a series of steps, and each of which was to answer specific questions about the relation. Based on the results presented for each of the projects we have made a number of conclusions regarding the interactions between stance width and the control of standing balance.

5.1.1 Stability Range

In Chapter 3 we began our investigation into the effects of stance width variations by mapping the region of stabilizing active gains for each stance. The results showed that the magnitude of the gains within the stability regions decreased with increased stance. It was not surprising that lower gains would be stabilizing for wide stance; however, we did find it interesting that the high gains were unstable in wide stances. This result contradicts common perception that wide stance is more stable simply because it has a wider base of support. If that were the case, the stabilizing gains of narrow stance would

have been a low-magnitude subset of the stabilizing gains of wide stance. The results showed that overall stability could not be obtained by maintaining a high level of active stiffness for all stances. A high level of stiffness may provide stability for a narrow stance, but the same stiffness would induce unstable oscillations in a wider stance. It was this discovery that led to the next phase of the investigation that sought to explain why this variation occurred and define the underlying cause.

5.1.2 Dynamic Response Variation

In Chapter 3 we also evaluated the effects of stance variation by quantifying the stance-dependent changes in the dynamic response of the system. The results showed that the effective stiffness of the responses increases with increased stance width and responses became unstable as the stiffness exceeded a stable threshold. This stable threshold is the result of the delay of active control. A stiffness increase is correlated with an increase in response frequency. Because the system has a temporal delay, the phase of the delay increases with frequency resulting in unstable oscillations. Thus, the instability that occurs with high gains is the result of the delay in feedback control. However, the increase in stiffness that results from stance width increases is the result of an occurrence of mechanical origin.

5.1.3 Mechanical Leverage

We evaluated the mechanics of the structure to determine the cause of the stance-dependent change in stiffness. Again, common perception is that increasing stance width makes the system stiffer because it sets the legs at an angle, allowing them to direct perturbation forces along their axis rather than as bending forces that must be balanced by joint torque. Instead, our results showed that stance width variation alters two important aspects of the physical system: the mechanical impedance of the structure and the mechanical leverage of the controlled mechanical system. Mechanical impedance is the

structure's resistance to movement when subjected to a perturbation. This aspect of stance increase is the common understanding of increased stiffness with increased stance, and it is true for the bipedal standing model. Increased stance width results in decreased initial displacement magnitude. Perturbation impedance is therefore important to the overall stability of the system; however, it primarily affects the initial displacement due to the perturbation and not the dynamics of the post perturbation response. The change in the dynamics of the post-perturbation response is the result of a stance dependent alteration of the mechanical leverage of the system. Increasing stance width increases the mechanical leverage of the system thereby changing the interaction between the controller and the structure. This relationship is what's important to the stability and behavior of the system. Feedback gains must be matched to the mechanical structure. If gains are too high the system, the system oscillates, if gains are too low, the system falls. Changing stance width is like changing the gain of the system; so changing stance width requires a change of the feedback gains so that the system remains stable.

5.1.4 Intrinsic Effects

Our results showed that intrinsic stiffness increases the stability of the postural system. This increased stability is manifested as an increase in the stabilizing gain regions for each stance, facilitating stable postural responses for a wider range of active gains for each stance. It also increases the stability of postural responses for each set of parameters. This increased stability of the responses is manifested as decreased initial displacement, decreased settling time, and decreased oscillation magnitude and frequency.

5.1.5 SWAG Function

We characterized a stance-dependent change in mechanical leverage through mechanical analysis of postural kinematics, and showed that it is the cause of the changing dynamics of postural responses under changing stance width. The analysis

showed that mechanical leverage acts as a gain in the control loop of the system. By scaling the feedback gain of the controller by the reciprocal of that leverage, or more specifically, the reciprocal of the change in leverage, we showed that consistent postural performance could be maintained under stance width variations. We called this function of gain scaling the SWAG function (Stance Width Adjustment of Gain Function). The true benefit of the SWAG function is that it enables a stable system to remain stable after changes in stance width.

5.2 Future Research Directions

The work presented in this dissertation has well defined a relation between stance width and control. However, there are variations of this work that could provide more detail on some of the elements studied here or insight into other specific postural scenarios. One specific variation of this work would be to scale the model up to human proportions and evaluate the SWAG factor on a human scale. This scaling would be necessary to evaluate some of the implications presented in this chapter. With the scaling, feedback delay of the postural controller would also need to be adjusted. The adjustment of feedback delay may also present interesting dynamic implications for the cat scaled system.

Another direction of future research would be to expand the model of the SWAG function and develop system identification methods that extract the intrinsic and active components of postural responses. Since the model produces response dynamics, active gains could be assumed to scale by the SWAG function and optimization methods could be used to identify scaling of intrinsic stiffness across stances.

This research could be expanded to greater complexity to investigate dynamic variation of intrinsic stiffness. Because intrinsic stiffness of muscles can be modulated through activation, dynamic models could vary the magnitude of intrinsic stiffness during the postural response.

These paths of future research each vary in their levels of complexity, but they all incorporate the variation of mechanical dynamics that is associated with stance width. Continuation of this research along any of these paths could help improve our understanding of postural control, thereby bringing us closer to better treatments for impairments and better control for our standing robots.

5.3 Implications

The conclusions of this dissertation describe the relation between stance width and postural control, and from this description, predictions can be made regarding the effects of parameter variations. These predictions have implications that may affect rehabilitation therapies and the studies of human and animal postural control. They may also have implications on the development of control strategies for humanoid standing robotics.

5.3.1 Human/Animal Posture

This research has shown that feedback gains must be reduced with increased stance width in order to maintain postural stability. This reduction is required because of a change in the mechanics of the postural configuration, therefore it is reasonable to assume that a similar change occurs in the mechanics of human and animal posture. So with such changes, we predict that the feedback gain for postural control in humans and animals must also be reduced with increased stance width if joint kinematics are used in the feedback process. However, if CoM kinematics are used in the feedback process, it is possible that *less* scaling would be required, but some scaling would still be necessary due to the irrelevance of the leg/CoM displacement ratio and the changing relation between torque and CoM acceleration. Also, it must be emphasized that these results show that gain reduction would be required because of the changing leverage of the

postural configuration, not because of the decreased displacement magnitude resulting from increased “passive” stiffness of the mechanical system.

The conclusions of this study and the use of the SWAG function may assist future studies and provide some insight into past studies of human and animal postural control by helping to explain results that show variations of activation levels during postural changes. Activation changes could occur for postural adjustments other than stance width, including squatting, bending, and loading (carrying extra mass). The SWAG could also be used to predict changes in muscle activation after postural adjustment.

The use of the SWAG function may also influence clinical research in the detection of postural impairments. Because the SWAG function predicts changes in control requirements under stance variation and the dynamic model can show changing activity levels for different magnitudes of gain and perturbation, the postural responses of patients and subjects could be compared to the model to determine if gain adjustments are being made after stance variations.

Eventually, the results of our research may influence clinical therapies by facilitating the suggestion of compensation methods for balance-impaired patients. The suggestions would originate from an understanding of the postural system, enabling a physician to suggest postures in which the effects of a balance impairment are minimized. The understanding attained in this research may also be used to develop devices, both passive and active, that increase intrinsic stiffness and thereby increase the stability of balance-impaired patients.

5.3.2 Robot Posture

As the field of robotics continues to grow, and there is more of a need for standing robots to emulate humans and animals, use of the SWAG function could facilitate compliant behavior that will be required for these systems. The SWAG function would serve as bridge between high impedance and passive dynamic robotics. The

scaling of gain would enable the production of forceful responses when necessary and passive responses when force is not required. Reference to the SWAG function could also suggest standing postures that lower power consumption for standing autonomous robots, thereby increasing battery life and their overall usefulness.

APPENDIX A

MODEL PROGRAMS

5.4 AUTOLEV MODEL

```
%       File:  Jlinks60.al
%--------------------------------------------------------------------
%                 Default Settings

AutoZ       OFF           % Program introduces Zees automatically
Digits      7             % Significant digits
%--------------------------------------------------------------------
%                 Newtonian, bodies, frames, particles, points
Newtonian   N
Bodies      A, B, C
Frames      L1, L2
Points      NA, AB, BC, CN, NCO
%--------------------------------------------------------------------
%      Variables, constants, and specified
MotionVariables'  qA", qB", qC"     % qA', qB', qC' are generalized speeds
Variables       FA{2}, FC{2}                % Contact forces
Constants       aA=.000             % Acceleration coefficient at A
Constants       aC=.000             % Acceleration coefficient at C
Constants       dA=0              % Damping coefficient at A
Constants       dC=0              % Damping coefficient at C
Constants       kA=00               % Stiffness coefficient at A
Constants       kC=00               % Stiffness coefficient at C
Constants       LA=0.1397, LB=0.04445, LC=0.1397        % Lengths(meters)
Specified       g=9.81              % Gravitational acceleration
Specified        LN = .04445 % stance width
Specified        accel = 0.0    % lateral acceleration
Specified        TAA = -aA*QA"      % Acceleration Torque on A
Specified        TAC = -aC*QC"      % Acceleration Torque on C
Specified        TDA = -dA*QA'      % Damping Torque on A
Specified        TDC = -dC*QC'      % Damping Torque on C
Specified        TKA = -kA*QA       % Stiffness Torque on A
Specified        TKC = -kC*QC       % Stiffness Torque on C
Specified        TA = TKA+TDA       % Total Active Torque at A
Specified        TC = TKC+TDC       % Total Active Torque at C
ZEE_NOT = [FA1, FA2, FC1, FC2]
%--------------------------------------------------------------------
%      Mass and inertia
Mass        A=mA=.162, B=mB=1.35, C=mC=.162
Inertia     A, 7.14E-05,3.38E-04,2.71E-04,-5.4E-11,0.0,-3.21E-6
```

```
Inertia     B, 1.36E-3,2.19E-3,1.42E-3,0.0,-2.07E-8,-1.04E-4
Inertia     C, 7.14E-05,3.38E-04,2.71E-04,-5.4E-11,0.0,-3.21E-6
%-------------------------------------------------------------------
%       Geometry relating unit vectors
Dircos(B, L1, Space123, pi, 0, -pi/2)
Dircos(B, L2, Space123, 0, 0, -pi/2)
Simprot(N, B, 3, qB)
Simprot(L1, A, 3, qA)
Simprot(L2, C, 3, qC)
%-------------------------------------------------------------------
%       Position vectors
P_AB_NA> = LA*A1>
P_AB_BC> = LB*B1>
P_BC_CN> = LC*C1>
P_NA_CN> = LN*N1>
P_AB_Ao> = .0561*A1>
P_AB_Bo> = 0.5*LB*B1> + .0192*B2>
P_BC_Co> = .0561*C1>
P_NA_NCO> = 0.5*LN*N1>
%-------------------------------------------------------------------
%       Angular velocities
W_B_N> = qB'*B3>
W_L1_B> = 0>
W_L2_B> = 0>
W_A_B> = qA'*A3>
W_C_B> = qC'*C3>
%-------------------------------------------------------------------
%       Velocities
MotionVariables'  vx'
%V_NA_N> = 0>
V_NA_N> = vx*N2>
V2pts(N, A, NA, Ao)
V2pts(N, A, NA, AB)
V2pts(N, B, AB, Bo)
V2pts(N, B, AB, BC)
V2pts(N, C, BC, Co)
V2pts(N, C, BC, CN)
%-------------------------------------------------------------------
%       Motion constraints
Auxiliary[1] = Dot( V_CN_N>, N1> )      % Dot( V_CN_N>, N1> ) = 0
Auxiliary[2] = Dot( V_CN_N>, N2> )      % Dot( V_CN_N>, N2> ) = 0
Auxiliary[3] = Dot( V_NA_N>, N2> )      % Dot( V_NA_N>, N1> ) = 0
%Auxiliary[4] = Dot( V_NA_N>, N2> )      % Dot( V_NA_N>, N2> ) = 0
Constrain( Auxiliary[qB',qC',vx] )        % Solve for qB', qC', vx
%-------------------------------------------------------------------
%       Angular accelerations
```

```
ALF_A_N> = Dt( W_A_N>, N )
ALF_B_N> = Dt( W_B_N>, N )
ALF_C_N> = Dt( W_C_N>, N )
%----------------------------------------------------------------------
%       Accelerations of particles and mass centers of bodies
A_NA_N> = 0>
A2pts(N, A, NA, Ao)
A2pts(N, A, NA, AB)
A2pts(N, B, AB, Bo)
A2pts(N, B, AB, BC)
A2pts(N, C, BC, Co)
%----------------------------------------------------------------------
%       Forces
Gravity(-g*N2> + accel*N1>)
Force_NA> = FA1*N1> + FA2*N2>
Force_CN> = FC1*N1> + FC2*N2>
Torque(B/A, TA*A3>)         % Torque on A
Torque(B/C, TC*C3>)         % Torque on C
%----------------------------------------------------------------------
%       Equations of motion
Zero = Fr() + FrStar()
%Kane( FC1, FC2)
Kane( FC1, FC2, FA2)
%----------------------------------------------------------------------
%       Units system for CODE input/output conversions
UnitSystem  kg,meter,sec
%----------------------------------------------------------------------
%       Integration parameters and values for constants and variables
Input  tFinal=3.1, integStp=0.001, absErr=1.0E-07, relErr=1.0E-07
Input  qA=0 rad, qB=0 rad, qC=0 rad % Initial values
%----------------------------------------------------------------------
%       Quantities to be output from CODE
LOOP> = P_NA_AB> + P_AB_BC> + P_BC_CN> + P_CN_NA>
Config[1] = Dot( Loop>, N1> )         % Should always equal 0
Config[2] = Dot( Loop>, N2> )         % Should always equal 0
COM = Dot(P_NCO_BO>, N1>)             % CoM Excursion
COMU = Dot(P_NCO_BO>, N2>)            % CoM Vertical Excursion
COMV = Dot(V_BO_N>, N1>)              % CoM Excursion Velocity
COMUV = Dot(V_BO_N>, N2>)             % CoM Vertical Excursion Velocity
COMA = Dot(A_BO_N>, N1>)              % CoM Excursion Acceleration
ECheck = NiCheck()                    % Checking function
Output t, qA rad, qB rad, qC rad, COM cm, COMU cm
Output qA' rad/sec, qB' rad/sec, qC' rad/sec, COMV cm/s, COMUV cm/s
Output qA" rad/s^2, qB" rad/s^2, qC" rad/s^2, COMA cm/s^2
Output TA, TC, TAA, TAC, TDA, TDC, TKA, TKC, FC1, FC2, FA2
Output Config[1], Config[2], ECheck
```

```
%---------------------------------------------------------------------
%       Code generation for numerical solution
CODE Dynamics() jlinks60nz.c
%---------------------------------------------------------------------
%       Record Autolev responses
Save jlinks60nz.all
```

REFERENCES

Alexandrov AV, Frolov AA, Horak FB, Carlson-Kuhta P, and Park S. Feedback equilibrium control during human standing. *Biological Cybernetics* V93: 309-322, 2005.

Barin K. Evaluation of a generalized model of human postural dynamics and control in the sagittal plane. *Biol Cybern* 61: 37-50, 1989.

Brown LA, Jensen JL, Korff T, and Woollacott MH. The translating platform paradigm: perturbation displacement waveform alters the postural response. *Gait Posture* 14: 256-263, 2001.

Collins S, Ruina A, Tedrake R, and Wisse M. Efficient bipedal robots based on passive-dynamic walkers. *Science* 307: 1082-1085, 2005.

Collins SH, Wisse M, and Ruina A. A three-dimensional passive-dynamic walking robot with two legs and knees. *International Journal of Robotics Research* 20: 607-615, 2001.

Day BL, Steiger MJ, Thompson PD, and Marsden CD. Effect of vision and stance width on human body motion when standing: implications for afferent control of lateral sway. *J Physiol* 469: 479-499, 1993.

Donelan JM, Shipman DW, Kram R, and Kuo AD. Mechanical and metabolic requirements for active lateral stabilization in human walking. *J Biomech* 37: 827-835, 2004.

Full RJ, and Koditschek DE. Templates and anchors: neuromechanical hypotheses of legged locomotion on land. *J Exp Biol* 202: 3325-3332, 1999.

Gage WH, Winter DA, Frank JS, and Adkin AL. Kinematic and kinetic validity of the inverted pendulum model in quiet standing. *Gait Posture* 19: 124-132, 2004.

He J, Levine WS, and Loeb GE. Feedback gains for correcting small perturbations to standing posture. *Automatic Control, IEEE Transactions on* 36: 322-332, 1991.

Henry SM, Fung J, and Horak FB. Control of stance during lateral and anterior/posterior surface translations. *Rehabilitation Engineering, IEEE Transactions on [see also IEEE Trans on Neural Systems and Rehabilitation]* 6: 32-42, 1998a.

Henry SM, Fung J, and Horak FB. Effect of stance width on multidirectional postural responses. *J Neurophysiol* 85: 559-570, 2001.

Henry SM, Fung J, and Horak FB. EMG responses to maintain stance during multidirectional surface translations. *Journal of Neurophysiology* 80: 1939-1950, 1998b.

Hirai K, Hirose M, Haikawa Y, and Takenaka T. The development of Honda humanoid robot. In: *Robotics and Automation, 1998 Proceedings 1998 IEEE International Conference on*1998, p. 1321-1326 vol.1322.

Hogan N. Adaptive control of mechanical impedance by coactivation of antagonist muscles. *Automatic Control, IEEE Transactions on* 29: 681-690, 1984.

Horak FB, Dimitrova D, and Nutt JG. Direction-specific postural instability in subjects with Parkinson's disease. *Exp Neurol* 193: 504-521, 2005.

Horak FB, Frank J, and Nutt J. Effects of dopamine on postural control in parkinsonian subjects: scaling, set, and tone. *J Neurophysiol* 75: 2380-2396, 1996.

Horak FB, and Nashner LM. Central programming of postural movements: adaptation to altered support-surface configurations. *J Neurophysiol* 55: 1369-1381, 1986.

Huyghues-Despointes CM, Cope TC, and Nichols TR. Intrinsic properties and reflex compensation in reinnervated triceps surae muscles of the cat: effect of activation level. *J Neurophysiol* 90: 1537-1546, 2003a.

Huyghues-Despointes CM, Cope TC, and Nichols TR. Intrinsic properties and reflex compensation in reinnervated triceps surae muscles of the cat: effect of movement history. *J Neurophysiol* 90: 1547-1555, 2003b.

Ishida A, Imai S, and Fukuoka Y. Analysis of the posture control system under fixed and sway-referenced support conditions. *IEEE Trans Biomed Eng* 44: 331-336, 1997.

Jeka J, Kiemel T, Creath R, Horak F, and Peterka R. Controlling human upright posture: velocity information is more accurate than position or acceleration. *J Neurophysiol* 92: 2368-2379, 2004.

Joyce GC, and Rack PM. Isotonic lengthening and shortening movements of cat soleus muscle. *J Physiol* 204: 475-491, 1969.

Kearney RE, Stein RB, and Parameswaran L. Identification of intrinsic and reflex contributions to human ankle stiffness dynamics. *IEEE Trans Biomed Eng* 44: 493-504, 1997.

Kiemel T, Oie KS, and Jeka JJ. Multisensory fusion and the stochastic structure of postural sway. *Biol Cybern* 87: 262-277, 2002.

Kirby RL, Price NA, and MacLeod DA. The influence of foot position on standing balance. *Journal of Biomechanics* 20: 423-427, 1987.

Koditschek DE, Full RJ, and Buehler M. Mechanical aspects of legged locomotion control. *Arthropod Structure & Development* 33: 251-272, 2004.

Kubow TM, and Full RJ. The role of the mechanical system in control: a hypothesis of self-stabilization in hexapedal runners. *Philosophical Transactions of the Royal Society of London Series B-Biological Sciences* 354: 849-861, 1999.

Kuo AD. An optimal control model for analyzing human postural balance. *IEEE Trans Biomed Eng* 42: 87-101, 1995.

Kuo AD, Donelan JM, and Ruina A. Energetic consequences of walking like an inverted pendulum: step-to-step transitions. *Exerc Sport Sci Rev* 33: 88-97, 2005.

Lockhart DB. Prediction of Muscle Activation Patterns During Postural Perturbations Using a Feedback Control Model. *Masters Thesis, Georgia Institute of Technology, School of Mechanical Engineering* 2005.

Loeb GE, Brown IE, and Cheng EJ. A hierarchical foundation for models of sensorimotor control. *Exp Brain Res* 126: 1-18, 1999.

Macpherson JM. Changes in a postural strategy with inter-paw distance. *J Neurophysiol* 71: 931-940, 1994.

Macpherson JM. Strategies that simplify the control of quadrupedal stance. I. Forces at the ground. *J Neurophysiol* 60: 204-217, 1988.

Macpherson JM, and Fung J. Weight support and balance during perturbed stance in the chronic spinal cat. *Journal of Neurophysiology* 82: 3066-3081, 1999.

Macpherson JM, Lywood DW, and Van Eyken A. A system for the analysis of posture and stance in quadrupeds. *J Neurosci Methods* 20: 73-82, 1987.

Maki BE, and Ostrovski G. Scaling of postural responses to transient and continuous perturbations. *Gait & Posture* 1: 93-104, 1993.

McGeer T. Dynamics and control of bipedal locomotion. *J Theor Biol* 163: 277-314, 1993.

McGeer T. Passive bipedal running. *Proc R Soc Lond B Biol Sci* 240: 107-134, 1990.

Mcgeer T. Passive Dynamic Walking. *International Journal of Robotics Research* 9: 62-82, 1990.

Mirbagheri MM, Barbeau H, and Kearney RE. Intrinsic and reflex contributions to human ankle stiffness: variation with activation level and position. *Experimental Brain Research* 135: 423-436, 2000.

Morasso PG, and Schieppati M. Can muscle stiffness alone stabilize upright standing? *J Neurophysiol* 82: 1622-1626, 1999.

Nichols TR, and Houk JC. Improvement in linearity and regulation of stiffness that results from actions of stretch reflex. *J Neurophysiol* 39: 119-142, 1976.

Park JH, and Chung H. ZMP compensation by online trajectory generation for biped robots. In: *Systems, Man, and Cybernetics, 1999 IEEE SMC '99 Conference Proceedings 1999 IEEE International Conference on*1999, p. 960-965 vol.964.

Park S, Horak FB, and Kuo AD. Postural feedback responses scale with biomechanical constraints in human standing. *Exp Brain Res* 154: 417-427, 2004.

Patla AE, Ishac MG, and Winter DA. Anticipatory control of center of mass and joint stability during voluntary arm movement from a standing posture: interplay between active and passive control. *Exp Brain Res* 143: 318-327, 2002.

Peterka RJ. Sensorimotor integration in human postural control. *J Neurophysiol* 88: 1097-1118, 2002.

Peterka RJ. Simplifying the complexities of maintaining balance. In: *IEEE Eng Med Biol Mag*2003, p. 63-68.

Peterka RJ, and Loughlin PJ. Dynamic regulation of sensorimotor integration in human postural control. *J Neurophysiol* 91: 410-423, 2004.

Pratt G. Low impedance walking robots. *INTEGRATIVE AND COMPARATIVE BIOLOGY* 42: 175-181, 2002.

Prince F, Winter DA, and Archer SE. Assessment of postural control during quiet stance with different foot configurations. *Gait & Posture* 3: 110-110, 1995.

Rietdyk S, Patla AE, Winter DA, Ishac MG, and Little CE. NACOB presentation CSB New Investigator Award. Balance recovery from medio-lateral perturbations of the upper body during standing. North American Congress on Biomechanics. *J Biomech* 32: 1149-1158, 1999.

Ruina A. Nonholonomic stability aspects of piecewise holonomic systems. *Reports on Mathematical Physics* 42: 91-100, 1998.

Ruina A, Bertram JEA, and Srinivasan M. A collisional model of the energetic cost of support work qualitatively explains leg sequencing in walking and galloping, pseudo-elastic leg behavior in running and the walk-to-run transition. *Journal of Theoretical Biology* 237: 170-192, 2005.

Sorao K, Murakami T, and Ohnishi K. A unified approach to ZMP and gravity center control in biped dynamic stable walking. In: *Advanced Intelligent Mechatronics '97, IEEE/ASME International Conference on*1997, p. 112.

Ting LH, Full RJ, Blickhan R, and Tu MS. Is Static Stability Important in Hexapedal Runners. *American Zoologist* 30: A135-A135, 1990.

Torres-Oviedo G, Macpherson JM, and Ting LH. Muscle synergy organization is robust across a variety of postural perturbations. *J Neurophysiol* 96: 1530-1546, 2006.

van der Kooij H, Jacobs R, Koopman B, and Grootenboer H. A multisensory integration model of human stance control. *Biol Cybern* 80: 299-308, 1999.

van der Kooij H, Jacobs R, Koopman B, and van der Helm F. An adaptive model of sensory integration in a dynamic environment applied to human stance control. *Biol Cybern* 84: 103-115, 2001.

Van Der Linde RQ. Active leg compliance for passive walking. In: *Robotics and Automation, 1998 Proceedings 1998 IEEE International Conference on*1998, p. 2339-2344 vol.2333.

van der Linde RQ. Design, analysis, and control of a low power joint for walking robots, by phasic activation of McKibben muscles (vol 15, pg 599, 1999). *Ieee Transactions on Robotics and Automation* 15: 1145-1145, 1999a.

van der Linde RQ. Passive bipedal walking with phasic muscle contraction. *Biological Cybernetics* 81: 227-237, 1999b.

Vukobratovic M, and Juricic D. Contribution to the synthesis of biped gait. *IEEE Trans Biomed Eng* 16: 1–6, 1969.

Winter DA, Patla AE, Ishac M, and Gage WH. Motor mechanisms of balance during quiet standing. *J Electromyogr Kinesiol* 13: 49-56, 2003.

Winter DA, Patla AE, Prince F, Ishac M, and Gielo-Perczak K. Stiffness control of balance in quiet standing. *J Neurophysiol* 80: 1211-1221, 1998.

Winter DA, Prince F, Frank JS, Powell C, and Zabjek KF. Unified theory regarding A/P and M/L balance in quiet stance. *J Neurophysiol* 75: 2334-2343, 1996.

Winter DA, Prince F, and Patla A. Validity of the inverted pendulum model of balance in quiet standing. *Gait & Posture* 5: 153-154, 1997.

Wisse M, Schwab AL, van der Linde RQ, and van der Helm FCT. How to keep from falling forward: Elementary swing leg action for passive dynamic walkers. *Ieee Transactions on Robotics* 21: 393-401, 2005.

Yamaguchi J, Soga E, Inoue S, and Takanishi A. Development of a bipedal humanoid robot-control method of whole body cooperative dynamic biped walking. In: *Robotics and Automation, 1999 Proceedings 1999 IEEE International Conference on*1999, p. 368-374 vol.361.

VITA

Jevin E. Scrivens

Jevin was born in Tampa, Florida. He attended public schools in Miami and Tampa, received a B.S. in Mechanical Engineering from Florida A&M University, Tallahassee, Florida, in 1995 and a S.M. in Mechanical Engineering from Massachusetts Institute of Technology, Cambridge, Massachusetts in 1997. He then worked for Procter and Gamble and Walt Disney World as a Mechanical Engineer before coming to Georgia Tech to earn a doctorate in Bioengineeering. When he is not working on his research, Mr. Scrivens enjoys playing with his children, playing soccer, and building stuff.